DYNAMIC MODELING, PARAMETER IDENTIFICATION, PAYLOAD ESTIMATION, AND NON-CONTACT ARM GEOMETRY SENSING OF CABLE SHOVELS

by

Abdol Rasul Rasuli

B.A.Sc., Iran University of Science and Technology, Tehran, Iran, 1992
M.A.Sc., K.N.T. University of Technology, Tehran, Iran, 1995

A THESIS SUBMITTED IN PARTIAL FULFILLMENT OF THE
REQUIREMENTS FOR THE DEGREE OF

DOCTOR OF PHILOSOPHY

in

THE FACULTY OF GRADUATE STUDIES

(Electrical and Computer Engineering)

THE UNIVERSITY OF BRITISH COLUMBIA

(Vancouver)

December 2012

ABSTRACT

This thesis presents the application of the least squares estimation technique in identification of the cable shovel parameters and monitoring its payload. Both detailed and simplified dynamic models of the cable shovel are derived by modeling the DC motors and analyzing such nonlinear effects as inertia, Coriolis, centripetal, and friction. Mathematical methods, including the interactive Newton-Euler technique, have been used to obtain the kinematic and dynamic equations of the shovel, and establish the relationship between the shovel parameters and the payload inside the bucket. The cable shovel bucket is also referred to as "dipper". An on-line parameter identification scheme was developed and experimentally verified in order to estimate the cable shovel parameters. A data acquisition system was installed on a P&H2100 cable shovel in the Sarcheshmeh Copper mine, located in Iran, where it logged the cable shovel data for several loading cycles. The payload was dynamically estimated using the simplified dynamic cable-shovel model I developed. The accuracy and repeatability of the algorithm has been verified based upon the cable shovel data logged during its normal operation at the mine.

In the course of this thesis project, I also devised a novel approach for non-contact sensing of the dynamic arm-geometry of the cable-shovel. A prototype sensor apparatus was designed and assembled that measures the dipper handle angle, the swing angle, and the dipper handle length. Different sensors such as gyroscopes, magnetometers, accelerometers, and a laser sensor are integrated into Arm Geometry Sensor (AGS) apparatus. The AGS apparatus is installed on the saddle block and measures all cable shovel joint variables without having direct physical contact with the links or joints. The AGS apparatus was employed during field trials on the on the P&H2100 cable shovel and verified to effectively sense the shovel joint variables with acceptable accuracy.

The results of our research can be extended to intelligent shovel excavation (ISE) technology, the study of material diggability in surface mining, the monitoring of interactive forces during excavation, and the enhanced safety and productivity during dump truck loading.

PREFACE

This thesis presents the research that I conducted throughout my PhD study. My research supervisors were Prof. William Dunford and Dr. Shahram Tafazoli. They have provided guidance and modifications all along my thesis work and in the course of writing the manuscripts. I was responsible for developing the models, selecting the required sensors, conducting the field trials, analyzing the data logged in the field trials, compiling the results and conclusions, as well as preparing the manuscripts. I received significant software and hardware development support from engineers and scientists at Motion Metrics International Corp for preparing the data logger used in the field trial.

A version of Chapter 3 has been submitted for journal publication and is also patent pending in both Canada and USA:

A. Rasuli, S. Tafazoli Bilandi, and W. Dunford, "A Novel Approach to Non-Contact, Absolute Sensing of the Arm Geometry for Electric Cable Shovels," Submitted

S. Tafazoli, A.M. Ahani, and A. R. Rasuli, "Method and Apparatus for Determining a Spatial Positioning of Loading Equipment," US Patent application 13154230, Canada patent application 84122-8, June 6, 2011.

A version of Chapter 5 has been submitted for journal publication:

A. Rasuli, S. Tafazoli Bilandi, and W. Dunford, "Dynamic Modeling, Parameter Identification, and Payload Estimation of Mining Cable Shovels," Submitted

TABLE OF CONTENTS

LIST OF TABLES

LIST OF FIGURES

NOMENCLATURE

θ_i angular rotation of revolute joint i

θ_1 angular displacement of the swing joint

θ_2 angular displacement of the boom joint

θ_3 angular displacement of the saddle block joint

ϕ_s angular acceleration of the sheave

α_7 angle between the hoist rope and the horizontal line in point A

α_6 angle of F_{Sheave} and the vertical line

α_3 angle between the hoist rope and the dipper handle

α_5 angle between the dipper handle and the vertical line

α_4 angle between the boom and the suspension cable

δ angle between the hoist rope and the sheave with respect to vertical line in point A

$u_A(t)$ armature supply voltage of the DC motor

$i_A(t)$ armature current of the DC motor

$\omega_m(t)$ angular speed of the DC motor

τ_{Boom} boom torque (Equal to τ_2)

L_B boom length

$o_0 x_0 y_0 z_0$ coordinate frame of the swing revolute joint

$o_1 x_1 y_1 z_1$ coordinate frame of the boom revolute joint

$o_2 x_2 y_2 z_2$ coordinate frame of the saddle block revolute joint

$o_3 x_3 y_3 z_3$ coordinate frame of the crowd prismatic joint

$o_4 x_4 y_4 z_4$ coordinate frame of the end-effector

T_{04} coordinate transformation from the end-effector(bucket) frame to the base frame

$A_{i-1,i}$	coordinate transformation matrix from farm o_i to frame o_{i-1}
i_{CA}	crowd motor armature current
i_{CF}	crowd motor field current
K_C	coefficient function of the crowd motor torque coefficient and the crowd gear ratio
K_H	coefficient function of to the hoist motor torque coefficient, the hoist gear ratio, and the hoist drum radius
f_{c3}	Coulomb friction of joint 2
f_{c4}	Coulomb friction of joint 3
f_C	Coulomb friction matrix
A_{Hoist}	cross section area of the hoist cable
$C(q)$	Christoffel Symbol Matrix
c_i	$Cos\theta_i\ (i = 1, 2, 3)$
c_{23}	$Cos(\theta_2 + \theta_3)$
L_m	DC motor armature inductance
R_m	DC motor armature resistance
K_m	DC motor torque constant as well as the back electromotive force constant
J_m	inertia of the DC motor
f_{vm}	DC motor viscous friction coefficient
f_{cm}	DC motor coulomb friction coefficient
T_{mLoad}	DC motor instantaneous load torque
L_{af}	DC motor field-armature mutual inductance
$i_f(t)$	DC motor field current
L_{BS}	distance from the saddle block to the sheave
l_{SD}	distance from the sheave to the center of the dipper
X_{Drum}	displacement of the hoist cable in point A

X_{Hoist}	displacement of the hoist cable in point D
F_{Drum}	force applied by drum to the hoist rope at point A
F_B	force applied by the hoist rope to the sheave at point B
F_C	force applied by the sheave hoist rope to the hoist rope at point C
F_{Hoist}	force applied by the hoist rope to the dipper at point D
F_{Sheave}	force applied by the sheave to the boom
F_{SC}	force applied by the suspension cable to the boom
F_4	force exerted to the dipper handle by the prismatic joint
F_{Crowd}	force exerted to the dipper handle by the crowd motor
F_{Hoist}	force exert to the dipper by the hoist rope
F_{load}	force exerted by the end-effector on external objects or the payload
τ_{FS}	friction between the sheave and the hoist cables
$G(q)$	gravity vector
L_{AB}	hoist cable length from drum to sheave (Point A to Point B)
L_{CD}	hoist cable length from sheave to the dipper (Point C to Point D)
M_{AB}	hoist cable weight from drum to sheave (Point A to Point B)
M_{CD}	hoist cable weight from sheave to the dipper (Point C to Point D)
F_{Hx}	horizontal force applied to the dipper by the hoist rope
i_{HA}	hoist motor armature currents
i_{HA_1}	hoist motor #1 armature current
i_{HA_2}	hoist motor #2 armature current
i_{HF}	hoist motor field currents
l_{laser}	length measured by laser sensor
d_i	linear displacement of prismatic joint i
a_i	length of link i
d_4	linear displacement of the crowd joint which corresponds to the linear

	movement of the dipper handle relative to the saddle block or the distance from the saddle block to the center of the dipper
M_i	mass of link i
I	moment of inertia
a_1	perpendicular distance from z_0 to z_1 (the length of link 1)
a_2	perpendicular distance from z_1 to z_2 (the length of link 2)
a_3	perpendicular distance from z_2 to z_3 (the length of link 3)
m_{Load}	payload inside the dipper
R_i^{i-1T}	rotation matrix from frame i into $i-1$ frame
r_S	radius of the sheave
I_S	rotational inertia of the sheave
F_{BX}	reaction force on the boom along horizontal line resulted by F_{SC} and $F_{Sheaves}$
F_{BY}	reaction force on the boom along vertical line resulted by F_{SC} and $F_{Sheaves}$
s_i	$Sin\theta_i \, (i = 1, 2, 3)$
s_{23}	$Sin(\theta_2 + \theta_3)$
τ_1	swing torque
i_{SA}	swing motor armature current
i_{SF}	swing motor field currents
$D(q)$	symmetric joint-space inertia matrix or manipulator inertia tensor
k_{SC}	spring coefficient of the suspension cable
γ_{Hoist}	spring modulus of the hoist cable
τ_3	torque exerted by revolute joint to the dipper handle
M_d	the total mass of the dipper and the dipper handle
L_{COGO}	the fixed perpendicular distance from the center of the gravity of the dipper and the dipper handle to the dipper bail
$\dot{\theta}_3$	the angular velocity of the saddle block joint

$\ddot{\theta}_3$	the angular acceleration of the saddle block joint
$\dot{d}_4$	the linear velocity of the crowd joint
$\ddot{d}_4$	the linear acceleration of the crowd joint
$\dot{r}_{cd}$	the linear velocity of the center of the dipper and the dipper handle
$\ddot{r}_{cd}$	the linear acceleration of the center of the dipper and the dipper handle
I_3	the inertia tensor of the COG of the dipper and the dipper handle
I_{ZZ3}	the moment of inertia of the COG of the dipper and the dipper handle around z_2 axis when the object is rotated around z_2 axis
ω_i^i	the angular velocity of link i in frame i
$\dot{\omega}_i^i$	the angular acceleration of link i in frame i
$\ddot{q}_{C_i}^i$	the linear acceleration of the center of mass of link i in frame i
$\ddot{q}_i^i$	the linear acceleration of the origin of frame i in frame i
τ_i	torque of joint i
r_{cd}	vector from o_3 to the center of gravity of the dipper and the dipper handle
F_{Hy}	vertical force applied to the dipper by the hoist rope
f_{v3}	viscous friction of joint 2
f_{v4}	viscous friction of joint 3
$r_{i-1,i}^i$	vector from origin of frame $i-1$ to origin of frame i
r_{i,C_i}^i	vector from the origin of frame i to the center of mass C_i
q	vector of the generalized joint coordinate describing the pose of the manipulator
$\dot{q}$	vector of joint velocities
$\ddot{q}$	vector of joint accelerations
f_V	viscous friction matrix

τ vector of generalized forces (including torques)

ρ_{Hoist} weight per unit length of the hoist rope

3DOFOT   3 Degree of Freedom Orientation Tracker

ACKNOWLEDGEMENTS

DEDICATION

To

My parents Monir and Mohammad,

My wife Marjan

and

My daughter Atlasi

1 INTRODUCTION

1.1   Introduction and Motivation

In open-pit mining, very large machines are used to load and transfer material. Cable shovels, with a maximum dipper capacity of 120 tonnes per scoop, load massive dump trucks with raw material.   These dump trucks, with a maximum capacity of about 400 tonnes, transport the material to the crusher and the downstream processing plant.

Overloading these dump trucks lessens their engine and tire life and may damage the truck frames. Overloading causes fatigue and early failure which consequently results in excessive maintenance costs. In the lack of a weight measurement system, the shovel operator estimates the weight of material in the dump truck based on its volume. For this reason, the trucks are normally underloaded in order to avoid problems associated with overloading. However, underloading may also result in a significant loss in production. Therefore, underweight and overweight payloads in dump trucks potentially cause lost production, labour inefficiency, reduced engine and tire life, truck frame damage, and excessive truck component wear [1, 2]. Studies show that an accurate cable shovel payload monitoring system can approximately save 10% of the mining cost for each dump truck [1-5].

Commercial payload monitoring systems have been developed to determine the payload inside the cable shovel dipper before unloading to the dump truck. These systems estimate the net weight based on the motor dynamics, the known cable shovel geometry, and the known tare weight. The performance of such measurement systems have reported to have 10% error in the estimation of the payload that is not acceptable [1- 5]. A main factor contributing to these errors is that the existing payload monitoring systems do not effectively model the complex dynamic operation of such equipment. In addition, these systems do not compensate the environmental effects on the equipment, such as temperature and altitude of mine where the shovel is located. Load-sensing pin is recently used to sense the payload inside the dipper [5]. Using load-sensing pin requires mechanical modification on the shovel sheave or the dipper bail. Besides, load-sensing pin only sense the hoist rope forces and ignore the force generates by the crowd motor.

Last but not least, load-sensing pin is functional for sensing the payload when the dipper is motionless. In order to be effective, a measurement system has to be capable of accurately and repeatedly performing measurements within a small error even when the dipper moves. For example an acceptable error is within ±2% [1-5]. Otherwise, the problems of overloading and underloading would persist.

Weighing the load onboard each dump truck as a substitute for the excavator payload monitoring system is a regular production monitoring method. The majority of the dump trucks employed in mining come with a payload monitoring equipment onboard, as standard equipment. However, these onboard systems inherently have an error of approximately 10% and, in order to achieve this accuracy, a truck must be completely motionless on a horizontal loading surface. These dump truck payload monitoring systems estimate the amount of material loaded on the truck tray by sensing pressure on the truck suspension. A major weighing error in these onboard monitoring systems may be generated due to a loss of suspension pressure as a result of oil leakage from the truck's suspension. Shock-loading of the pressure sensors reduces their service life and adds to the already considerable cost of maintenance of these truck weighing systems. Electric shovels, by contrast, weigh using electrical measurements from motors and motion sensors. The cables carrying these signals are located in cable trays in the protected housing of the shovel. Another advantage of cable shovel based payload monitoring system is that a typical mine has a 4:1 ratio of dump trucks to shovels. Hence, fewer systems are needed for installation and maintenance. Furthermore, since the shovel operator is the main person controlling the load dumped on the truck, it makes sense to display the dynamic payload weight directly to the shovel operator so that proper adjustments can be made on the fly to optimize loaded material on the truck tray. Cable shovels also must be protected against overloading. Depending on the density of the material being excavated by the shovel and how the ground has been blasted, cable shovels may execute excessive force when digging. If the dipper cutting force and payload frequently exceed the fatigue threshold specified by the hoist rope manufacturer the hoist rope will break. Breakage of the hoist rope can cause a significant impact in the operations of the mine. Replacing a broken hoist rope takes approximately two days if the replacement is available on site. Due to the fundamental job of the cable shovel in a mine,

it has been estimated that the cost of one hour of shovel downtime is $200,000 while the hourly downtime cost of a dump truck is $50,000.

1.2 Observation, Machine Specification and Summary of Payload Monitoring System

Figure 1 illustrates the various key components of a typical cable shovel. The dipper is suspended from the hoist rope, which is connected to a hoist drum, which is mounted on the machinery deck. Consequently, rotation of the hoist drum lowers or elevates the dipper. The hoist drum is coupled to two, identical fast-response DC motors through a double-reduction gear. The dipper is also supported by an arm called the crowd arm or the dipper handle.
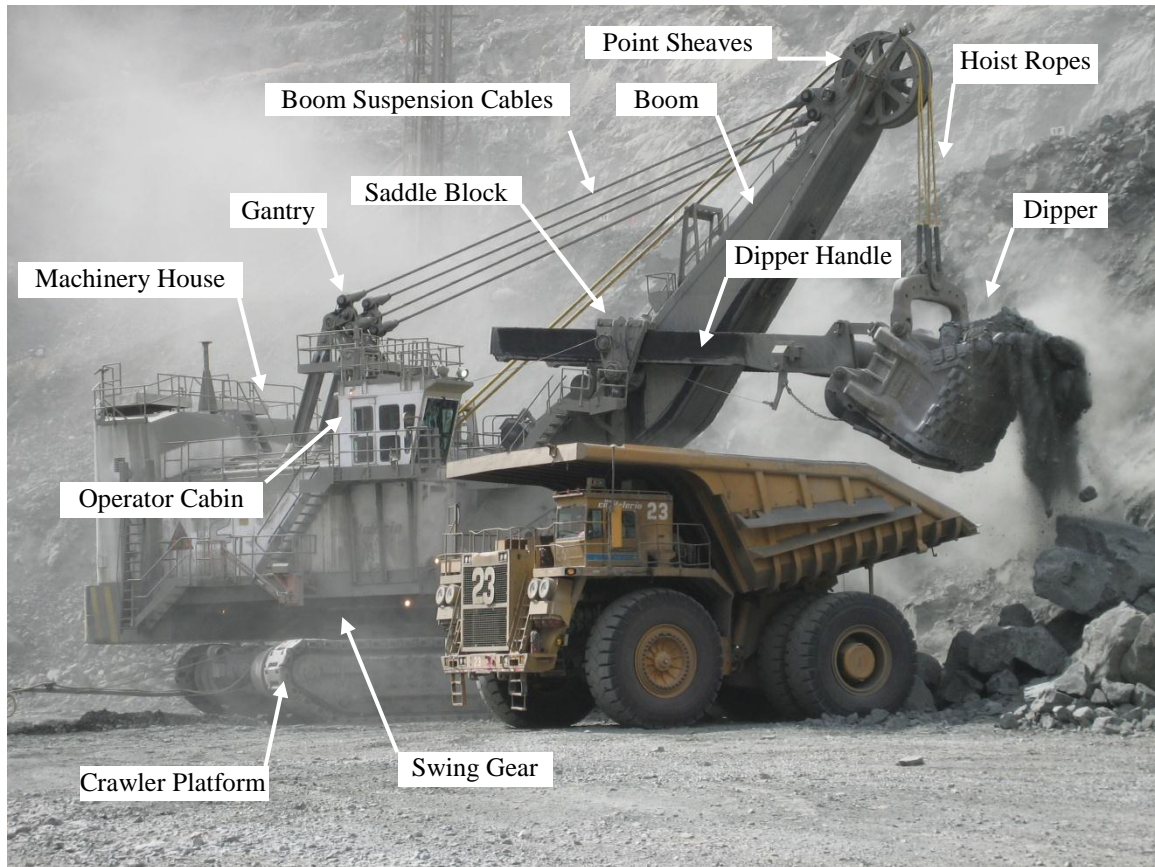
Figure 1: Key components of a typical P&H cable shovel

The attachment of the dipper handle to the boom is secured by the saddle block. The saddle block limits the dipper handle to only forward or backward movement. The hoist cable allows both the saddle block and the dipper handle to pivot freely. To control lateral

movement of the dipper arm in the saddle block, the dipper arm is slotted in a rack and pinion gear. This engages a drive pinion mounted in the saddle block. The drive pinion is actuated by an electric motor, crowd, that causes the extension or retraction of the dipper arm relative to the saddle block. Hence, the digging force is generated by both the hoist rope and the crowd motor. Alternating current (AC) is supplied to the shovel through a tail cable, which is connected to the electrical distribution system of the mine through a switch house. The crowd, the hoist, and the swing motors are all driven independently by their own motor controllers. The drive technology used in the P&H cable shovel is a DC motor connected to phase-controlled thyristor rectifiers [6-10]. The motors are all separately excited DC motors built in ratings up to 2000 horsepower. The core of power control for the motors is a bank of four-quadrant thyristor converters. These rectify a three-phase AC waveform to DC at the required voltage. A six-pulse thyristor bridge feeds the field of the DC motors. Based on our field trail, the crowd and swing motors both have a nominally fixed field current. However, the hoist field current has two different fixed values during hoisting and lowering. The boom suspension cables, which connect the upper portion of the boom to the stay structure, are under tension at all operating conditions. The lengths of these cables partially vary depending on the dipper position and the load on the dipper and consequently the angle of boom will change accordingly.

Figure 2 represents a block diagram of the proposed indirect payload monitoring system. The cable shovel dynamic payload monitoring system measures the swing, crowd, and hoist motor currents and then estimates actuator torques and forces required by the cable shovel. Joint variable sensors measure the swing angle, the dipper angle, and the crowd extension length. Dynamic payload monitoring is performed using the kinematic and the simplified dynamic equations of the cable shovel. The following parameters can also be calculated: the digging cycle, the cutting force, the swing-loaded and swing-empty time segment of the loading cycle, and so on. The shovel parameters are either not available or they vary with temperature and other factors. As a result, these cable shovel parameters must be estimated.
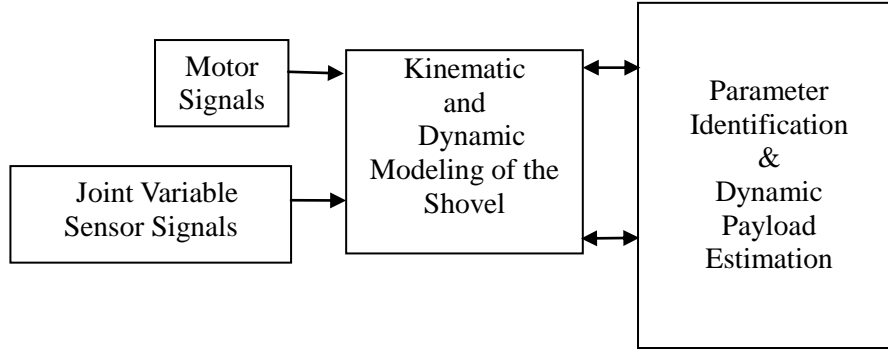
Figure 2: Block diagram of the proposed payload monitoring system

1.3 Thesis Objectives

The major objectives of the thesis are:

1. To build a dynamic model of a cable shovel that accurately simulates various factors including DC motors, inertia, Coriolis-effect, centripetal forces, gravity, and spring effect of the cables, and friction.

2. To formulate a linear relationship between the currents driving the cable shovel motor and the generalized forces applied to its joints.

3. To identify cable shovel parameters using the least-squares estimation technique.

4. To establish the relationship between sensed motor currents and joint variables, and the payload weight inside the shovel dipper using the experimentally identified linearized shovel model.

5. To devise an innovative non-contact method of sensing the geometry of the cable shovel arm and bucket.

6. To experimentally demonstrate the accuracy and repeatability of the arm geometry sensing apparatus and the payload estimation algorithm.

1.4 Literature Review

In this section, I review related work in the area of the dynamic modeling of cables shovels. I also discuss parameter identification of robot dynamics and DC motors, and the

cable shovel arm geometry sensing.

1.4.1   Cable Shovel Dynamic Modeling

Many researchers have investigated robotic excavation in recent years.   Most of this work is limited to the discussion of hydraulically driven equipment, similar in design to a conventional backhoe excavator or front-end-loader. A series of rotational joints are used in typical hydraulic excavators to actuate the boom, the stick, and bucket. In contrast, cable shovels (also known as electric rope shovel) operate differently and are substantially larger. Typically a cable shovel employs a mechanical system consisting of one rotational and one sliding joint to actuate its dipper. Cable shovels also generally have limited on-board sensing, typically, encoders on drive motors, and motor current and voltage sensors.

A number of authors have investigated cable shovels.   These researchers have focused mainly on the mine 'diggability' [11-19], collision avoidance [10, 20-28], enhanced energy efficiency and productivity [14, 16, 29-34], and autonomous excavation [11, 30, 35, 36].

A significant body of relevant work was conducted at the University of Alberta by Frimpong et al. [11-19] in recent years. They have developed a dynamic cable shovel model by analyzing the main functional components (the dipper handle and the dipper) employing an iterative Newton-Euler method. The model includes the main terms that influence the performance of a cable shovel, such as the linear and the angular motions of dipper handle and dipper. Based on the dynamic model, Frimpong et al. have identified that the material properties to be excavated, the geometrical and physical properties of the dipper handle and dipper, as well as the digging strategies are the main factors that determine the required crowd and hoist forces which determine the performance of a cable shovel. The rotation of the upper structure was not modeled in their work. Furthermore, formulation of the dynamic model presented by Frimpong et al. depends on precise knowledge of various kinematic and dynamic parameters which characterize a particular cable shovel and must be obtained from the shovel specifications provided by manufacturers.

Cork [35] used data derived from motor current sensors to detect dipper fullness. His

6

method was based on estimating the force applied at the dipper teeth. This calculation was based on sensing motor currents and was resolved into a Cartesian velocity, using the kinematic equations of the shovel.

Hendricks et al. [37] developed a dynamic model for cable shovels using Euller-Lagrange formulation without including the resistive external forces from the mine environments. Daneshmend et al. [38] dealt with the same problem using an iterative Newton-Euler formulation. However that work did not include the dipper handle crowd, which is very important for a complete description of the dynamic behavior of a cable shovel .

McAree et al. [3, 4, 39] have modeled a cable shovel as a manipulator with three degrees of freedom considering the swing revolute joint, the dipper revolute joint, and the dipper handle prismatic joint. However, they have assumed the boom angle is fixed, the hoist-rope is without mass, and that the boom suspension cable and the hoist-rope are inextensible. The cable shovel manufacturer (P&H) has provided various cable shovel parameters such as dimensions, masses, inertias and motor parameters for McAree to use.

In this thesis, the P&H cable shovel is treated as a robotic manipulator with three revolute and one prismatic joint: the cab swing angle θ_1, the boom joint angle θ_2, the saddle block joint angle θ_3, and the crowd joint displacement d_4 which corresponds to the linear movement of the dipper handle relative to the saddle block. This thesis will investigate for the first time the effect of the following mechanisms:

- the variation in the dipper-handle length caused by its rotation
- the point-sheave torque and hoist-cable torque on the torque of the boom
- the suspension cable-spring

1.4.2   Parameter Identification of Robot Dynamics

Experimental identification of the robot dynamics has been studied by many researchers for the past 25 years [40-46]. The rigid-body dynamics of a manipulator can be transformed to one that is linear in its parameters and thus allows the application of a linear least-squares estimation (LSE) [42, 43, 47-50]. However, knowledge of the inertial parameters of the robot manipulators is required for any modeling of advanced

control algorithms and robot-dynamics. These parameters can be estimated using the manipulator joint torques and forces along with the manipulator joint variables. Unfortunately the cable shovels are not equipped with joint force/torque sensors, and consequently they need to be derived from motor currents. The main shortcoming with this method is that the joint torque/force estimation accuracy is limited by unmodeled joint friction and actuator dynamics.

Since the cable shovel manufacturer does not provide accurate information regarding the modelling parameters of the cable shovel, I must establish a reliable method for generating a precise model of the cable shovel. The cable shovel model depends upon knowing the inertia, mass and center of mass of each link but, as the number of parameters increase with the number of degree of freedom (DOF), the model also increases in complexity. This involves much more computational work.

The link parameters that require estimation are:

- Mass

- Inertia tensor

- Center of mass

- Friction parameters

Tafazoli et al. [42] estimated the gravitational parameters of a mini-excavator from static measurements . They considered the differences between adjacent joint-torques in order to decouple the estimation problem and improve their modeling accuracy. They also determined the nonlinear dynamic equation of the mini-excavator assuming a plane open-kinematic chain for the three links that form the excavator arm. Next, they regrouped the dynamic equations to derive a set of parameters that linearize the equations. A similar approach is proposed in this thesis for the first time for cable shovels.

Liu [40] used a base-mounted force-and-torque sensor to statically estimate the mass of a manipulator. This manipulator is mounted on a force sensor with six-degrees-of-freedom. The reaction forces and moments at its base can be measured at different manipulator-positions and base-orientations. While this method is effective for some applications, it still cannot estimate all of the inertial properties of the manipulator.

As stated earlier, to identify the cable shovel parameters and to estimate the payload

in the cable shovel dipper I require measuring the hoist torque, the crowd force, and the swings torque. Installation of a torque meter on the cable shovel motor is difficult and requires considerable retrofitting and mechanical modification.

Because of the difficulty in installing torque sensors in cable shovels, I must use an indirect method and calculate the torque from the DC motor signals. This implies that the torque cannot be obtained from deflection of the motor shaft but must be derived from various motor signals, such as current, voltage, and motor speed.

Meester [51] designed a microcomputer-controlled torque-calculator that used an indirect method for torque measurement on DC motor drives. The device calculates torque from voltage, current, and speed signals, as well as using some stored motor parameters and characteristics. Such values of parameters and characteristics for the cable shovel DC motors are not available. Therefore, Messter's technique is not practical for our application.

Habbadi [52] presented a mathematical development of the new identification approach based upon the parametric drive model and on the prior knowledge of the time variation of the drive velocity, current, and the supply voltage of the DC motor. This approach can be accomplished only when the shovel drives are working normally or, at specific instant during unloading when the motion has a known velocity profile and the dipper is empty. The major drawback to this approach for the identification of the cable shovel motor parameters is that this procedure should run while there is no load on the motor shaft.

In this thesis I identify various cable shovel parameters, motor torque coefficients, and joint frictions. These have been derived from the relevant variables logged during the normal operation of the cable shovel. I also make an estimate of the generated joint-torque. A major advantage here is that I do not need to obtain any information from the shovel manufacturer in order to build a dynamic model of the cable shovel or estimate its payload. As the result, our payload monitoring system can adapt itself to variations in the environment that otherwise might alter the cable shovel parameters or alter the motor characteristics. Moreover, in order to measure these parameters, I will not interrupt the operation of the cable shovel.

1.4.3 Cable Shovel Arm Geometry and Joint Variable Extraction

The enormous size of these shovels limits the operator's vision and this limitation causes injuries in some mines. In recent years several studies that recommended more efficient techniques for monitoring the precise position of the dipper shovels [20-22, 24, 25, 36, 53, 54] have been performed. Ghassemi et al. [55-57] used two biaxial accelerometers to estimate each joint angle in hydraulic shovels. The approach is capable only of sensing roll and pitch angles and cannot measure the yaw or swing angle. Furthermore, two accelerometers must be installed in separate locations on the shovel to measure just one angle. Because of the shovel size, positioning several sensors which must include wiring on different parts of the cable shovel will be quite difficult. Even if the technique was adopted for the cable shovel, it will not be able to sense the crowd extension either. Hence, two additional sensors will be needed for swing and crowd length measurement.

Roberts et al. [36] used a two dimension laser-scanner to create a 3D digital terrain map for large excavators. Kashani et al. [20, 22] used a 2D laser-scanner on hydraulic shovels and cable shovels that assist in bucket steering or 'localizing' and aids in the control of the shovel arm-geometry. Lin [24, 25] utilized a stereo vision camera to estimate the cab swing angle in P&H cable shovels in an outdoor lighting environment. These techniques are slow and require a relatively powerful CPU. Unfortunately, sunlight and dust, which are present at all mining environments, may degrade accuracy and performance of the laser device.

This thesis presents a novel approach to the non-contact sensing of the arm geometry of the cable shovel and to determine the exact coordinates of the bucket position. Just one AGS apparatus is needed to measure all of the cable shovel joint variables. In our proposed sensor apparatus, only one cable is required to transfer the sensor data to the operator's cabin. The apparatus is comprised of an advanced dynamic 3D orientation sensor and one laser sensor. This apparatus is able to measure each of the cable shovel joint variable indirectly, without having any physical contact with the joint or links. The sensor is robust to cable shovel vibration and the harsh mining environment. Furthermore, the installation of our proposed AGS apparatus does not require any mechanical modification to the existing cable shovel and can be accomplished in approximately one hour. The response time of the sensor is only 20 milliseconds, which

is adequate for our application as demonstrated experimentally later.

2   CABLE SHOVEL DYNAMIC MODELING

2.1   Introduction

The kinematic and dynamic equations of P&H type cable shovel are developed in this chapter.   An iterative Newton-Euler technique is used to develop the dynamic equations. These equations relate the joint and motor torques to cable shovel joint variables using various cable shovel parameters. The following are presented in this chapter for the first time:

- the effect of variation in the dipper handle length caused by its rotation
- the effect of the point sheave torque and hoist cable torque on the torque of the boom
- the suspension cable spring effect
- the hoist cable spring effect

2.2   Kinematics of the Cable Shovel

The Denavit-Hartenberg (DH) convention is used here to determine kinematic equations of the cable shovel [48-50]. This convention is widely used in robotics for open kinematic chains.

The P&H cable shovel is indeed a robotic manipulator, with three revolute and one prismatic joint. Its joint variables are:

- the cab swing angle θ_1
- the boom joint angle θ_2
- the saddle block or the dipper joint-angle θ_3
- the crowd joint displacement d_4, that corresponds to the linear movement of the dipper handle relative to the saddle block

It is important to remember that the boom joint angle corresponds to a passive joint with very limited range of motion. Note that this boom is attached to the shovel body by the boom suspension cables. Because of the elasticity of the suspension cables the boom has

some limited movements during the shovel operation specially during digging and when the dipper is full.

Figure 3 represents the cable shovel DH coordinate frame assignments and the joint variables. Figure 4 represents a simplified model of the cable shovel. Table 1 represents the DH parameters of the shovel.

First, let us assume the cable-shovel is located on a flat, level surface. Assuming the cable shovel as a series of links, with a frame rigidly attached to each link, we can express the location and orientation of the bucket or the end-effecter (frame Fr_4) with respect to the base frame Fr_0 as [48, 50]:

$$T_{04} = A_{01}(\theta_1)A_{12}(\theta_2)A_{23}(\theta_3)A_{34}(d_4) \tag{1}$$

Where A_{ij} are the homogenous transformations that represent the translation and rotation of the frame j with respect to the frame i, θ_i and d_i are the joint variables associated with the motion of the link i with respect to the link $i-1$, and $i=1,2,3,4$.
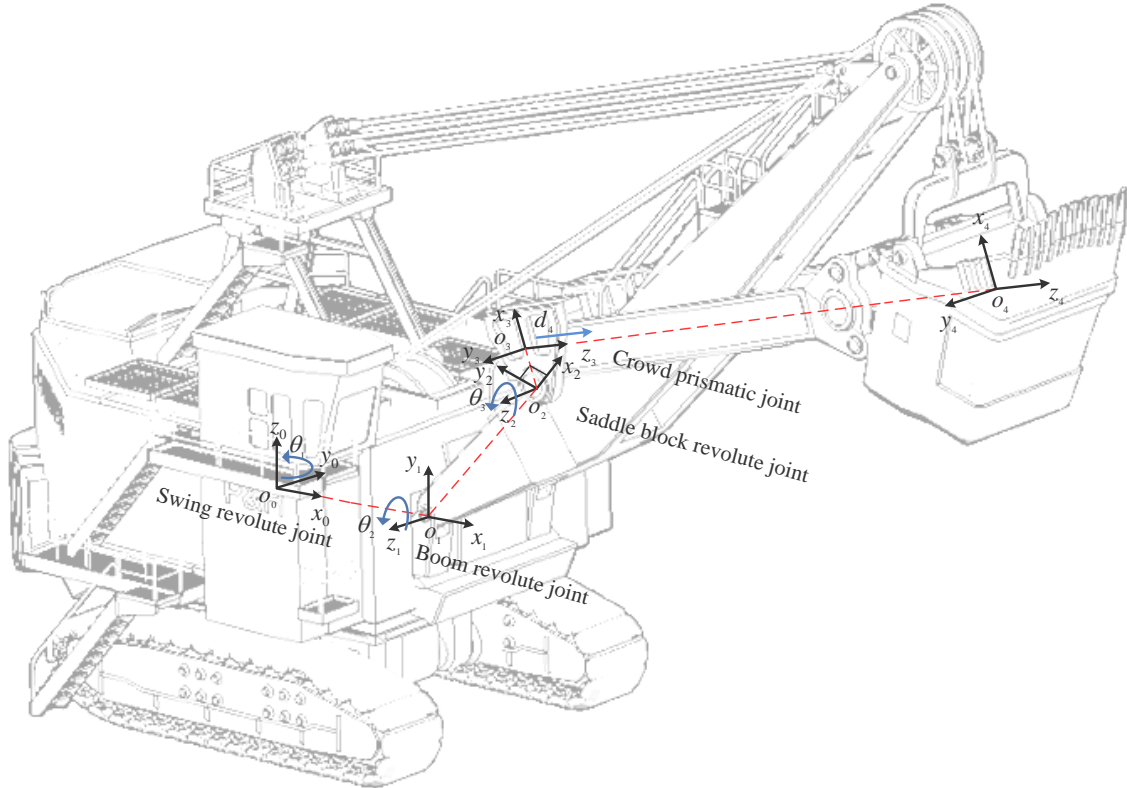
Figure 3: P&H cable shovel schematics identifying the DH coordinate frame assignments joint variables

13
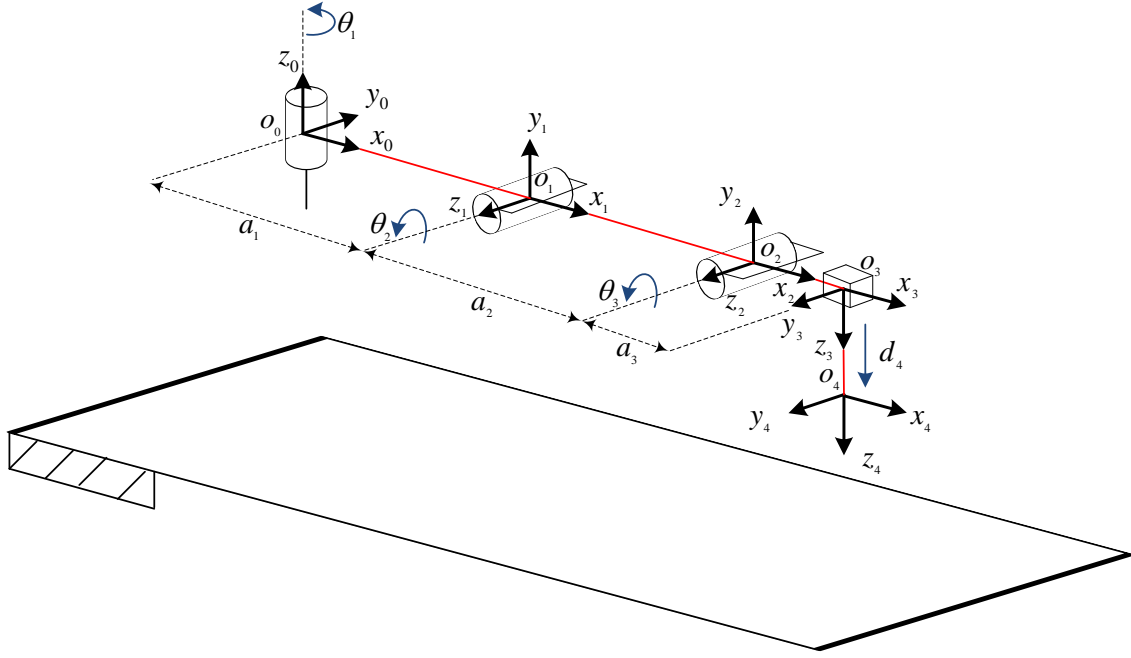
Figure 4: Conventional representations of the joints and the links of the cable shovel

Table 1: DH parameter table for a 4 DOF cable shovel

Parameter Joint number	θ_i	d_i	a_i	α_i
J_1	θ_1	0	a_1	$\dfrac{\pi}{2}$
J_2	θ_2	0	a_2	0
J_3	θ_3	0	a_3	$\dfrac{\pi}{2}$
J_4	0	d_4	0	0

Joint homogeneous transformation matrixes are as follow:

$$
A_{01} = \begin{bmatrix} c_1 & 0 & s_1 & a_1 c_1 \\ s_1 & 0 & -c_1 & a_1 s_1 \\ 0 & 1 & 0 & 0 \\ 0 & 0 & 0 & 1 \end{bmatrix} , \quad A_{12} = \begin{bmatrix} c_2 & -s_2 & 0 & a_2 c_2 \\ s_2 & c_2 & 0 & a_2 s_2 \\ 0 & 0 & 1 & 0 \\ 0 & 0 & 0 & 1 \end{bmatrix} , \quad A_{23} = \begin{bmatrix} c_3 & 0 & s_3 & a_3 c_3 \\ s_3 & 0 & -c_3 & a_3 s_3 \\ 0 & 1 & 0 & 0 \\ 0 & 0 & 0 & 1 \end{bmatrix}
$$

$$
A_{34} = \begin{bmatrix} 1 & 0 & 0 & 0 \\ 0 & 1 & 0 & 0 \\ 0 & 0 & 1 & d_4 \\ 0 & 0 & 0 & 1 \end{bmatrix} \tag{1}
$$

Hence, the transformation from the frame 4 back to the base frame can be represented as follows:

$$
T_{04} = \begin{bmatrix} c_1 c_{23} & s_1 & c_1 s_{23} & c_1 s_{23} d_4 + c_1 c_{23} a_3 + c_1 c_2 a_2 + c_1 a_1 \\ s_1 c_{23} & -c_1 & s_1 s_{23} & s_1 s_{23} d_4 + s_1 c_{23} a_3 + s_1 c_2 a_2 + s_1 a_1 \\ s_{23} & 0 & -c_{23} & -c_{23} d_4 + s_{23} a_3 + a_2 s_2 \\ 0 & 0 & 0 & 1 \end{bmatrix} \tag{2}
$$

Where s_i, c_i, s_{23}, and c_{23} represent $Sin\theta_i$, $Cos\theta_i$, $Sin(\theta_2 + \theta_3)$, and $Cos(\theta_2 + \theta_3)$, respectively.

2.3   Dynamic Analysis

An effective dynamic model of a manipulator will create a relationship between the actuator forces (and torques) and the joint variables (i.e., joint angles and displacements). A dynamic model of the cable shovel can be useful for:

- simulating its motion
- analyzing the cable shovel structure
- implementing payload and cutting(digging) force monitoring algorithms

- implementing advanced collision avoidance algorithm, and

- designing advanced closed-loop trajectory control algorithms

There are two classical approaches to dynamic modeling of open kinematic chain (serial) manipulators: the Euler-Lagrange, and the Newton-Euler. The Euler-Lagrange formulation is energy based and conceptually simple and systematic to derive. Newton-Euler formulation is based on a recursive algorithm to derive the model and is computationally more efficient since it exploits the typically open structure of the manipulator kinematic chain [48-50].

The Recursive Newton-Euler approach (RNE) [48-50] is performed by first stepping forward through the chain of links to compute the kinematic parameters of the links (i.e. velocity, angular velocity, acceleration & angular acceleration) and then stepping backwards through the links and using Newton's Second Law $F = ma$, and Eulers equations $\tau = I\alpha$, to compute the joint torques, where m is the mass, a is the linear acceleration, I is the moment of inertia, and α is the angular acceleration. The cable shovel structure can be considered a 4DOF serial manipulator when the hoist cables can be replaced with an imaging rotary actuator. It is also important to note that the boom joint is indeed a passive joint. The resulting dynamic equations for our 4DOF manipulator is given by:

Forward chain for 1 to 4:

The base frame is fixed, therefore:

$$\omega_0^0 = \begin{bmatrix} 0 & 0 & 0 \end{bmatrix} \tag{3}$$

$$\dot{\omega}_0^0 = \begin{bmatrix} 0 & 0 & 0 \end{bmatrix} \tag{4}$$

$$\ddot{q}_0^0 = \begin{bmatrix} 0 & 0 & g \end{bmatrix} \tag{5}$$

These vectors are the initial conditions for the velocities and acceleration, and g is the gravitational constant.

$$\omega_1^1 = \begin{bmatrix} 0 & \dot{\theta}_1 & 0 \end{bmatrix} \tag{6}$$

$$\dot{\omega}_1^1 = \begin{bmatrix} 0 & \ddot{\theta}_1 & 0 \end{bmatrix} \tag{7}$$

$$\ddot{q}_1^1 = \begin{bmatrix} -\dot{\theta}_1^2 a_1 & g & -\ddot{\theta}_1 a_1 \end{bmatrix} \tag{8}$$

$$\ddot{q}_{c1}^1 = \begin{bmatrix} (-\dot{\theta}_1^2 a_1 - \dot{\theta}_1^2 a_1 r_{c1}) & g & (-\ddot{\theta}_1 a_1 - \ddot{\theta}_1 a_1 r_{c1}) \end{bmatrix} \tag{9}$$

$$\omega_2^2 = \begin{bmatrix} \dot{\theta}_1 s_2 & \dot{\theta}_1 c_2 & \dot{\theta}_2 \end{bmatrix} \tag{10}$$

$$\dot{\omega}_2^2 = \begin{bmatrix} (\ddot{\theta}_1 s_2 + c_2 \dot{\theta}_2 \dot{\theta}_1) & (\ddot{\theta}_1 c_2 - s_2 \dot{\theta}_2 \dot{\theta}_1) & \ddot{\theta}_2 \end{bmatrix} \tag{11}$$

$$\ddot{q}_2^2 = \begin{bmatrix} s_2 g - c_2 \dot{\theta}_1^2 a_1 - \dot{\theta}_1^2 c_2^2 a_2 - \dot{\theta}_2^2 a_2 \\ c_2 g + s_2 \dot{\theta}_1^2 a_1 + s_2 \dot{\theta}_1^2 c_2 a_2 + \ddot{\theta}_2 a_2 \\ a_2(\ddot{\theta}_1 c_2 - 2 s_2 \dot{\theta}_2 \dot{\theta}_1) - \ddot{\theta}_1 a_1 \end{bmatrix}^T \tag{12}$$

$$\ddot{q}_{c2}^2 = \begin{bmatrix} s_2 g - c_2 \dot{\theta}_1^2 a_1 - \dot{\theta}_1^2 c_2^2 a_2 - \dot{\theta}_2^2 a_2 - r_{c2}(\dot{\theta}_1^2 c_2^2 + \dot{\theta}_2^2) \\ c_2 g + s_2 \dot{\theta}_1^2 a_1 + s_2 \dot{\theta}_1^2 c_2 a_2 + \ddot{\theta}_2 a_2 + r_{c2}(s_2 \dot{\theta}_1^2 c_2 a_2 + \ddot{\theta}_2) \\ a_2(\ddot{\theta}_1 c_2 - 2 s_2 \dot{\theta}_2 \dot{\theta}_1) - \ddot{\theta}_1 a_1 - r_{c2}(\ddot{\theta}_1 c_2 - 2 s_2 \dot{\theta}_2 \dot{\theta}_1) \end{bmatrix}^T \tag{13}$$

$$\omega_3^3 = \begin{bmatrix} \dot{\theta}_1 s_{23} & \dot{\theta}_{23} & -c_{23} \dot{\theta}_1 \end{bmatrix} \tag{14}$$

$$\dot{\omega}_3^3 = \begin{bmatrix} (\ddot{\theta}_1 s_{23} + \dot{\theta}_1 s_{23}) & \ddot{\theta}_{23} & (\ddot{\theta}_1 s_{23} - \dot{\theta}_1 c_{23}) \end{bmatrix} \tag{15}$$

17

$$\ddot{q}_3^{\,3} = \begin{bmatrix} \alpha_1 & \beta_1 & \delta_1 \end{bmatrix} \tag{16}$$

Where:

$$\alpha_1 = c_3(s_2 g - c_2\,\dot{\theta}_1^2\,a_1 - \dot{\theta}_1\,c_2{}^2 a_2 - \dot{\theta}_2^2\,a_2) + s_3(c_2 g + s_2\,\dot{\theta}_1^2\,a_1 + s_2\,\dot{\theta}_1\,c_2 a_2 + \ddot{\theta}_2\,a_2)$$
$$- a_3\,\dot{\theta}_{23}^2 + (c_{23}\,\dot{\theta}_1)^2 a_3$$

$$\beta_1 = a_2(-\ddot{\theta}_1\,c_2 + s_2\,\dot{\theta}_2\,\dot{\theta}_1) - \ddot{\theta}_1\,a_1 + a_2 s_2\,\dot{\theta}_2\,\dot{\theta}_1 + a_3[s_3(c_2\,\dot{\theta}_2\,\dot{\theta}_1 + s_2\,\dot{\theta}_1^2 + c_2\,\dot{\theta}_3\,\dot{\theta}_1)$$
$$- c_3(c_2\,\dot{\theta}_1 - s_2\,\dot{\theta}_3\,\dot{\theta}_1 - s_2\,\dot{\theta}_2\,\dot{\theta}_1)] + a_3\,\ddot{\theta}_{23} + s_{23}\,\dot{\theta}_1$$

$$\delta_1 = s_3(s_2 g - c_2\,\dot{\theta}_1^2\,a_1 - \dot{\theta}_1\,c_2{}^2 a_2 - a_2\,\ddot{\theta}_2) - c_3(c_2 g + s_2\,\dot{\theta}_1^2\,a_1 + s_2\,\dot{\theta}_1\,c_2 a_2 + \ddot{\theta}_2\,a_2)$$
$$- a_3\,\ddot{\theta}_{23} - a_3 s_{23}\,\dot{\theta}_1^2\,c_{23}$$

$$\ddot{q}_{c3}^{\,3} = \begin{bmatrix} \alpha_2 & \beta_2 & \delta_2 \end{bmatrix} \tag{17}$$

Where:

$$\alpha_2 = c_3(s_2 g - c_2\,\dot{\theta}_1^2\,a_1 - \dot{\theta}_1\,c_2{}^2 a_2 - \dot{\theta}_2^2\,a_2) + s_3(c_2 g + s_2\,\dot{\theta}_1^2\,a_1 + s_2\,\dot{\theta}_1\,c_2 a_2 + \ddot{\theta}_2\,a_2)$$
$$- a_3\,\dot{\theta}_{23}^2 + (c_{23}\,\dot{\theta}_1)^2 a_3 - r_{c3}[\dot{\theta}_{23}^2 + (c_{23}\,\dot{\theta}_1)^2]$$

$$\beta_2 = a_2(-\ddot{\theta}_1\,c_2 + s_2\,\dot{\theta}_2\,\dot{\theta}_1) - \ddot{\theta}_1\,a_1 + a_2 s_2\,\dot{\theta}_2\,\dot{\theta}_1 + a_3[s_3(c_2\,\dot{\theta}_2\,\dot{\theta}_1 + s_2\,\dot{\theta}_1^2 + c_2\,\dot{\theta}_3\,\dot{\theta}_1)$$
$$- c_3(c_2\,\dot{\theta}_1 - s_2\,\dot{\theta}_3\,\dot{\theta}_1 - s_2\,\dot{\theta}_2\,\dot{\theta}_1)] + a_3\,\dot{\theta}_{23}\,s_{23}\,\dot{\theta}_1 + r_{c3}[s_3(c_2\,\dot{\theta}_2\,\dot{\theta}_1 + s_2\,\dot{\theta}_1^2 + c_2\,\dot{\theta}_3\,\dot{\theta}_1)$$
$$- c_3(c_2\,\dot{\theta}_1 - s_2\,\dot{\theta}_3\,\dot{\theta}_1 - s_2\,\dot{\theta}_2\,\dot{\theta}_1)] + r_{c3}\,\dot{\theta}_{23}\,s_{23}\,\dot{\theta}_1$$

$$\delta_2 = s_3(s_2 g - c_2\,\dot{\theta}_1^2\,a_1 - \dot{\theta}_1\,c_2{}^2 a_2 - a_2\,\ddot{\theta}_2) - c_3(c_2 g + s_2\,\dot{\theta}_1^2\,a_1 + s_2\,\dot{\theta}_1\,c_2 a_2 + \ddot{\theta}_2\,a_2)$$
$$- a_3\,\ddot{\theta}_{23} - a_3 s_{23}\,\dot{\theta}_1^2\,c_{23} - r_{c3}\,\ddot{\theta}_{23} - r_{c3} s_{23}\,\dot{\theta}_1^2\,c_{23}$$

$$\omega_4^4 = \left[\dot{\theta}_1 s_{23} \quad \dot{\theta}_{23} \quad -c_{23}\dot{\theta}_1 \right] \tag{18}$$

$$\dot{\omega}_4^4 = \left[(\ddot{\theta}_1 s_{23} + \dot{\theta}_1 c_{23}) \quad \ddot{\theta}_{23} \quad (\dot{\theta}_1 s_{23} - \ddot{\theta}_1 c_{23}) \right] \tag{19}$$

$$\ddot{q}_4^4 = \left[\alpha_3 \quad \beta_3 \quad \delta_3 \right] \tag{20}$$

Where:

$$\alpha_3 = c_3 (s_2 g - c_2 \dot{\theta}_1^2 a_1 - \dot{\theta}_1^2 c_2^2 a_2 - \dot{\theta}_2^2 a_2) + s_3 (c_2 g + s_2 \dot{\theta}_1^2 a_1 + s_2 \dot{\theta}_1^2 c_2 a_2 + \ddot{\theta}_2 a_2)$$
$$- a_3 \dot{\theta}_{23}^2 + (c_{23}\dot{\theta}_1)^2 a_3 + 2 d_4 \dot{\theta}_{23} + d_4 \ddot{\theta}_{23} - d_4 s_{23} \dot{\theta}_1^2 c_{23}$$

$$\beta_3 = a_2 (-\ddot{\theta}_1 c_2 + s_2 \dot{\theta}_2 \dot{\theta}_1) - \ddot{\theta}_1 a_1 + a_2 s_2 \dot{\theta}_2 \dot{\theta}_1 + a_3 [s_3 (c_2 \dot{\theta}_2 \dot{\theta}_1 + s_2 \dot{\theta}_1^2 + c_2 \dot{\theta}_3 \dot{\theta}_1)$$
$$- c_3 (c_2 \dot{\theta}_1^2 - s_2 \dot{\theta}_3 \dot{\theta}_1 - s_2 \dot{\theta}_2 \dot{\theta}_1)] + a_3 \dot{\theta}_{23} s_{23} \dot{\theta}_1 - 2 d_4 s_{23} \dot{\theta}_1 - d_4 \dot{\theta}_{23} \dot{\theta}_1^2 c_{23}$$
$$- d_4 [c_3 (c_2 \dot{\theta}_2 \dot{\theta}_1 + s_2 \dot{\theta}_1^2 + c_2 \dot{\theta}_3 \dot{\theta}_1) + s_3 (c_2 \dot{\theta}_1^2 - s_2 \dot{\theta}_3 \dot{\theta}_1 - s_2 \dot{\theta}_2 \dot{\theta}_1)]$$

$$\delta_3 = s_3 (s_2 g - c_2 \dot{\theta}_1^2 a_1 - \dot{\theta}_1^2 c_2^2 a_2 - a_2 \dot{\theta}_2^2) - c_3 (c_2 g + s_2 \dot{\theta}_1^2 a_1 + s_2 \dot{\theta}_1^2 c_2 a_2 + \ddot{\theta}_2 a_2)$$
$$- a_3 \ddot{\theta}_{23} - a_3 s_{23} \dot{\theta}_1^2 c_{23} + \ddot{d}_4 - d_4 (s_{23} \dot{\theta}_1)^2 - d_4 \dot{\theta}_{23}^2$$

$$\ddot{q}_{c4}^{\;4} = \begin{bmatrix} \alpha_4 & \beta_4 & \delta_4 \end{bmatrix}$$

Where:

$$\alpha_4 = c_3(s_2 g - c_2 \dot{\theta}_1^2 a_1 - \dot{\theta}_1^2 c_2{}^2 a_2 - \dot{\theta}_2^2 a_2) + s_3(c_2 g + s_2 \dot{\theta}_1^2 a_1 + s_2 \dot{\theta}_1^2 c_2 a_2 + \ddot{\theta}_2 a_2)$$
$$- a_3 \dot{\theta}_{23}^2 + (c_{23}\dot{\theta}_1)^2 a_3 + 2\dot{d}\,\dot{\theta}_{23} + d_4 \ddot{\theta}_{23}$$
$$- d_4 s_{23} \dot{\theta}_1^2 c_{23} + r_{c4}\ddot{\theta}_{23} - r_{c4} s_{23}\dot{\theta}_1^2 c_{23}$$

$$\beta_4 = a_2(-\ddot{\theta}_1 c_2 + s_2 \dot{\theta}_2 \dot{\theta}_1) - \ddot{\theta}_1 a_1 + a_2 s_2 \dot{\theta}_2 \dot{\theta}_1 + a_3[s_3(c_2 \dot{\theta}_2 \dot{\theta}_1 + s_2 \dot{\theta}_1^2 + c_2 \dot{\theta}_3 \dot{\theta}_1)$$
$$- c_3(c_2 \dot{\theta}_1 - s_2 \dot{\theta}_3 \dot{\theta}_1 - s_2 \dot{\theta}_2 \dot{\theta}_1)] + a_3 \ddot{\theta}_{23} s_{23}\dot{\theta}_1 - 2\dot{d}_4 s_{23}\dot{\theta}_1$$
$$- d_4 \ddot{\theta}_{23}\dot{\theta}_1^2 c_{23} - d_4[c_3(c_2 \dot{\theta}_2 \dot{\theta}_1 + s_2 \ddot{\theta}_1 + c_2 \dot{\theta}_3 \dot{\theta}_1) - r_{c4}\ddot{\theta}_{23}\dot{\theta}_1 c_{23}$$
$$+ s_3(c_2 \ddot{\theta}_2 - s_2 \dot{\theta}_3 \dot{\theta}_1 - s_2 \dot{\theta}_2 \dot{\theta}_1)] - r_{c4}[c_3(c_2 \dot{\theta}_2 \dot{\theta}_1 + s_2 \ddot{\theta}_1 + c_2 \dot{\theta}_3 \dot{\theta}_1)$$
$$+ s_3(c_2 \ddot{\theta}_2 - s_2 \dot{\theta}_3 \dot{\theta}_1 - s_2 \dot{\theta}_2 \dot{\theta}_1)]$$

$$\delta_4 = s_3(s_2 g - c_2 \dot{\theta}_1^2 a_1 - \dot{\theta}_1^2 c_2{}^2 a_2 - a_2 \dot{\theta}_2^2) - c_3(c_2 g + s_2 \dot{\theta}_1^2 a_1 + s_2 \dot{\theta}_1^2 c_2 a_2 + \ddot{\theta}_2 a_2)$$
$$- a_3 \ddot{\theta}_{23} - a_3 s_{23}\dot{\theta}_1^2 c_{23} + \ddot{d}_4 - d_4(s_{23}\dot{\theta}_1)^2 - d_4 \ddot{\theta}_{23} - c_{c4}(s_{23}\dot{\theta}_1)^2$$
$$- r_{c4}\ddot{\theta}_{23}$$

Having computed the velocities and accelerations by forward recursion from the base link to the end effector, the forces and torques can be also calculated by a backward recursion [48, 50]:

The backward chain from 4 to 1 is as follows:

$$f_4 = M_4[s_3(s_2 g - c_2 \dot{\theta}_1^2 a_1 - \dot{\theta}_1^2 c_2{}^2 a_2 - a_2 \dot{\theta}_2^2) - c_3(c_2 g + s_2 \dot{\theta}_1^2 a_1 + s_2 \dot{\theta}_1^2 c_2 a_2 + \ddot{\theta}_2 a_2)$$
$$- a_3 \ddot{\theta}_{23} - a_3 s_{23}\dot{\theta}_1^2 c_{23} + \ddot{d} - d_4(s_{23}\dot{\theta}_1)^2 - d_4 \ddot{\theta}_{23}$$
$$- c_{c4}(s_{23}\dot{\theta}_1)^2 - r_{c4}\ddot{\theta}_{23}] + f_{v4}\dot{d}_4 + f_{c4}\,\mathrm{sgn}(\dot{d}_4)$$

$$\tau_3 = (-M_4[s_3(s_2 g - c_2 \dot{\theta}_1^2 a_1 - \dot{\theta}_1^2 c_2^2 a_2 - a_2 \ddot{\theta}_2) - c_3(c_2 g + s_2 \dot{\theta}_1^2 a_1 + s_2 \dot{\theta}_1^2 c_2 a_2 + \ddot{\theta}_2 a_2)$$

$$-a_3 \ddot{\theta}_{23} - a_3 s_{23} \dot{\theta}_1^2 c_{23} + \ddot{d}_4 - d_4(s_{23}\dot{\theta}_1)^2 - d_4 \ddot{\theta}_{23} - c_{c4}(s_{23}\dot{\theta}_1)^2 - r_{c4}\ddot{\theta}_{23}\,]$$

$$-M_3[s_3(s_2 g - c_2 \dot{\theta}_1^2 a_1 - \dot{\theta}_1^2 c_2^2 a_2 - a_2 \ddot{\theta}_2) - c_3(c_2 g + s_2 \dot{\theta}_1^2 a_1 + s_2 \dot{\theta}_1^2 c_2 a_2 + \ddot{\theta}_2 a_2)$$

$$-a_3 \ddot{\theta}_{23} - a_3 s_{23} \dot{\theta}_1^2 c_{23} - r_{c3}\ddot{\theta}_{23} - r_{c3}s_{23}\dot{\theta}_1^2 c_{23}])(a_3 + r_{c3})$$

$$+M_4(c_3(s_2 g - c_2 \dot{\theta}_1^2 a_1 - \dot{\theta}_1^2 c_2^2 a_2 - a_2 \ddot{\theta}_2) + s_3(c_2 g + s_2 \dot{\theta}_1^2 a_1 + s_2 \dot{\theta}_1^2 c_2 a_2 + \ddot{\theta}_2 a_2)$$

$$-a_3 \ddot{\theta}_{23} - (c_{23}\dot{\theta}_1)^2 a_3 + 2\dot{d}_4 \ddot{\theta}_{23} + d_4 \ddot{\theta}_{23} - d_4 s_{23}\dot{\theta}_1^2 c_{23} + r_{c4}\ddot{\theta}_{23}$$

$$-r_{c4}s_{23}\dot{\theta}_1^2 c_{23})(d_4 + r_{c4}) + I_4(s_{23}\dot{\theta}_1^2 c_{23}) + M_4(s_3(s_2 g - \dot{\theta}_1^2 c_2^2 a_2 - a_2 \ddot{\theta}_2)$$

$$-c_3(c_2 g + s_2 \dot{\theta}_1^2 a_1 + s_2 \dot{\theta}_1^2 c_2 a_2 + \ddot{\theta}_2 a_2) - a_3 \ddot{\theta}_{23} - a_3 s_{23}\dot{\theta}_1^2 c_{23} + \ddot{d}_4$$

$$-d_4(s_{23}\dot{\theta}_1)^2 - d_4 \ddot{\theta}_{23} - c_{c4}(s_{23}\dot{\theta}_1)^2 - r_{c4}\ddot{\theta}_{23})r_{c3} + I_3 s_{23}\dot{\theta}_1^2 c_{23} + f_{v3}\dot{\theta}_3 + f_{c3}\dot{\theta}_3$$

<div align="right">(23)</div>

As the equations for τ_1 and τ_2 are quite lengthy they have not been included in this thesis. The dynamic equations of a serial manipulator such as the cable shovel can be written on the following general form:

$$D(q)\ddot{q} + C(q,\dot{q})\dot{q} + f_V \dot{q} + f_C \operatorname{sgn}(\dot{q}) + G(q) = \tau \qquad (24)$$

Where:

q is the vector of the generalized joint coordinate describing the pose of the manipulator

$\dot{q}$ is the vector of joint velocities

$\ddot{q}$ is the vector of joint acceleration

$D(q)$ is the symmetric joint-space inertia matrix or manipulator inertia tensor

$C(q)$ describes the Coriolis and centripetal effects matrix

f_V is the viscous friction coefficient matrix

f_C is the Coulomb friction coefficient matrix

$G(q)$ is the gravity loading vector

τ is the vector of generalized joint forces(including torques)

2.4 Relationship Between Joint Torques and Motor Torques

The torques discussed until now are the joint torques. However, DC motors via transmissions (gearboxes and ropes) move the links in the cable shovel. Therefore, the equation showing the relationships between DC motor torques and joint torques must be obtained. The swing and the crowd joints are actuated by DC motors and power is transmitted by gear boxes, whose equations have been extensively developed in the literature [58, 59]. I use current and voltage transducers to detect the electrical operating parameters of the swing, hoist and crowd motors. The joint torques can be calculated from these signals.

The other power transmission units are:
- the hoist (including the gear, the drum, and the ropes) and
- the boom (with no actuator).

Figure 5 and Figure 7 represent the different forces that are applied to the elements of the mechanical structure.

Where:

F_{Drum} is the force applied by drum to the hoist rope at point A

F_B is the force applied by the hoist rope to the sheave at point B

F_C is the force applied by the sheave hoist rope to the hoist rope at point C

F_{Hoist} is the force applied by the hoist rope to the dipper at point D

F_{Sheave} is the force applied by the sheave to the boom

F_{SC} is the force applied by the suspension cable to the boom

τ_{Boom} is the boom torque or τ_2

F_{BX} is the reaction force on the boom along horizontal line resulted by F_{SC} and

        $F_{Sheaves}$

F_{BY} is the reaction force on the boom along vertical line resulted by F_{SC} and

        $F_{Sheaves}$

X_{Drum} is the displacement of the hoist cable in point A

X_{Hoist} is the displacement of the hoist cable in point D

r_s is the radius of the sheave

δ is the angle between the hoist rope and the sheave with respect to vertical line at point A

α_7 is the angle between the hoist rope and the horizontal line in point A

α_6 is the angle of F_{Sheave} and the vertical line

α_3 is the angle between the hoist rope and the dipper handle

α_5 is the angle between the dipper handle and the vertical line

α_4 is the angle between the boom and the suspension cable

L_B is the boom length

L_{AB} is the hoist cable length from drum to sheave (Point A to Point B)

L_{CD} is the hoist cable length from sheave to the dipper (Point C to Point D)
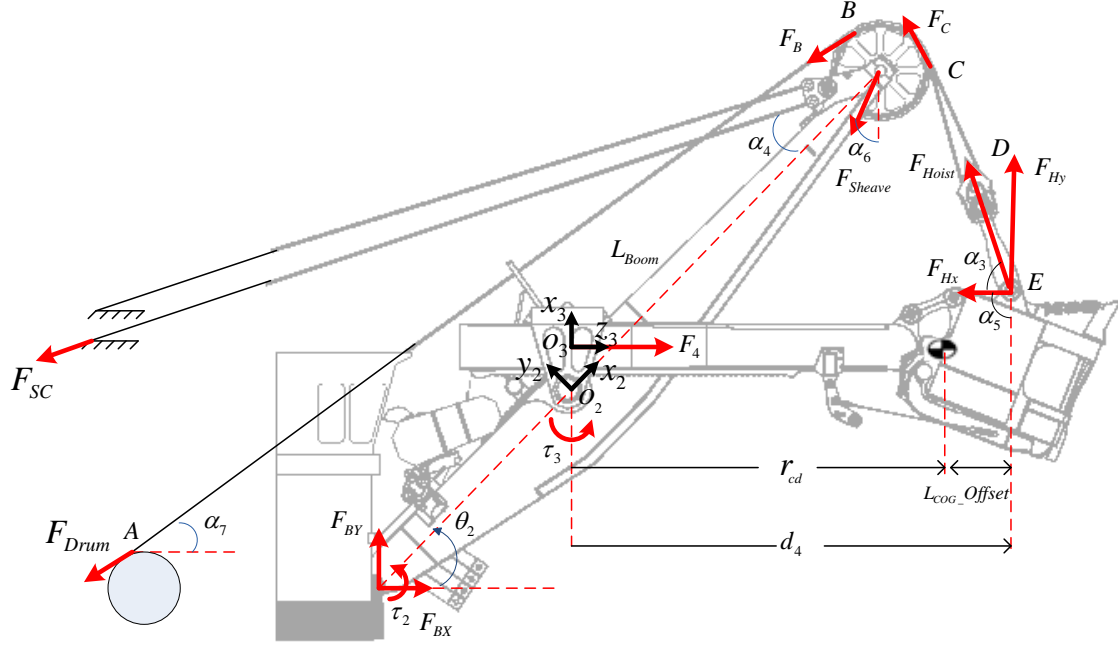
Figure 5: Forces apply to the elements of the mechanical structure

While the hoist rope is wound on the drum, the angle between the hoist rope and the sheave δ, changes as shown in Figure 6.

If we consider two parts for the hoist rope from the sheave location, as shown in figure Figure 7.a, force equations can be written as:

$$F_{Drum} = \frac{1}{Cos\delta}\left(M_{AB}\ddot{X}_{Drum} - gM_{AB}Sin\alpha_7 + F_B \right) \tag{25}$$

$$F_{Hoist} = M_{CD}\ddot{X}_{Hoist} + F_C + gM_{CD}Cos(\alpha_3 + \alpha_5) \tag{26}$$

$$\tau_{Sheave} = (F_B - F_C)r_s = I_s\ddot{\phi}_s + \tau_{FS} \tag{27}$$
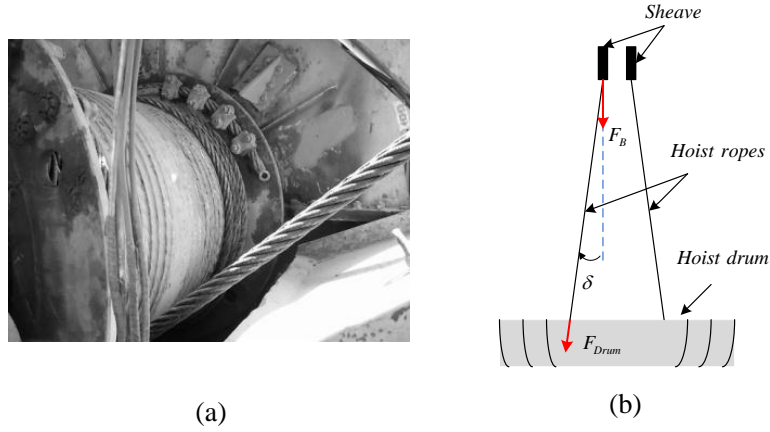
Figure 6: a) The drum and the hoist rope b) The front view of drum, hoist rope, and sheave

Where:

M_{AB} is the hoist cable mass from drum to sheave (Point A to Point B)

M_{CD} is the hoist cable weight from sheave to the dipper (Point C to Point D)

ϕ_s is the angular acceleration of the sheave

I_S is the rotational inertia of the sheave

τ_{FS} is the friction between the sheave and the hoist cables

X is the cable displacement

Consequently F_{Hoist} and F_{Sheave} can be written as:

$$F_{Hoist} = M_{CD}\ddot{X}_{Hoist} + gM_{CD}Cos(\alpha_3 + \alpha_5) - \frac{I\alpha + \tau_{FS}}{r}$$
$$+ F_{Drum}Cos\delta - M_{AB}\ddot{X}_{Drum} + gM_{AB}Sin\alpha_7$$

(28)

$$F_{Sheaves} = -Cos(\alpha_3 + \alpha_5)[F_{Hoist} - M_{CD}\ddot{X}_{Hoist} + gM_{CD}Cos(\alpha_3 + \alpha_5)]$$
$$+ Sin\alpha_7[F_{Drum}Cos\delta - M_{AB}\ddot{X}_{Drum} + gM_{AB}Sin\alpha_7]$$

(29)
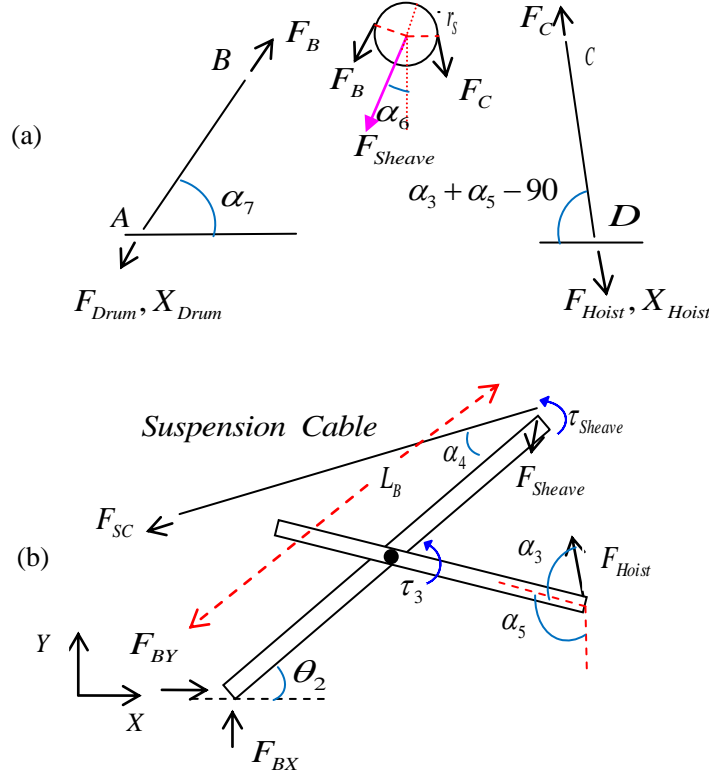
Figure 7: The side view of hoist Rope, sheave, boom, and crowd along with forces apply to them

Let us assume an equivalent torque τ_{eq} that represents the force F_{Hoist} as it is felt in the saddle block:

$$\tau_{eq} = \tau_3 = F_{Hoist} d_4 Sin\alpha_3 \tag{30}$$

Where d_4 is the crowd joint displacement. τ_{Boom}, which is the function of $F_{Sheaves}$ and the spring effect of suspension cables is given by:

$$F_{BX} = F_{SC} Cos(\theta_2 - \alpha_4) + F_{Sheave} Sin\alpha_6 \tag{31}$$

$$F_{BY} = F_{SC} Sin(\theta_2 - \alpha_4) + F_{Sheave} Cos\alpha_6 \tag{32}$$

$$F_{SC} = K_{SC} \Delta X \tag{33}$$

$$\tau_{Boom} = \tau_2 = -\tau_{Sheave} + [F_{Sheave} Sin(\alpha_1 + \alpha_6) - F_{SC} Sin\alpha_4] L_B \quad If \ \alpha_6 < 90 - \theta_2 \tag{34}$$

$$\tau_{Boom} = \tau_2 = -\tau_{Sheave} + [-F_{Sheave} Sin(\alpha_1 + \alpha_6) - F_{SC} Sin\alpha_4] L_B \quad If \ \alpha_6 >= 90 - \theta_2 \tag{35}$$

Where K_{SC} is the spring coefficient of the suspension cable, and τ_{Boom} is equal to τ_2.

The total force applies to the crowd prismatic joint is equal to:

$$F_4 = F_{Crowd} - F_{Hoist}Cos\alpha_3 \tag{36}$$

Where F_{Crowd} is the force exerted on the dipper handle by the crowd motor and F_4 is the force exerted to the dipper handle by the prismatic joint.

I have considered the hoist-rope as a rigid body until now, whereas in reality it is elastic and its length changes under the mass of the dipper or payload. As shown by de Silva in [59], the corresponding spring effect can be modelled as follows:

$$\frac{F_{Drum}}{S^2 X_{Drum}} = \frac{M_{AB}}{\frac{M_{AB}}{3}S^2 + K_{AB}} \tag{37}$$

$$\frac{F_{Hoist}}{S^2 X_{Hoist}} = \frac{M_{CD}}{\frac{M_{CD}}{3}S^2 + K_{CD}} \tag{38}$$

$$K_{AB} = \frac{A_{Hoist}\gamma_{Hoist}}{L_{AB}} \tag{39}$$

$$K_{CD} = \frac{A_{Hoist}\gamma_{Hoist}}{L_{CD}} \tag{40}$$

$$M_{AB} = L_{AB}.\rho_{Hoist} \tag{41}$$

$$M_{CD} = L_{CD}.\rho_{Hoist} \tag{42}$$

Where A_{Hoist} is cross section area of the hoist cable, γ_{Hoist} is the spring modulus of the hoist cable, S is the Laplace transformation operator, and ρ_{Hoist} is the weight per length unit of the hoist cable. In equations (38) and (39) the equivalent lumped mass concentrated at the free ends of the hoist cable is equal to one third of the cable mass.

2.5   Dipper Handle Linear Movement Caused by Rotation

A closer look at the dipper handle and the shipper pinion reveals that as the dipper handle rotates, the effective length of the dipper handle changes despite the crowd motor and the shipper pinion being stationary. Figure 8 represents the dipper handle, the shipper pinion, and the saddle block in cable shovels. Therefore, a more accurate model is required. The effective length of the dipper handle is the distance from the end effector or the dipper to the point of contact between the dipper handle and the gear along the dipper

handle. This linear movement is caused by the rotation of the dipper handle on the shipper pinion. In other words, the saddle block joint angle θ_3 variations alter the crowd joint displacement d_4 as represented in Figure 9. This figure illustrates the dipper handle movement on the shipper pinion. The dashed rectangle shows the position of the dipper handle if we assume one complete turn rotation for the shipper pinion. In practice, the dipper handle or the saddle block joint angle θ_3 variations are usually between $-45°$ to $45°$.
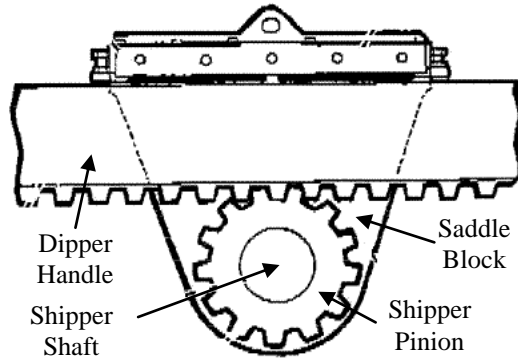
Figure 8 : Dipper handle and shipper pinion
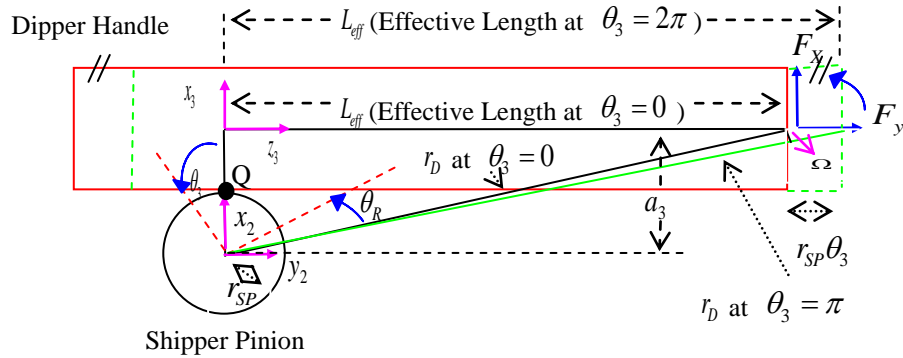
Figure 9: Dipper handle movement on the shipper pinion

According to Figure 9 :

r_{SP} is the radius of the Shipper Pinion

28

θ_3 is the rotation angle of x_3 around y_2 axis

θ_R is the rotation angle of the end effector in a view from the center of the shipper pinion

a_3 is the distance from the center of the shipper pinion and the center of the dipper handle or distance from z_2 to z_3 along the x_3 axis

L_{eff} is the effective length of the dipper handle at $\theta_3 = 0$

r_D is the distance between centers of the gear to the end effector.

The two factors below prevent the end effecter from following a complete circle:

- Changes in the crowd length because of rotation
- Instantaneous change of the center of rotation

The variation in the length of the dipper handle generated by rotation of dipper handle is calculated as follows:

$$\Delta d = r_{SP}\theta_3 \tag{43}$$

Which means the prismatic joint moves $r\theta_3$ as the revolute joint rotates θ_3. Below equations represent the relationship between θ_R and θ_3:

$$\theta_3 = \theta_R + Sin^{-1}(\frac{\Omega}{r_D}) \tag{44}$$

In cable shovels $\Omega \langle\langle r_D$, therefore:

$$\theta_3 \approx \theta_R + \frac{\Omega}{r_D} \Rightarrow \theta_3 \approx \theta_R \tag{45}$$

Finally, the variation of the dipper handle will be the total of the variation of the above prismatic joint plus the variation of the main prismatic joint generated by the crowd motor. d_4 will be replaced by d_{PR} in equations (23) and (24) where:

29

$$d_{PR} = d_4 + r_{SP}\theta_3 \tag{46}$$

Equation (47) will provide the accurate distance between the dipper and the point of intersection between the shipper pinion and the dipper handle, represented as point Q in Figure 9 . This length value has a significant effect on the force balance about point Q.

The presence of the hoist rope to actuate the crowd rotational joint indeed creates an intercoupling between the rotational and prismatic action of the crowd even if the shipper-pinion arrangement was replaced by a basic prismatic actuator. If the prismatic joint is activated, obviously d_4 will change. However, due to the presence of the hoist ropes, the joint angle θ_3 will also change even if the hoist motors are not actuated. The reverse scenario would not be true, i.e., if the hoist motor is actuated θ_3 will obviously change as a result. However, due to the shipper-pinion arrangement, the prismatic joint displacement will also change by a factor of $r_{SP}\theta_3$.

2.6 P&H Cable Shovel Actuator Dynamics and Drives

The drive technology used in the P&H cable shovel is DC motor connected to phase-controlled thyristor rectifiers. These motors are all separately- excited DC motors built in ratings of up to 2000 horsepower.

The behavior of the DC motors is described by the following fundamental equations [60, 61]:

$$u_A(t) - K_m \omega_m(t) = L_A \frac{di_A(t)}{dt} + R_A i_A(t) \tag{47}$$

$$K_m = L_{af} i_f(t) \tag{48}$$

And mechanical equation is:

$$K_m i_A(t) - T_{m.Load}(t) = J_m \frac{d\omega_m(t)}{dt} + f_{vm}\omega(t) + f_{cm}sign[\omega_m(t)] \tag{49}$$

Where

$\quad$ $u_A(t)$ $\quad$ is the motor armature supply voltage

$\quad$ $i_A(t)$ $\quad$ is the motor armature current

$\omega_m(t)$ is the motor angular velocity

L_m is the motor armature inductance

R_m is the motor armature resistance

K_m represents the torque constant as well as the back-electromotive-force constant

L_{af} is the field-armature mutual inductance

$i_f(t)$ is the motor field current

J_m is the motor inertia

f_{vm} is the motor viscous friction coefficient

f_{cm} is the motor coulomb friction torque

T_{mLoad} is the motor instantaneous load torque.

The motor drives in the P&H cable shovels are four-quadrant thyristor converters that rectify a three-phase AC signal to a DC signal at the required voltage as represented in Figure 10. With this arrangement the motors powering the cable shovel are able to operate both as a motor or a generator, since the armature currents and directional torque can be reversed very quickly [7, 62]. There are inductors connected in series with the thyristors that limit the current circulating in the thyristors. The field of the motors in the P&H cable shovel is fed by a six-pulse thyristor bridge as represented in Figure 11. Our experiments in the field show that the crowd and swing motors have a fixed field currents; however, the hoist field current has two different fixed values: one for hoisting and another for lowering.
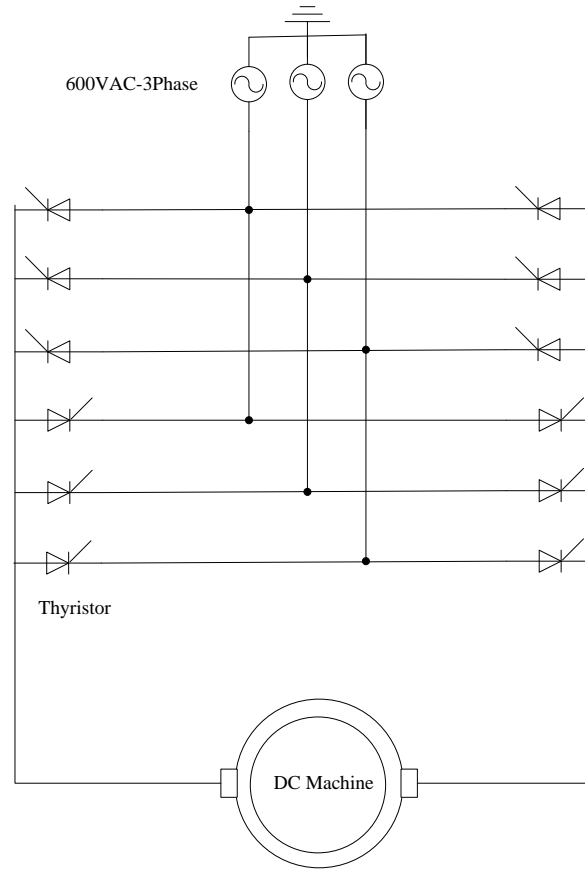
Figure 10: Four-Quadrant Three-Phase Rectifier DC machine drive
used in the P&H cable shovels
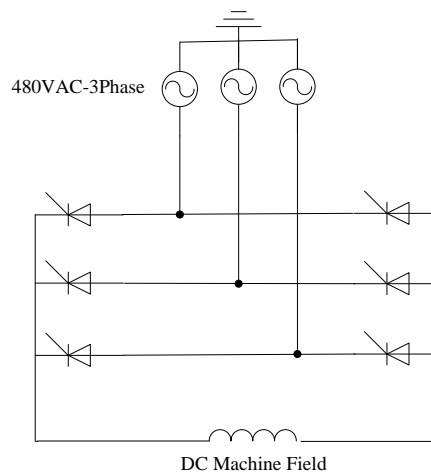
Figure 11: Six-Pulse Thyristor bridge feeds the field of the
DC motors used in the P&H cable shovels

3 A NOVEL CABLE SHOVEL JOINT VARIABLE SENSING DEVICE

3.1 Introduction

In this chapter I will explore two issues. First, I will discuss the conventional techniques that are used to sense the geometry of cable shovel arms. Second, I will present our novel approach that allows non-contact sensing of the shovel arm geometry. and also determine the exact coordinates of the bucket's position.

3.2 Conventional Techniques for Measuring the Cable-Shovel Joint Variables

Sensing the cable shovel joint variables such as swing angle, the dipper handle extension, the, and hoist rope expansion are currently obtained by detecting rotation of the swing, crowd, and hoist motors. These variables are achieved by the resolvers or encoders incorporating a component coupled to the motor gears [6, 23]. The angle between the crowd and the boom can by calculated by using the length of the crowd and the length of the hoist rope. The velocity and acceleration of the crowd, the angular velocity and angular acceleration of the machinery deck, and the angular velocity and angular acceleration of the boom are estimated by numerical differentiation of the crowd displacement, the machinery deck swing angle, and the boom angle, respectively.

For the reason that the hoist rope length is varied by tension, using the hoist motor shaft-based resolver signal to calculate the hoist rope length has some error. Moreover, the installation of the resolvers on the motor shaft is difficult and requires retrofitting and mechanical modifications. Another drawback of using resolvers is that they do not measure the absolute values but calculate these values based just on the motor rotation. One shortcoming becomes evident: if power to the arm monitoring system becomes disconnected in the middle of a cable shovel operation, then the resolvers cannot find the actual value of the joint variables when the power is or restored. Consequently, the zero point or the home position of the links must be defined whenever the system is energized.

In recent years, many researchers, such as Faxlin [63-69] have used a type of inertial sensor for tracking humans. These are constructed as micro-electromechanical

systems (or MEMS) that include gyroscopes with drift correction performed by referencing the Earth gravity for pitch and roll and which use the Earth's geomagnetic field for heading correction [70, 71]. Jimenez et al. [67] have used low-performance MEMS inertial sensors attached to a person's foot that detects step, stride length, comapass-heading and position-estimation. Although these sensors operate properly for tracking people, the steel structure of the cable shovel plus the magnetic field created by the DC motors and rectifiers significantly disturb the Earth's magnetic field which limits the accuracy of the heading angle.

3.3   Cable Shovel Arm Geometry

As discussed in chapter 2, in this thesis I treat the P&H cable-shovel as a robotic manipulator with three revolute joints and one prismatic joint, as shown in Figure 3. Thus I need to sense the cab swing angle θ_1, the boom joint angle θ_2, the saddle block joint angle θ_3, and the crowd joint displacement, d_4.

Because the cable shovel size is enormous, wiring the sensors will be difficult if we are to install several sensors on different parts of the machine. Furthermore, many field installations by engineers of Motion Metrics Int'l have revealed that electrical wires are much more prone to be damaged in the vicinity of the dipper or when there are multiple sensors near the movable joints. As shown later in this chapter, an innovative muti-sensor apparatus is introduced for the first time in this thesis for non-contact absolute sensing of the cable shovel. The optimal position for installing this sensor is between the operator's cabin and the saddle block represented by the red rectangle in Figure 12. While this location is easily reachable, it is also far enough from the dipper so that falling rocks cannot easily collide with the sensor.

According to the gear ratio between the hoist motor to the hoist cable, and the diameter of hoist drum, and including the maximum speed of the hoist-motor, I find that the maximum line-speed of the hoist-rope will be around 1 m/s. The maximum linear speed of the crowd or dipper handle is approximately 0.7 m/s.

Our experiments confirmed that the cable shovel joint variables must be sensed at least at the rate of 20Hz. The sensed variables are then used to estimate the following:

- Angular velocity and angular acceleration of the machinery deck swing $\dot{\theta}_1$, $\ddot{\theta}_1$

- Angular velocity and angular acceleration of the dipper handle $\dot{\theta}_3$, $\ddot{\theta}_3$

- Linear velocity and acceleration of the crowd (the dipper handle) $\dot{d}_4$, $\ddot{d}_4$

Figure 12: A suitable area for the installation of the arm-geometry sensor.

In summary, our arm geometry sensing device should have the following characteristics in order to be functional in mines:

- Be integrated in one enclosure in order to minimize the cabling

- Sense the cable shovel joint variables with 20ms response time

- Operate in the temperatures range from -40 $^{\circ}C$ to +60 $^{\circ}C$

- Acquire the cable shovel arm geometry without a complex and time consuming algorithm

- Be robust to cable shovel vibration and the harsh mining environment

35

- Can be installed without any mechanical modification on the shovel structure

3.4   Dipper Handle Length Measurement

Currently most non-contact displacement sensors are designed using either laser or ultrasonic technologies. Laser devices have fast response-time and are widely used in industrial application to sense distances of up to 70 meters that are quite adequate for our application.   The response time and measuring range of current ultrasonic devices do not meet our requirement for measuring the cable-shovel arm geometry.

Laser range-finder use either triangulation or a time-of-flight principle to measure distance [72-85]. Laser-triangulation calculates distance trigonometrically by measuring the angle between an emitted laser beam and a reflection of this beam, reflected off two mirrors. The laser, the two mirrors and a collection lens form a triangle.   Any change in distance correlates directly to a change in angle, which can be calculated. Usually the laser-emitter and the collection lens are installed in very close proximity within the sensor enclosure. However, triangulation is limited to measuring centimeter range distance with high precision since accuracy is reduced as distance is increased. The time-of-flight technique calculates the distance between the sensor and a target by measuring the time required for the laser beam to travel from the sensor to a target and return. This technique is effective for relatively long-range distance measurements.

I investigated the capabilities and the limitations of laser range-finders currently available, based on our intended application. For instance mine temperatures vary from $-40\,^{\circ}C$ to $+60\,^{\circ}C$, depending on the mine location.   Our distance sensor must be accurate and reliable in all mines and all times of the year. I evaluated the performance of the laser sensors in all possible conditions for the following parameters:

- Operating temperature range
- Sensor response time
- Effect of sunlight
- Effect of vibration

We know that the maximum length of the crowd is approximately 10 meters and its linear speed is around 0.7m/s [6, 86]. These values help us specify the laser sensor response time. In Table 2 below, I compare the specifications of various devices that

meet this criteria.

Table 2: Currently available laser sensors suitable for cable shovel crowd displacement sensing

Company	Model	Response Time (ms)	Range (Meters)	Accuracy (millimeters)	Temperature Range($^{\circ}C$)
Sick Group www.sick.com	DT500	250	0-30	3	-40 to 50
Schmitt Industries www.acuitylaser.com	AR1000	20	0-30	3	-10 to 50
Schmitt Industries www.acuitylaser.com	AR4100	1.3	0-17	3	-17 to 50
Jenoptik Group www.jenoptik.com	LDM42	20	0-30	3	-10 to 50
Waycon Positionsmesstechnik www.waycon.de	LLD-100-50	20	0-30	3	-10 to 50
Dimetix AG www.dimetix.com	DLS-BH-30	200	0-65	3	-40 to 50

The DT500 and DLS-BH-30 lasers are relatively slow for our application. However, their operating temperature ranges are appropriate for a mining environment. The speed, the accuracy, and the measuring range of AR1000, LDM42, and LLD-100-50 models are all adequate for our application. Similar to the DT500 laser sensor, the operating temperature range on these sensors can be enhanced by using a heater.

I tested different laser range finders in an effort to select a suitable model for our application. The following two major factors influenced our decision [74, 76]:

- Vibration effect
- Sunlight effect

In our first experiment the laser sensors were stationary, but the target was moved at the speed of 1m/s in an indoor environment. I found that the LDM42 could not track the target at 50Hz sampling rate when the target was moving at 1 m/s if the target was vibrated at the same speed. The LDM42 laser sensor generated an error message that

indicated there is too much difference between the measured distance and the pre-calculated value. These test results demonstrated that we require a faster laser sensor in order to measure the crowd length dynamically. I repeated the aforementioned experiments with another high speed laser sensing device, the AR4000, manufactured by Schmitt Industries. The AR4000 properly operated with 20mS response time. The color of the target or the speed of the target did not affect the AR4000 performance. The maximum target speed in our tests was 2 m/s.

To study the influence of sunlight on the laser performance, I ran a second experiment in an outdoor environment on a sunny day. In the first part of the experiment, the sun was shining toward the laser device, but was behind the target, putting the target in shadow, as shown in Figure 13. I made observations when the target was stationary and also when it was moving slowly. On this part of our experiment the LDM42 laser worked properly. The lens-hood on the LDM42, which is similar to a camera lens-hood, prevented stray sunlight from entering the laser lens directly. The AR4000 also performed similarly, without any difficulty.
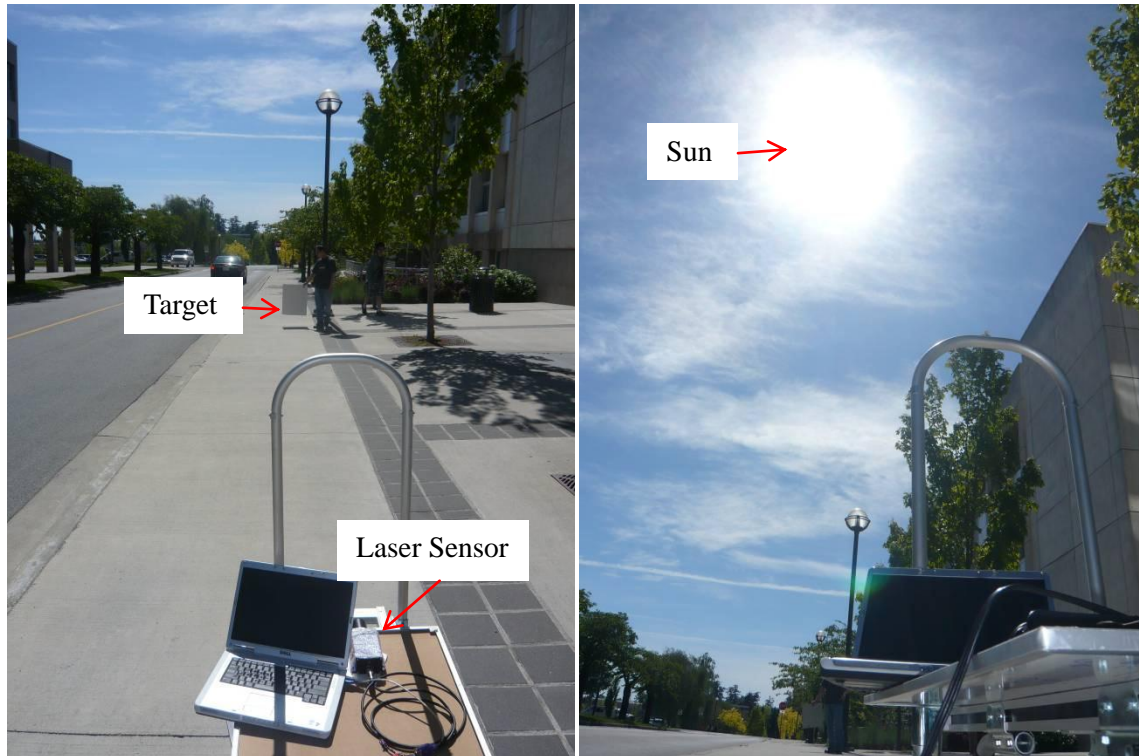
Figure 13: Testing the laser sensor: the laser, target, and sun are shown

In our next outdoor experiment, I swapped the position of the target and laser so that now the sun was shining from behind the laser and the target was fully illuminated by sunlight. On 90% of these tests the LDM42 sent an error message indicating that it was flooded by too much constant light. I believe the main reason that the LDM42 laser sensor failed is that the target reflected the too much sunlight. This problem could be solved simply by reducing the ambient light surrounding the target or by placing a sort of roof above the target. I observed that the AR4000 laser device performed well, regardless of target color, the direction of sunlight, or the speed at which I moved the target. In contrast, I discovered that the LDM42 laser range-finder to be inaccurate when the target is located outdoors or when the target moves quickly. Hence, a decision was made to incorporate the AR4000 laser sensor for our application.

3.5 Measurement of Dipper and Swing Angles

Suitable joint angle sensors are needed in virtually all manipulators that employ revolute joints. Both resolvers and encoders are used for this purpose is standard robotic application. However, modifying the joint-structure on a robot in order to install a properly aligned sensor is not a simple task and can be quite tedious. To locate the resolver-shaft in order that it is aligned properly with the rotation axis of the robot. This modification can be quite a tedious task. A remedy for this problem is to use a contact-free sensor to measure the joint-angles, using state-of-the-art silicon based MEMS orientation sensors.

As I stated in the first chapter, Ghassemi et al. [55, 57] used two biaxial accelerometers to estimate each joint-angles on hydraulic excavators. Then joint-angle measurements were taken under dynamic, real working conditions as shown in figure 14.
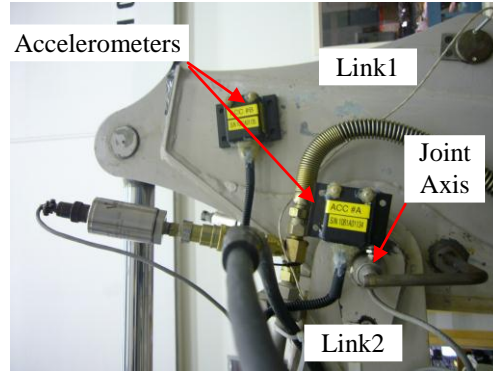
Figure 14: A pair of biaxial accelerometers installed on a hydraulic shovel
for measuring the joint angle

There is a clearance of approximately 10 cm between the crowd and the boom. This provide us with sufficient space to install the accelerometers. By installing the accelerometer pair on the saddle block there will be no need to use the hoist resolver as a sensor to measure the saddle block (or crowd) and boom joint angle. It is important to point out that this approach is capable of measuring only roll and pitch and cannot be used for sensing yaw or the swing angle. Furthermore, it requires installing two accelerometers for measuring each joint angle.

In the recent years, many researchers have used inertial sensors such as micro-electro-mechanical systems (MEMS) gyroscopes with drift correction performed by referencing the earth gravity for pitch and roll and the geomagnetic field for heading for human body tracking. Although these sensors operate properly for human motion tracking, the metal structure of the cable shovel and its DC motors and rectifiers significantly disturb the local earth magnetic field and limit the heading angle estimation

[64, 65, 69, 71]. One of the major challenges for measuring the joint angles in the cable shovel is presence of magnetic field and material in the vicinity. The DC motor drives in the P&H cable shovels are four-quadrant thyristor converters that generate enormous magnetic disturbance. The armature current of the DC motors could reach up to 3000A. Reducing the effect of the magnetic field disturbance on the yaw angle measurements has been a difficult task in this research.

Three Degrees of Freedom Orientation Tracker (3DOFOT) is a self-contained

sensor-system that measures three axes of orientation with respect to the Earth. Fortunately, a 3DOFOT device can provide us with the required joint-angles in the cable shovel. These 3DOFOT sensors can make computations and monitor the shovel movements using an earth-fixed co-ordinate reference system [68, 69]. However there still are some challenges remaining:

- transient accelerations
- vibration
- magnets or magnetic materials

The aforementioned issues are the main parameters that I considered in selecting an appropriate sensor for the cable shovel arm geometry. Table 3 compares four different 3DOFOT sensors available in the market.

Table 3: Existing 3DOFOT sensors in the market for the cable shovel arm geometry

Manufacturer	Model	Bandwidth (Hz)	Temperature Range($^\circ C$)	Accuracy (Degrees)
Polhemous Corp. www.polhemus.com	MINUTEMAN	75	0 to +50	+/-2
Xsens Corp. www.xsens.com	MTi	40	-20 to +50	Static: 0.5 Dynamic.: 2
InterSence Corp. www.isense.com	InertiaCube2+	180	0 to +50	1
MicroStrain Corp. www.microstrain.com	3DM-GX2	300	-40 to +50	Static: 0.5 Dynamic: 2

All of the 3DOFOT sensors listed in Table 3 measure the roll and pitch angles with high accuracy; however, our experiments have shown that the magnetic field disturbance or a metal object can affect the yaw angle measurement of most of these sensors. I tested different model and investigated the effect of vibration, magnetic field disturbance, and acceleration on their performances. The MTi sensor manufactured by XSENS outperformed its peers in its sensing the yaw angle and accordingly it was selected for our application. Chapter 4 of this thesis includes the results of using MTi in the field.

3.6   Innovative Cable Shovel Arm Geometry Sensor

I constructed an innovative, non-contact apparatus to measure the joint variables and active joints of the cable shovel. The proposed sensor integrated a laser range-finder and a 3DOFOT sensor in a single enclosure. This novel device minimizes the cabling required, and can be installed without any mechanical modification on the existing cable shovel.

The 3DOFOT device contains three accelerometers to measure linear accelerations (that is, sensitive to Earth gravity), three magnetometers to measure magnetic fields and three rate gyroscopes to measure the rate of rotation about each Cartesian axis. Further, these 3DOFOT sensors gather the outputs of the rate gyroscopes, the accelerometers and the magnetometers and then compute an estimate of the statistically-optimal 3D-orientation.   This can be accomplished with high accuracy and minimal drift under both static and dynamic conditions [66, 70]. The measurement of Earth gravity (by the 3D accelerometers) and Earth's magnetic-north (by the 3D magnetometers) compensate for any increasing drift-errors by integrating data from angular velocity provided by gyroscopes. This type of drift compensation is often called an Attitude and Heading Reference System (AHRS).

Recall the three challenges for sensing the joint angles: transient accelerations, vibration, and magnetic disturbance. I could minimize the effect of transient accelerations by installing an AGS sensor at a point where the transient accelerations are minimal.

This point is typically close to the centre of gravity of the link and—because any rotation around the centre of gravity converts into a centripetal acceleration located outside the center of rotation [70]. The enclosure for this apparatus is also shock at its centre of gravity and uses four spaced damping points, each with relatively low amplitudes, making the unit very stable (especially in pitch) so we can expect minimal transient accelerations. This is quite unlike an aircraft which can have a significantly longer duration in pitch acceleration about the axis of its wings or, in a different situation, a high standing softly-sprung truck that will experience longer lasting oscillations in pitch.

For best performance, the AGS sensor apparatus should be mechanically isolated from vibrations. Vibrations are measured directly by the accelerometers and these can

make the readings from the accelerometers invalid when the magnitude of the vibration is larger than the range of the accelerometer. As the result, the accelerometers saturate and their data cannot be used for the drift compensation in the roll/pitch measurement. Moreover, vibration may produce aliasing if the frequency of the vibration is higher than the bandwidth of the accelerometer. This can be observed as a low frequency oscillation. Further, high frequency vibrations often tend to have large acceleration amplitudes [70]. Concerning vibrations, the mount of the sensor apparatus itself has a natural frequency of around 20 Hz or lower. As a result, the vibrations become more attenuated as frequencies rise above 20 Hz. Therefore, the mount is effectively acting as a low-pass filter for the sensor thus enhancing the accuracy of our measurements.

As mentioned earlier ferromagnetic materials or magnets can affect the AGS sensor performance and accuracy. When a 3DOFOT sensor is placed close to a magnetic object, or contains ferromagnetic materials, then the measured magnetic field becomes distorted, causing an error in yaw (or heading) measurement. The Earth magnetic field can be significantly altered by ferromagnetic materials, permanent magnets, or very strong electric currents. The amount of disturbance depends on the distance between the AGS apparatus and the source of magnetic disturbance and also the amount of ferromagnetic material present. By installing the AGS sensor on the saddle-block I provide more than 10m distance between the sensor and the thyristor rectifiers of the cable-shovel, which I have identified as the major source of magnetic disturbance. Moreover, the magnetic disturbance generated by the cable shovel electrical circuitry can be completely calibrated and compensated for by using a specialized calibration procedure commonly known as a hard and soft iron calibration or magnetic field-mapping [70].

This sensor, that we'll call Apparatus 1, is shown in greater detail in Figure 15(a) [54]. Referring to Figure 15, Apparatus 1 includes a housing (2) and a mount (3) for securing the housing on the saddle block.

Apparatus 1 also includes:
- an orientation sensor (7) and
- a displacement sensor (8) mounted within the housing (1).
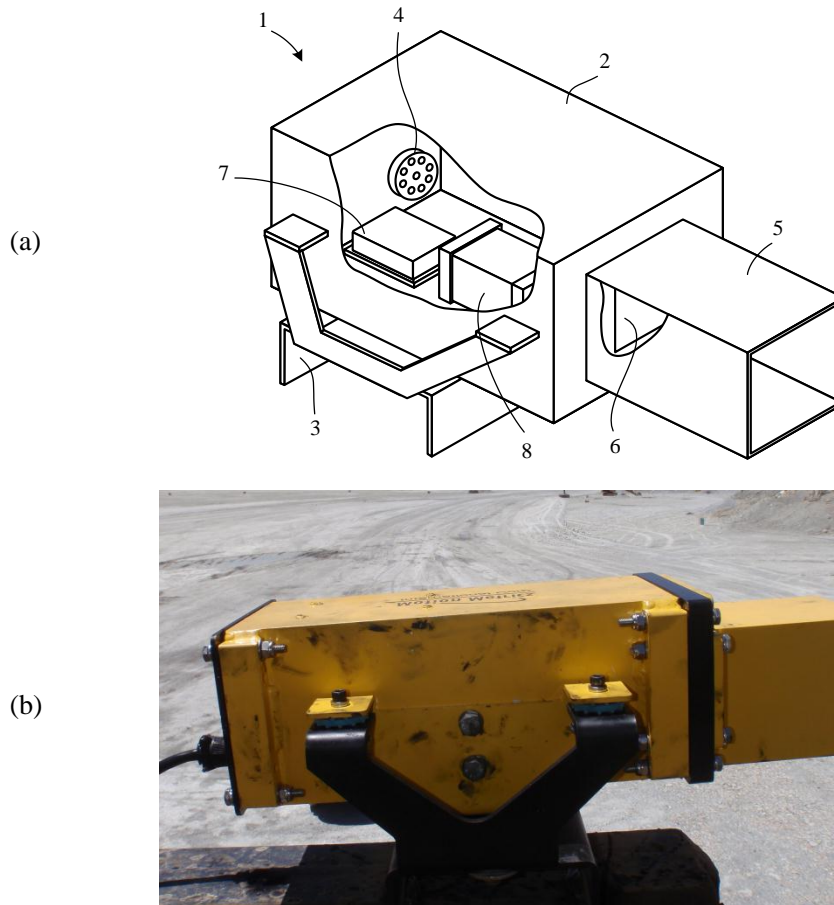
Figure 15: Cut-away perspective view of the AGS sensor (a)
and the senor installed on the shovel (b)

These sensors (7) and (8) are configured to produce spatial-positioning signals, including

- An orientation signal that defines the orientation of the saddle block and the dipper handle, and

- A displacement signal defining a displacement of the dipper relative to its support and

- A connector port (4) on the rear of the housing (1) for transmitting spatial-positioning signals from the sensors 7 and 8.

Apparatus 1 is also connected to a power supply for the sensors. In other embodiments, Apparatus 1 may include a wireless interface for transmitting the

spatial-positioning signals. In the model shown in Figure 15, the sensor (1) is a MEMS orientation-sensor such as the Xsens MTi.

Configuration-commands may be transmitted to the DSP via a serial port, using RS-323, RS-485, RS-422, or USB-compliant protocol. Power for operating the DSP and the various sensor elements is also connected to the sensors (7) and (8) though the connector port 4. Advantageously, the orientation sensor provides an accurate 3D orientation of the entire apparatus in any of a variety of signal formats. Further, the orientation sensor provides an accurate 3D orientation of the entire apparatus in any of a variety of signal formats. The orientation sensor (7) is also fully enclosed within the housing, which provides protection for the sensor elements when operating in a harsh environment such as a mine. In the layout shown in Figure 15, the displacement sensor (8) is a laser rangefinder such as the Acuity AR4000, manufactured by Schmitt Industries. The rangefinder also includes a processor circuit (not shown) that implements a modified measurement of the returning laser signal from an avalanche detector, (based upon the time-of-flight principle) which then generates a displacement signal. The signal provides an absolute measurement of the displacement between the housing (2) of the apparatus and the dipper. Referring again to Figure 15, the housing also includes a protective lens-hood (5) and a window made of lexan-sapphire (6) that allows the laser beam to be transmitted, while protecting the sensors inside from ingress of water and contaminants.

4 INSTRUMENTATION AND DATA LOGGING OF THE CABLE SHOVEL

In this chapter, I discuss the details of sensor installation on the cable-shovel, our field trials, the different scenarios that describe how our data was logged, and finally we discuss the data itself. This field trial was performed on a PH2100-XP cable shovel in the Mesesarchemshe Copper mine, located in central Iran. In chapter 5, we will employ the results of our field trial in order to indentify the cable shovel parameters.

4.1 Cable Shovel Joint Variables

As I stated earlier in section 1.4.2, in order to identify the cable shovel parameters, I must measure the joint variables and actuator torques simultaneously. I broadly discussed the measurement of cable shovel joint variables in Chapter 3. Because of the difficulty of installing torque meters directly on cable shovels, I must estimate the forces indirectly from electrical currents of the motors.

For this thesis I installed the sensors on a P&H2100 cable shovel, which has two swing motors. Power from these motors is transferred to the swing gear through a double-reduction spur gear transmission [6]. Because the armature and field wiring of both swing motors are connected in series, the armature and field currents are identical. As a result, only one current sensor is required to measure two field currents (of the two swing motors) and just one additional current sensor is required to measure the combined armature current of the two swing motors. The P&H2100 cable shovel has two hoist motors fed by two four-quadrant thyristor converters. Due to using two separate converters, the hoist armature currents of the two hoist motors are not the same. However, the field wiring of two hoist motors are connected in series and are fed by one six-pulse thyristor bridge. Therefore, the hoist field currents are identical and only one current sensor is required to measure the hoist field currents. Each hoist motor drives a double reduction gear. These gears are coupled to a common hoist drum gear. The P&H2100 cable shovel has one crowd motor mounted near the saddle block.

In summary, I measured the following variables during our field trail:

- Swing motor armature currents $i_{SA_1} = i_{SA_2}$

- Swing motor field currents $i_{SF_1} = i_{SF_2}$

- Hoist motor armature currents i_{HA_1} and i_{HA_2}

- Hoist motor field current $i_{HF_1} = i_{HF_2}$

- Crowd motor armature current i_{CA}

- Crowd motor field current i_{CF}

- Cab swing angle θ_1

- Boom joint angle θ_2

- Saddle block joint angle θ_3

- Crowd joint displacement d_4

- Cabin roll and pitch angles

4.2 DC Motor Current Measurement

A traditional technique for sensing current in DC motors is resistive current sensing. Using this technique, a shunt resistor is connected in series with the DC motor armature so that all of the current through the motor also flows through the resistor. The voltage drop across the shunt is proportional to the current flowing through the DC motor armature. The major drawbacks of this technique are that some modifications are required to the shovel existing electric circuits of the shovel and further, any high current conductors in the cable shovel must be relocated. Other disadvantages are lack of electrical isolation, voltage drop, and consequent energy loss.

Another transducer which is widely used for sensing DC current is the Hall Effect current sensor. This is non-contact DC current transducer that senses the magnetic field associated with the current flow through a conductor. The operational principle of the Hall effect current sensor has been discussed widely in literatures [87-89].

I chose a Hall Effect device with a split core as a suitable choice for our application. This device has a reasonable accuracy and linearity with current-overload capability and low power consumption. Moreover, the output of the sensor is isolated from the current carried in the conductor. The split core design allows us to install the device easily around the conductor carrying the current to the motor without the need to cut the cable. In this

47

thesis, I employed only this type of sensor, shown in Figure 16, for all motor current measurements.
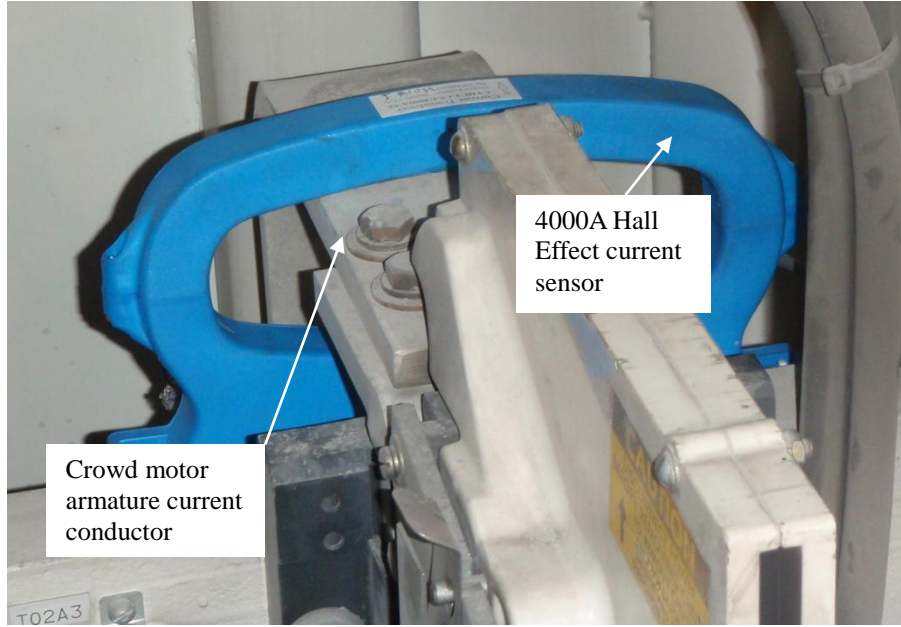
Figure 16: 4000A Hall Effect current sensor installed on the P&H2100 creowd motor armature conductor

4.3   System Hardware Diagram

Figure 17 illustrates my proposed configuration of the dynamic payload-monitoring system for P&H cable shovels.   Our novel AGS sensor measures:

- the cab swing angle θ_1
- the saddle block joint-angle θ_3
- the crowd extension d_4

The boom joint angle θ_2 is measured by an inclinometer.

A modified version of the standard Motion Metrics PC104 based embedded computer system was used. This system employs a Diamond-MM-32X-AT board for data acquisition.   This board has 32 analog inputs with 16-bit resolution and a 250 KHz sampling rate. A serial communication board reads data from the AGS through 12-wire cables connected through a junction box to the embedded system.

Together with Motion Metrics Engineers, I developed a graphical user interface that shows the arm geometry of the P&H2100 cable shovel on a touch screen monitor, including the shovel swing and the dipper handle position during the cable shovel operation. I remind the reader that the equations developed for this application have been presented earlier, in the section 2.2 of this thesis. This application is capable of logging 32 analog inputs along with the AGS reading at a 30 Hertz sample-rate. Table 4 represents the general specifications of the sensors being used in this project.

Table 4: General specifications for sensors used in the field trials

Sensor	Rated Input	Output Signal	Bandwidth (Hz)	Part No.
Swing 1 & 2 Armature Current	-1000 to 4000A	4-20mA	720	CYHCT-C5G-4000A-54
Crowd Armature Current	-1000 to 4000A	4-20mA	720	CYHCT-C5G-4000A-54
Hoist 1 Armature Current	-1000 to 4000A	4-20mA	720	CYHCT-C5G-4000A-54
Hoist 2 Armature Current	-1000 to 4000A	4-20mA	720	CYHCT-C5G-4000A-54
Swing 1& 2 Field Current	-100 to 200A	4-20mA	720	CYHCT-C9G-200A-54
Crowd Field Current	-100 to 200A	4-20mA	720	CYHCT-C9G-200A-54
Hoist 1&2 Field Current	-100 to 200A	4-20mA	720	CYHCT-C9G-200A-54
Laser Sensor for the crowd length measurement	0-17 M	RS422	770	AR4000
Inclinometer boom and the shovel Roll/Pitch measurement	0-20°	0-5V DC	6	CXTLA01
3DOFOT (MTi) for the dipper handle and the swing angle measurement	-180 to +180°	RS422	500	MTi
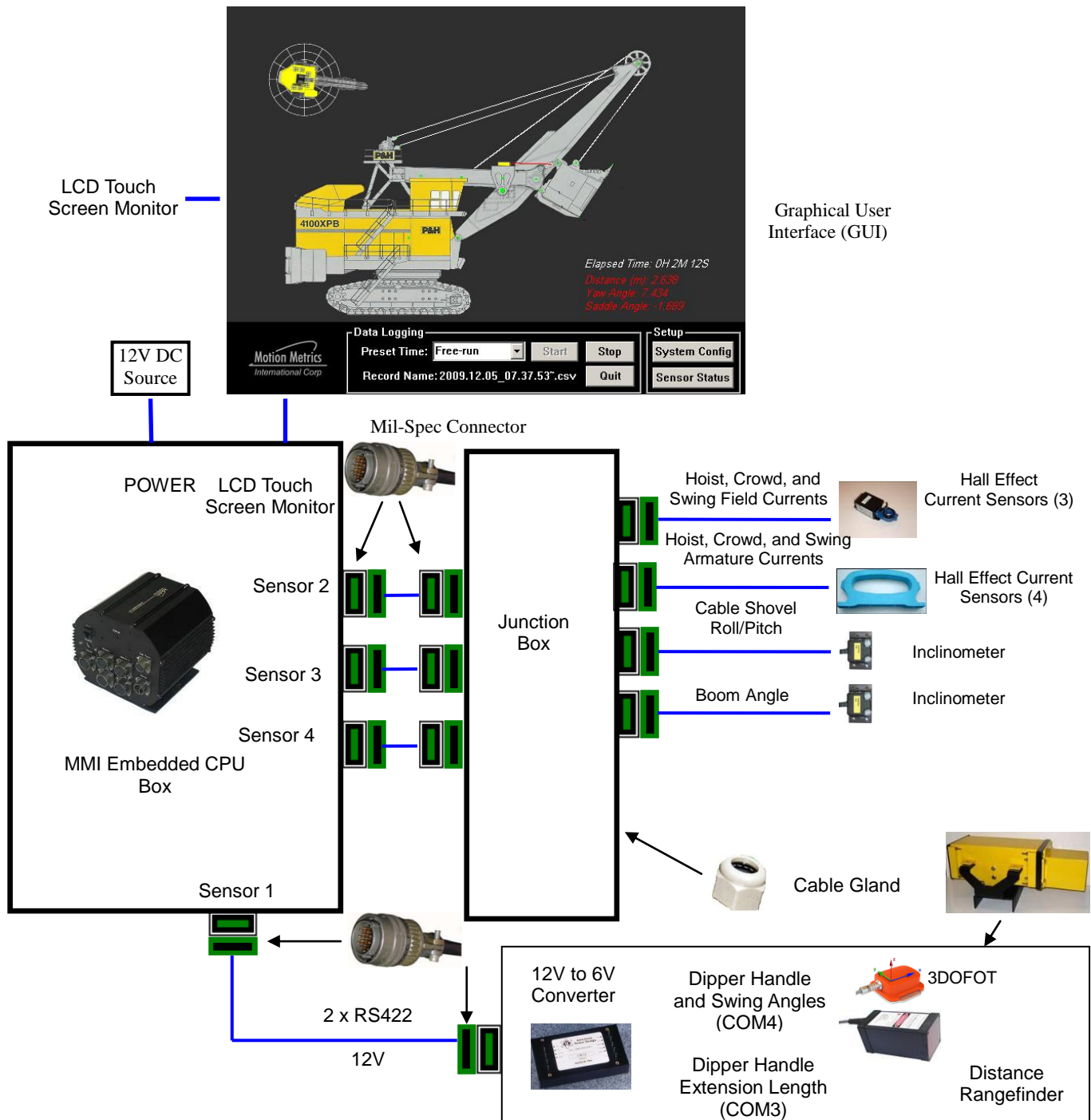
Figure 17 : Cable shovel payload monitoring components

4.4 Possible Location for AGS Installation

Figure 18 shows the possible location for the cable shovel AGS sensor installation on the top of the saddle block. The laser will aim at the dipper as shown in the Figure 19 and Figure 20. This location is far enough from the dipper so that rocks cannot hit the laser enclosure during ground engagement. Furthermore, I can use the existing electrical cable trays connecting the saddle block motor to the electrical room to wire AGS sensor to the operating room.

Figure 18: Saddle block top view

It is known that the laser performs better with a faster response time when the target is white and often referred to an 'cooperative' target. To further improve the laser performance, I can install a 'cooperative' target on the dipper handle as shown in Figure 20. The negative aspect of this approach is the cooperative target must be heavy and have a strong structure so that it does not vibrate during the shovel operation. Obtaining the mine approval to install a heavy object on the dipper handle may prove difficult.
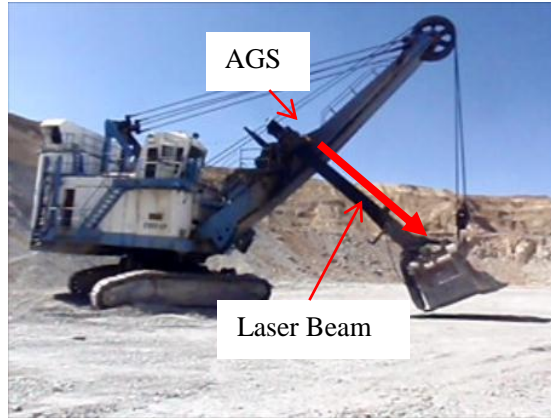
Figure 19: Laser sensor beam
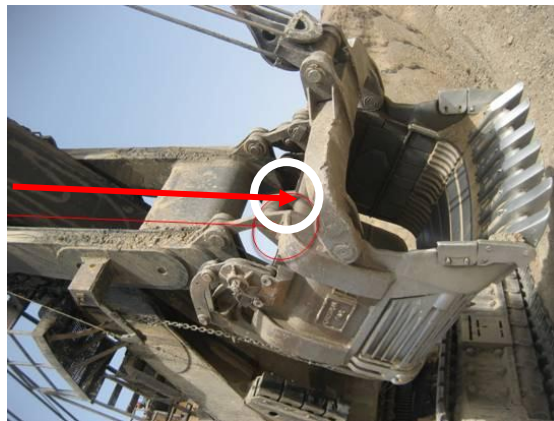
Figure 20: Laser beam reflecting from the dipper

Figure 21: Installation of a cooperative target on the dipper handle

4.5　Installation of the AGS on P&H Cable Shovel

I installed the AGS sensor apparatus on the saddle block of a P&H2100 cable shovel as shown in Figure 22. The installation process took less than two hours. The laser sensor

beam was aimed at the dipper in this position. I used the existing electrical cable trays connecting the crowd motor to the electrical room to wire the AGS cable to the operating room. By installing the arm geometry sensor apparatus on the saddle block, I measure the cab swing angle θ_1, the dipper handle or in the other word the saddle block joint angle θ_3, and the length of the extended crowd d_4 simultaneously. In this location, the arm geometry sensor rotates with the saddle block (the dipper handle) as represented in Figure 23 . Therefore, the angle, the angular velocity, and the angular acceleration of the AGS and the dipper handle are identical. The arm geometry sensor also swings with the shovel machinery house (the operator cabin) as represented in Figure 24. From this I know that at any instant the angle, the angular velocity, and the angular acceleration of the AGS and the shovel machinery (including the dipper, boom, and the operator cabin) are all identical. During the swing cycle, the lower portion of the shovel remains stationary.

The AGS remains stationary in respect to the dipper and measures the dipper handle extension d_4 while the dipper handle moves forward and backward as illustrated in Figure 25. While the cable shovel is operating, a touch screen monitor in the operator cabin instantaneously displays the joint variable values and the cable shovel three-dimensional arm-geometry as shown previously as the GUI in Figure 17.

The AGS apparatus installed on the saddle block has adequate distance from the cable shovel electrical room located underneath of the operator cabin. Consequently, I did not observe any sizable error in the yaw angle measurement by the AGS apparatus due to the disturbance of the magnetic field produced by the cable shovel rectifiers or electrical motors. In one experiment when I placed the AGS apparatus inside the operator cabin above the hoist and crowd thyristor rectifiers, and maintained the cable shovel in a fixed swing angle I noticed the yaw angle measured by the our apparatus drastically changed when the hoist or crowd motors started operating. This experiment confirmed that the top of the saddle block is a suitable location to install the AGS, where it is able to measure all cable shovel active joint variables while remaining relatively immune to electromagnetic noise generated by the cable shovel.

Figure 22: The arm geometry sensor apparatus (AGS) installed on a P&H cable shovel saddle block

Figure 23: Dipper and AGS positions at two different dipper handle angles

Figure 24: Shovel machinery and AGS positions at two different swing angles

Figure 25: Dipper and AGS positions for two different crowd extension lengths

The touch screen monitor installed in the cab shows the cable shovel arm geometry and joint variable values as represented in Figure 26. The software developed mainly by Motion Metrics engineers instantaneously displays the shovel's motion and arm-geometry.
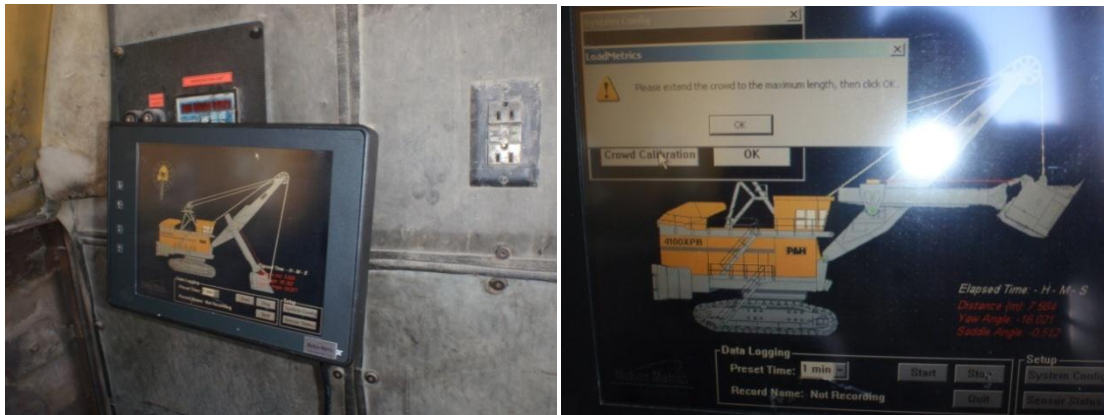
Figure 26: Graphical User Interface

4.6   Hall Effect Sensor Installation on DC Motors

As explained earlier, the P&H2100 cable shovel has two hoist motors, one crowd motor, and two swing motors [6], all of which separately excited DC motors. As stated earlier the armatures and fields of the swing motors are connected in series and have identical currents. However, each hoist motor armature has its own SCR driver which allows the hoist motor armature currents to be different. The fields of hoist motors are connected in series and consequently the hoist field currents are equal. In this work, three current sensors were installed to log two hoist motor armature and one field currents. Two current

sensors also measured the crowd armature and field currents. Current sensor specifications are shown in Table 4. Figure 27 and Figure 28 illustrate the installed armature and field current sensors respectively.
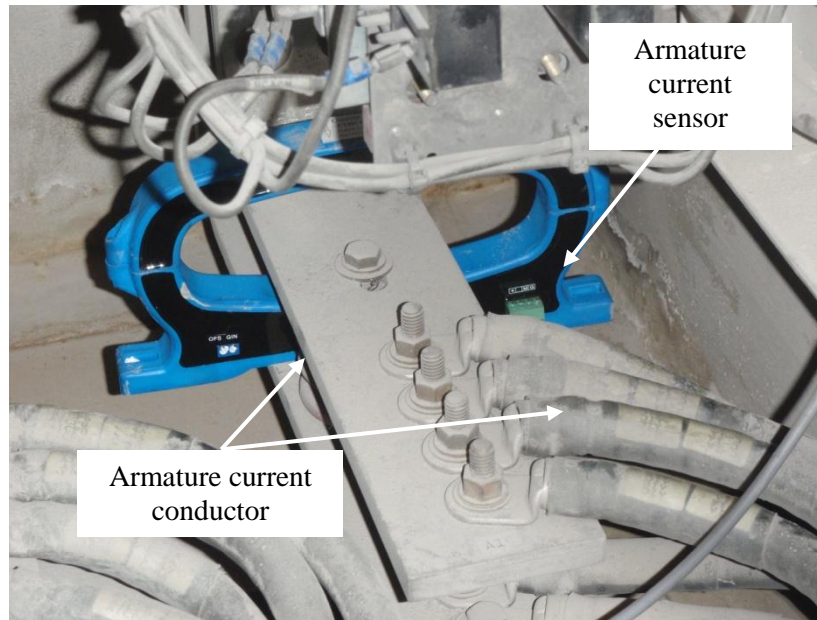
Figure 27: Armature current sensor installed in the field trail
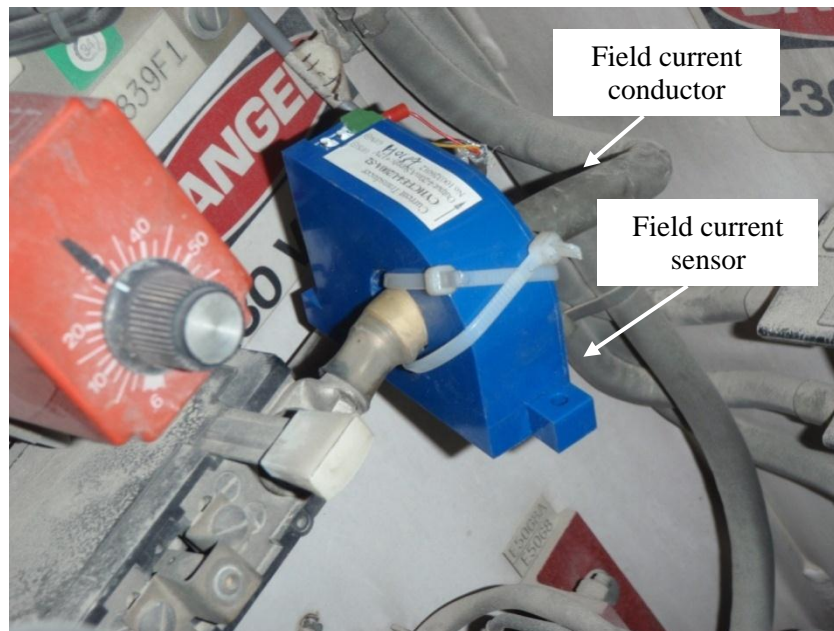
Figure 28: Field current sensor installed in the field trial

4.7   Boom Angle and the Cab Roll/ Pitch Sensor Installation

As explained in Chapter 1 the length of the suspension cables partially and slowly vary depending on the dipper position and its load. Consequently the angle of boom will change, represented by θ_2 in Figure 3. To measure this passive joint angle, I installed an inclinometer on the boom as shown in Figure 29. As shown in Table 4, the input range and the response time of the inclinometer are 20º and 200 ms, respectively.

Figure 29: The boom angle sensor installed on the cable shovel boom

Cable shovels quite often operate on non-level surface. To measure its roll and pitch angels with respect to the horizon I installed an inclinometer similar to the boom inclinometer in the operator cabin below the operator chair, as represented in Figure 30.

Figure 30: The cab roll/pitch angel sensor installed in the operator cabin

4.8   Data Logging During Shovel Operation

After I installed the sensors shown and verified their performance, I collected cable shovel data for different trajectories and payloads, noting as well the dipper fullness. The load being tested was dumped onto a waiting dump truck and weighed at a truck scale station located at the mine. The routines that I completed were as follows:

- The dipper handle moved horizontally to maximum and minimum extensions with only the crowd motor operating. Dipper loads: no load , full-load dipper, and 8420 kg

- The dipper handle moved vertically to its maximum and minimum extensions with only the hoist motor working. Dipper load: no load, , full-load dipper, and 8420 kg

- The operator cabin rotated from 0 º to 360 º angles with only the swing motor running. Dipper load: no load, full-load dipper, and 8420 kg load

- During the cable shovel digging cycle

- In this scenario, while the dipper door remained open (and the bucket empty), the operator went through a digging cycle in order to measure the cutting force.

- In all other experiments the cable shovel was operated normally

I carried out these experiments over four consecutive days, May 24-27, 2010. In our experiments, I logged the following signals:

- Two hoist motor armature currents i_{HA_1} & i_{HA_2}
- One crowd motor armature current i_{CA}
- One armature current for both swing motors, connected in series i_{SA}
- One field current for both hoist motors, connected in series i_{HF}
- One crowd motor field current i_{CF}
- One field current for two swing motors i_{SF}
- Dipper handle angle, relative to the horizontal plane (or with respect to the horizontal) θ_3
- Dipper handle extension d_4
- Shovel swing angle θ_1
- Shovel roll and pitch
- Boom angle θ_2

As stated earlier, the hoist motor field wirings and swing motor field wirings are connected in series. The logged sensor outputs for various scenarios listed in the previous page are plotted in the following figures:

Figure 31 shows two different values for the field current of the hoist motor: when the empty dipper moves upward and when the empty dipper moves downward.

Figure 32 shows the same signals as Figure 31, but with a full dipper. The hoist motor field current remains constant when the dipper is full.

Figure 31 and Figure 32 demonstrate the fact that the hoist armature current significantly increases when the dipper is full.

Figure 34 and Figure 35 illustrate that the field current for both the crowd and the swing motors remain relatively constant throughout different cycles of the cable shovel movements.
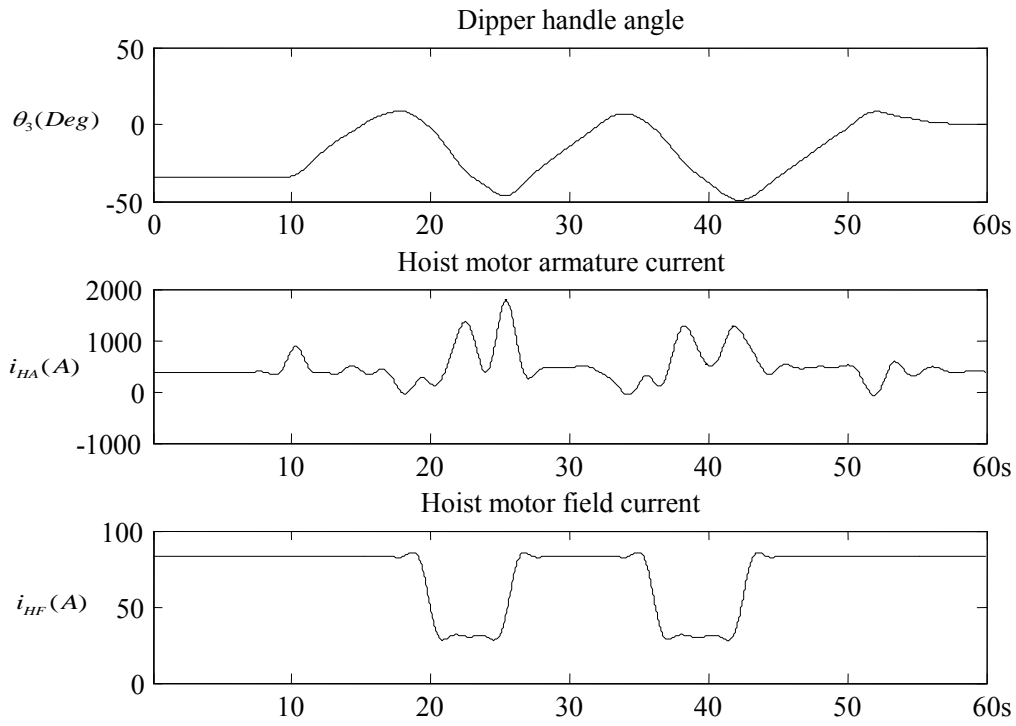
Figure 31: Dipper handle angle, the hoist motor armature, and field currents when the dipper moves upward and downward with zero load
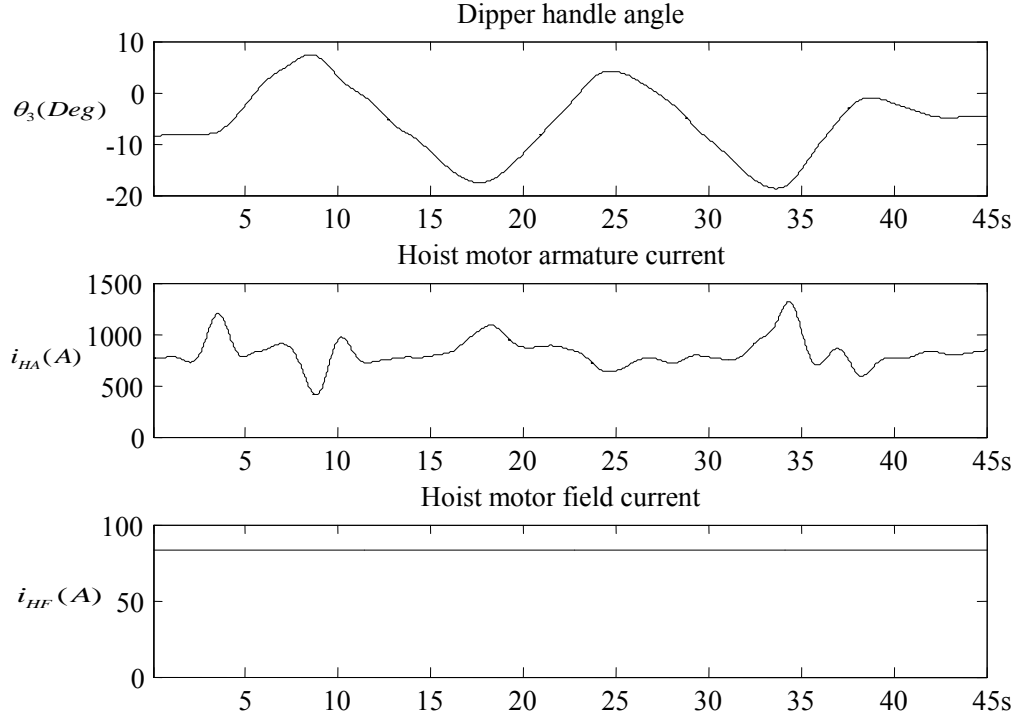
Figure 32: Cable-shovel dipper handle vertical angular movement vs. hoist motor armature and field currents when dipper is full
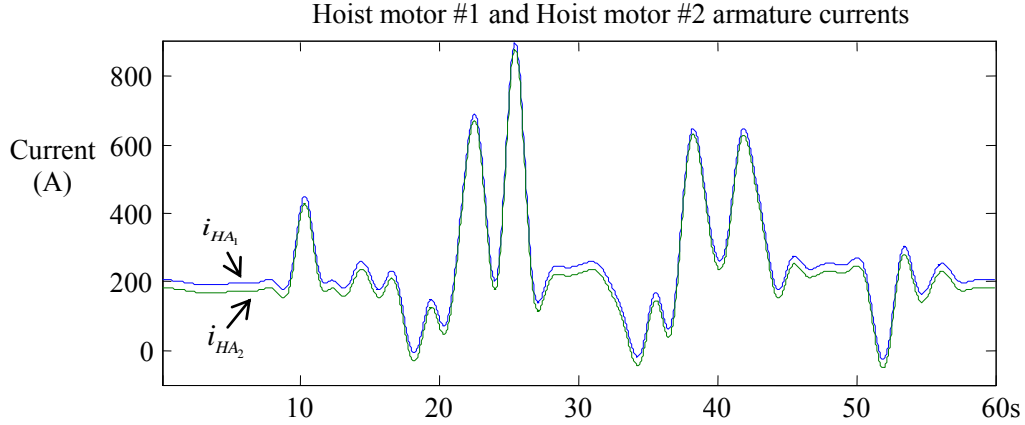
Figure 33: Armature currents of hoist motors #1 and #2 (when dipper is full and moving upward and downward)

Figure 33 demonstrates almost identical armature currents for the two hoist motors, despite having separate SCR motor drivers. Figure 34 shows the cable shovel dipper handle extension length and the crowd motor armature and field currents when the empty dipper moves forward and backward. Figure 35 shows the cable shovel swing angle and the swing motors armature and field currents when the shovel swings with an empty dipper.

Figure 36 shows several signals plotted in approximately one digging cycle, measured over a 30s time span. Note the significant rise in the crowd and hoist armature currents during a digging cycle.

Figure 37 represents the cable shovel dipper handle angle, swing angle, crowd length, swing armature current, crowd armature current, and hoist armature current for four cable shovel normal operation cycles over a 2-minute time span. Figure 38 represents the variation in boom joint angle during the four cycles shown in Figure 37.
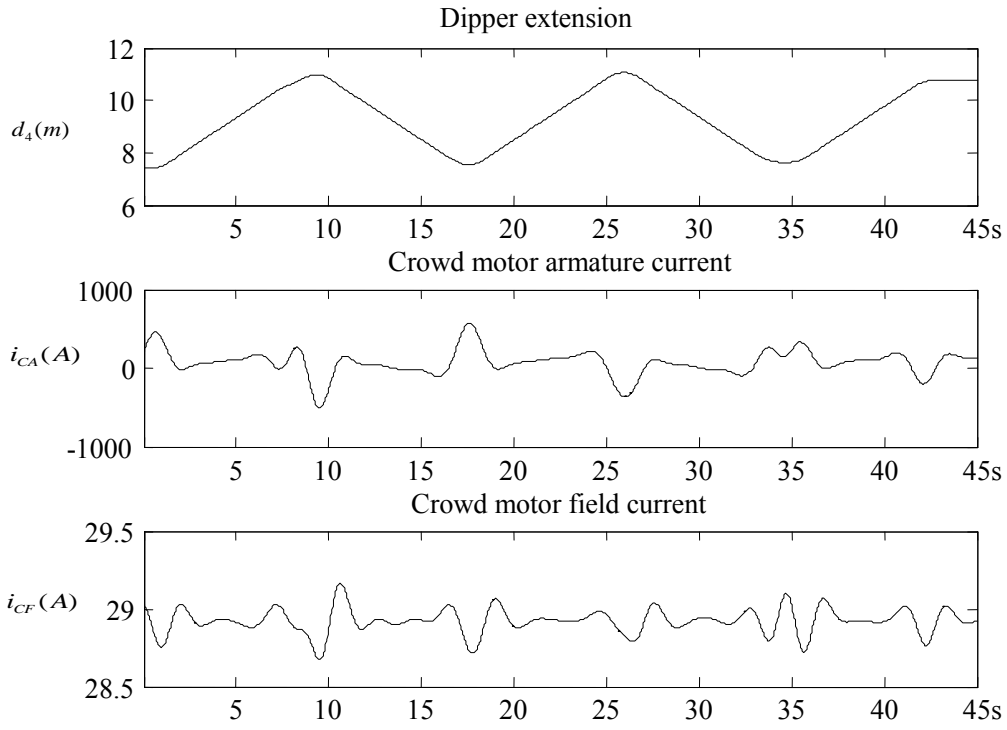
Figure 34: Dipper handle extension and the crowd motor armature and field currents when empty dipper moves forward and backward
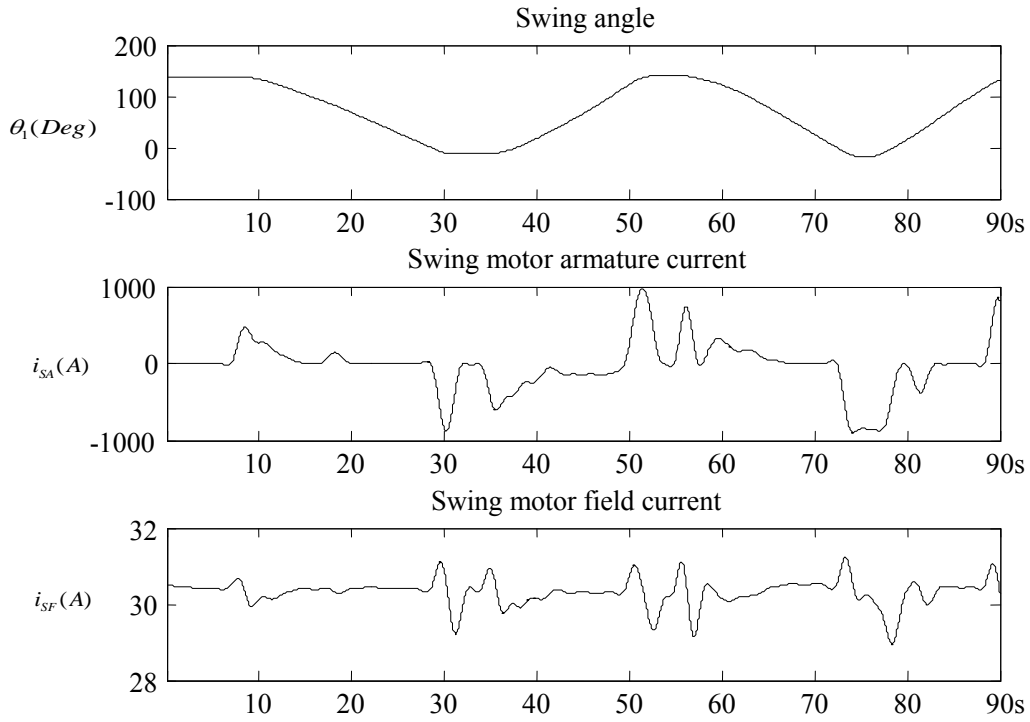
Figure 35: Swing motor armature and field currents when the dipper is empty
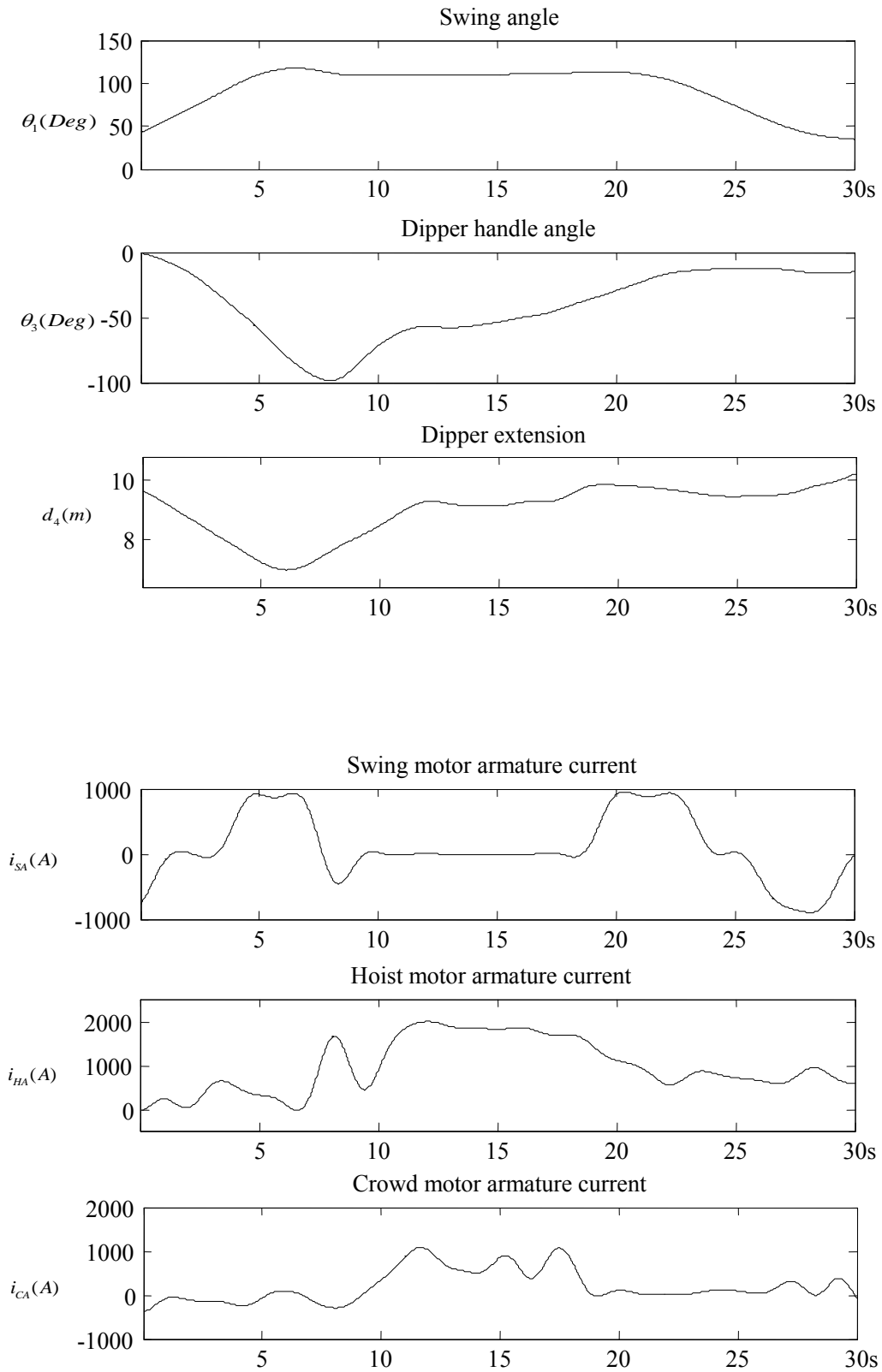
Figure 36: Nearly coincidental events during one digging cycle: swing angle, crowd length, swing armature current, crowd armature current and hoist armature current over 30 seconds
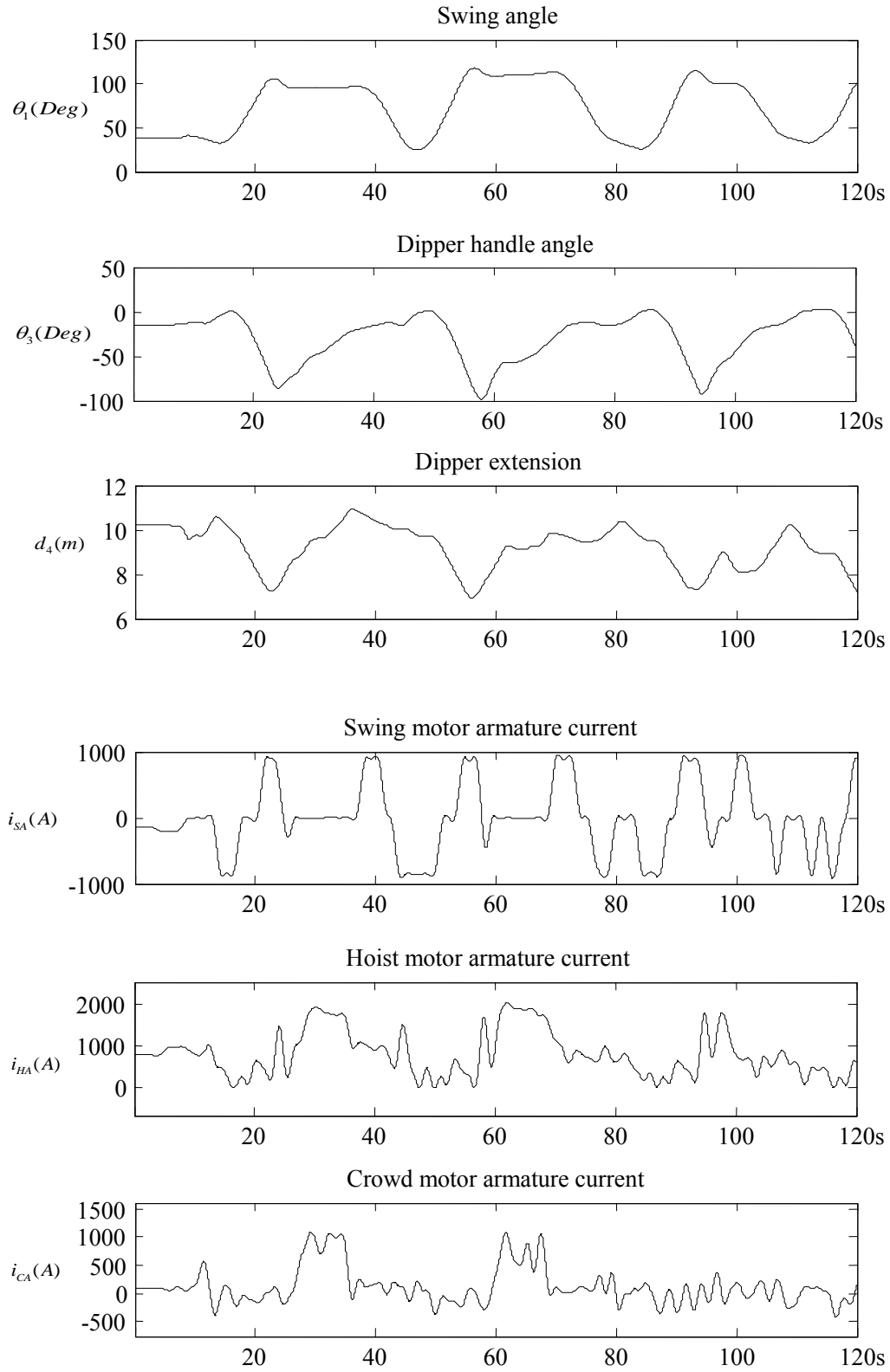
Figure 37: Cable shovel dipper handle angle, swing angle, crowd length, swing armature current, crowd armature current, and hoist armature current for four cable shovel normal operation cycles
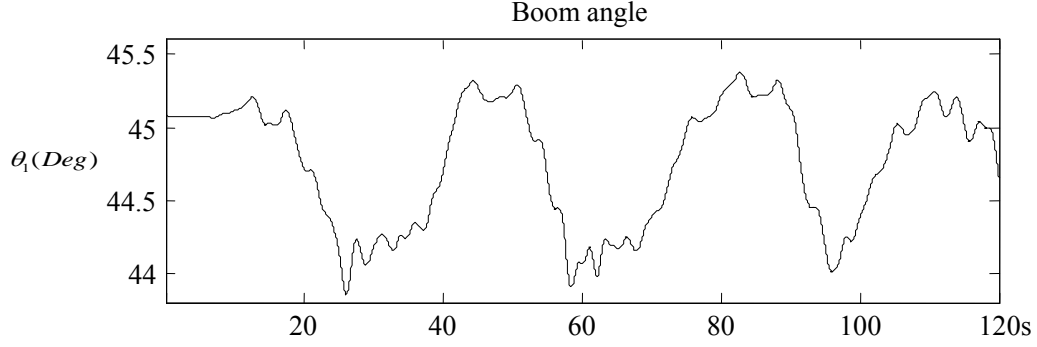
Figure 38: Variation in boom-angle for four typical shovel cycles shown in Figure 37

4.9   Velocitiy and Acceleration Estimation

To estimate the cable shovel dynamic parameters we require the cable shovel joint velocity and acceleration values. We can extract the velocities and accelerations of all joints by differentiating the position signals. However, estimation of the acceleration and velocity from position values will significantly magnify the noise. To reduce the noise amplified by differentiation, I used a first order low pass Butterworth-filter to eliminate this noise [90]. In order to avoid generating any of delay in our signals that I logged in our field test, I filtered all logged data including DC motor currents data.

Figure 39 and Figure 40 represent the crowd linear and angular velocity and acceleration achieved by differentiation and filtering the dipper handle angular. The dipper handle angle in this figure is the angle logged from the XSENS inertial sensor.
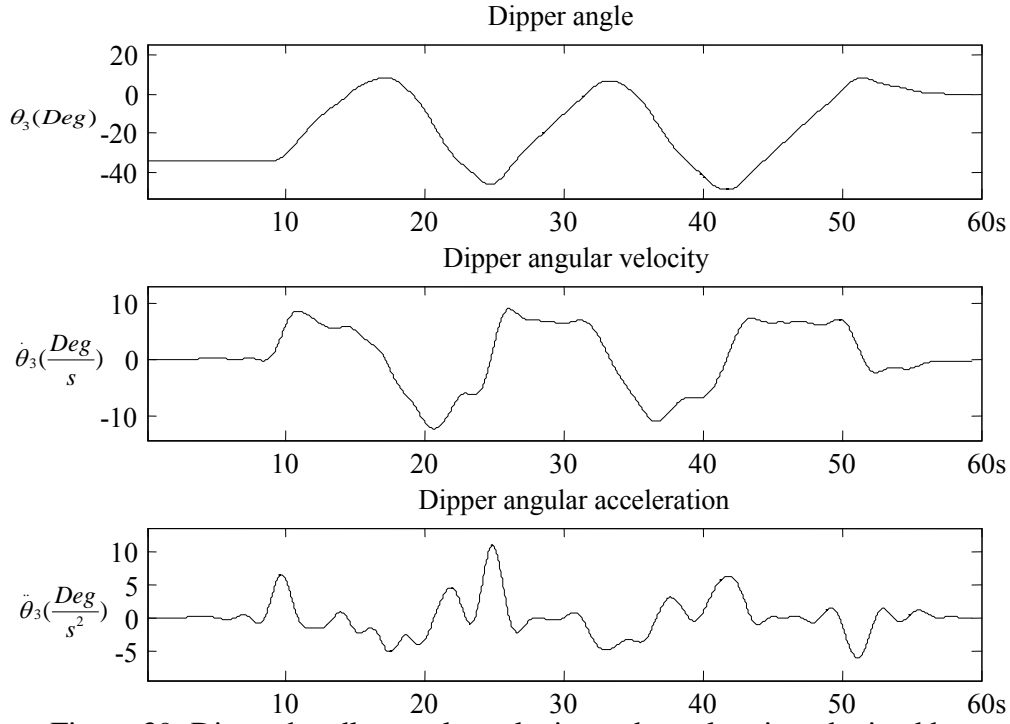
Figure 39: Dipper handle angular velocity and acceleration obtained by numerical differentiation and low-pass filtering the dipper handle angle
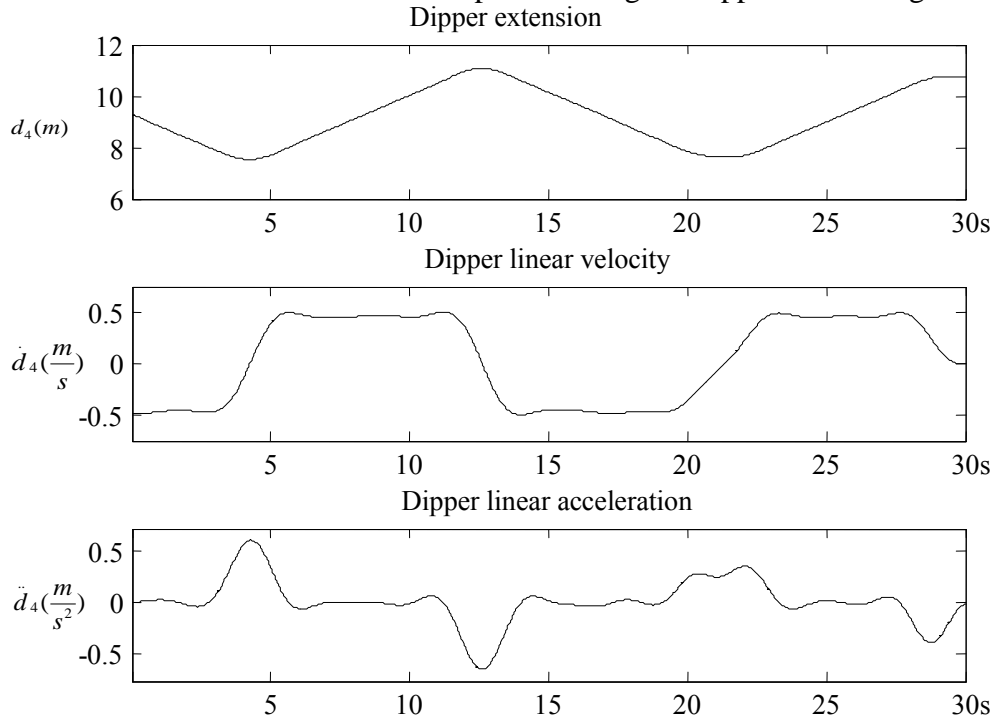
Figure 40: Dipper handle liner velocity and acceleration obtained by numerical differentiation and low-pass filtering of the dipper handle angle

5 CABLE SHOVEL PARAMETER IDENTIFICATION AND PAYLOAD ESTIMATION

In this chapter I discuss a simplified static and dynamic model of a typical cable shovel. Next, I present the different approaches to identify various parameters required for dynamic payload monitoring of the shovel. My experimental results are then compared to the payload measured using an accurate truck scale as benchmark.

5.1 Static Cable Shovel Equations Considering Dipper Handle Displacement and Rotation

I have already offered a detailed model of a typical cable shovel in section 2.4 of this thesis. In this section, I present a simplified discussion of the forces applied to the dipper and dipper handle in the static condition as depicted in Figure 42. I use this simplified model in order to estimate the cable shovel gravitational parameters

Our experimental results confirmed that the hoist motor toque significantly increases for the higher payload. As the main goal of this thesis is the dynamic payload monitoring of the cable shovel and in order to simplify the model, I consider only the degrees of freedom corresponding to the dipper handle joint angle Θ_3 (revolute joint), the crowd joint displacement d_4 (prismatic joint), and ignore the swing joint angle and the boom joint angle rotation. Furthermore, I assume perpendicular distance from z_2 to z_3 (the length of link 3) a_3 is equal to zero , and the coordinate frame of the saddle block revolute joint $o_2 x_2 y_2 z_2$ and coordinate frame of the crowd prismatic joint $o_3 x_3 y_3 z_3$ are located in the center of the saddle block assume as represented in Figure 41.
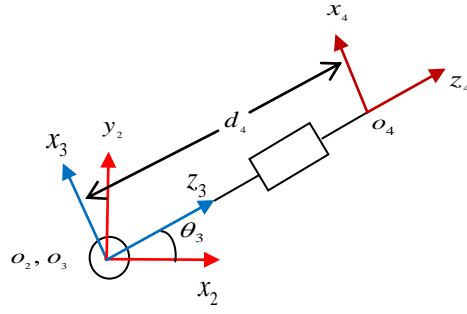
Figure 41: Vector diagram of dipper handle revolute joint and crowd prismatic joint
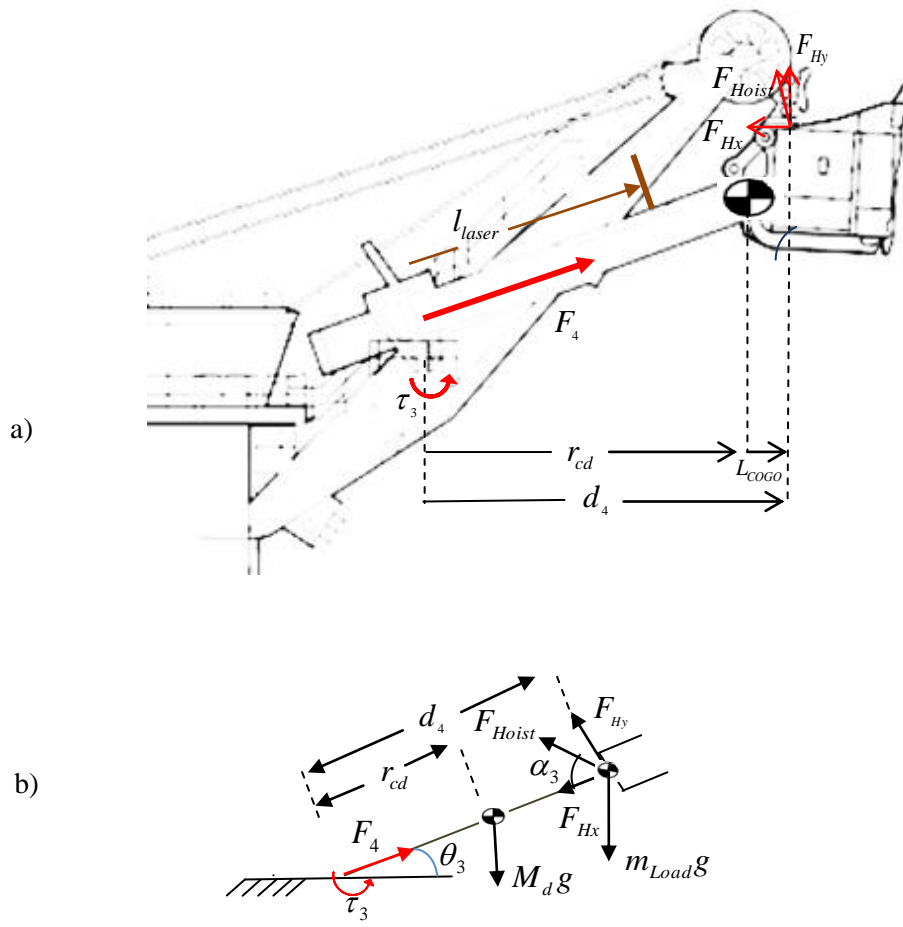
Figure 42: Forces exerted on the dipper handle and the dipper by the crowd motor and the hoist rope

The joint torque and force for the dipper handle revolute joint and the crowd prismatic joint can be computed from the related motor currents as follows:

$$F_4 = K_C i_{CA} \tag{50}$$

$$F_{Hoist} = K_H i_{HA} \tag{51}$$

$$F_{Hx} = F_{Hoist} Cos\alpha_3 \tag{52}$$

$$F_{Hy} = F_{Hoist} Sin\alpha_3 \tag{53}$$

$$\tau_3 = F_{Hoist} Sin\alpha_3 d_4 \tag{54}$$

Where α_3 is the angle between the hoist rope and the dipper handle, F_4 is the force exerted to the dipper by the crowd motor, F_{Hoist} is the force exerted to the dipper by the hoist rope, F_{Hy} is the component of the hoist force perpendicular to crowd, F_{Hx} is the component of the hoist force along the crowd, i_{HA} is the hoist motor armature current, i_{CA} is the crowd motor armature current, l_{laser} is the length measured by the laser sensor, L_{COG_Offset} is the fixed perpendicular distance from the center of the gravity of the dipper and the dipper handle to the dipper bail, K_C is the coefficient that is proportional to the crowd motor torque coefficient and the crowd gear ratio, and K_H is proportional to the hoist motor torque coefficient, the hoist gear ratio, and the hoist drum radius.

The moment balance about to the pivot point is:

$$M_d g r_{cd} c_3 + m_{Load} g d_4 c_3 = F_{Hoist} d_4 Sin\alpha_3 \tag{55}$$

Assuming no static friction, r_{cd} varies with the dipper position with respect to the saddle block and its value can be obtained as follows:

$$r_{cd} = d_4 - l_{COGO} \tag{56}$$

Therefore equation (62) can be written as:

$$M_d g d_4 c_3 - M_d g L_{COGO} c_3 + m_{Load} g d_4 c_3 = F_{Hoist} d_4 Sin\alpha_3 \tag{57}$$

The balance of force applied to the dipper handle along the z_3 axis is, assuming no static friction:

$$M_d g s_3 + m_{Load} g s_3 = F_4 - F_{Hoist} Cos\alpha_3 \tag{58}$$

From equations (51), (52), (58), and (59) I drive:

$$M_d g d_4 c_3 - M_d g L_{COGO} c_3 + m_{Load} g d_4 c_3 = k_H I_{HA} d_4 Sin\alpha_3 \tag{59}$$

$$M_d g s_3 + m_{Load} g s_3 = k_C I_{CA} - k_H I_{HA} Cos\alpha_3 \tag{60}$$

5.2 Computation of α_3 and Hoist Rope Length

As described earlier I used a 3DOFOT in our field trials for measuring the dipper handle angle and swing angle. I employed a laser sensor (or range-finder) to sense the extension of the dipper handle. $\theta_3 + \theta_2$ is directly measured by 3DOFOT (XSENS) sensor as follows:

$$\theta_3 = \theta_2 - XSENS_{Pitch} \tag{61}$$

The laser sensor measures the distance from the saddle block to the cooperative target installed on the dipper handle. The maximum crowd length measured by laser sensor in P&H2100BL cable shovel is 4.91m whereas the maximum value for d_4 is 10.79m. Therefore, d_4 is computed by adding following bias:

$$d_4 = l_{laser} + 5.89 \tag{62}$$

I obtained the angle α_3 and the hoist rope length from the sheave to the bail l_{SD} from the parameters measured by our AGS sensor apparatus and the cable shovel dimensions. The boom, the dipper handle, and the hoist rope form a triangle as shown in Figure 43 in red. Using the triangle:

$$l_{SD} = \sqrt{d_4^2 + L_{BS}^2 - 2L_{BS}d_4 Cos(\theta_2 - \theta_3)} \tag{63}$$

$$\alpha_3 = \cos^{-1}(\frac{l_{SD}^2 + d_4^2 - L_{BS}^2}{2l_{SD}d_4}) \tag{64}$$

Where L_{BS} is the distance from the saddle block to the sheave, l_{SD} is the distance from the sheave to the dipper, and d_4 is the distance from the saddle block to the center of the dipper. In the P&H2100BL cable shovel $\theta_2 = 45°$ is assumed to be fixed and $L_{BS} = 9.21m$.
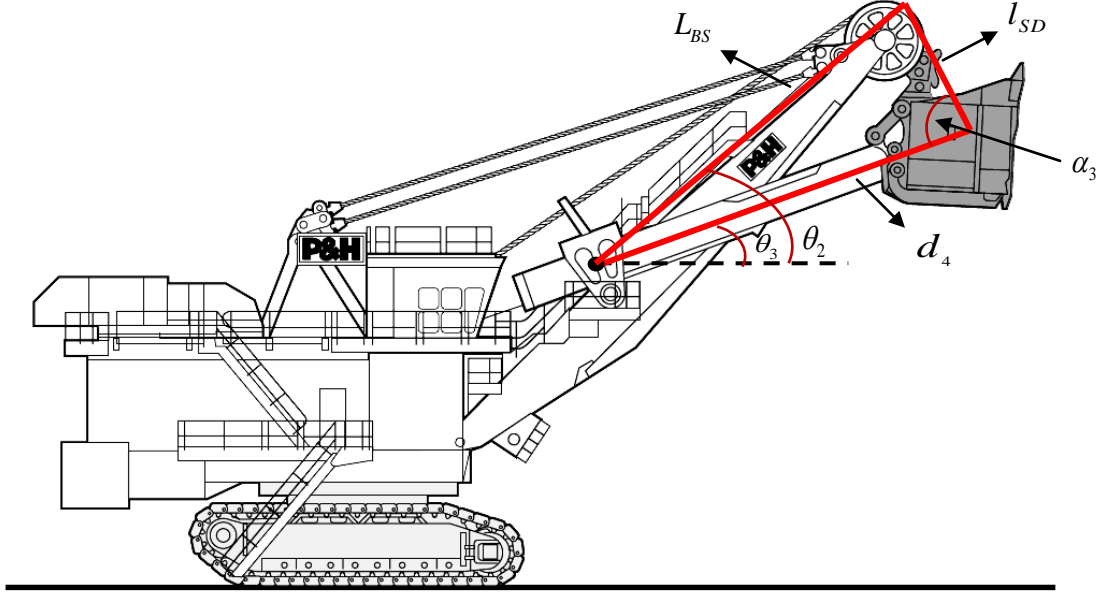
Figure 43: The triangle with on fixed side formed by the dipper handle,
the boom, and the hoist rope

5.3 Dynamic Analysis of Cable Shovel Considering Dipper Movements

As I explained earlier, I only considered the cable shovel dipper movements for the cable shovel payload estimation by modeling the dipper rotation and extension only. Since the dipper is fixed and cannot revolute around dipper handle, both dipper handle and the dipper are assumed as one rigid link. Hence, for the sake of dynamic payload monitoring, once again I assume the simplified two degrees of freedom manipulator model for the cable shovel, as shown in Figure 42. I utilize the Euler-Lagrange formulation method for our dynamic modeling:

$$\frac{d}{dt}\frac{\partial L}{\partial \dot{q}_i} - \frac{\partial L}{\partial q_i} = \tau_i \tag{65}$$

Where the Lagrangian is defined as $L = K - U$, and K and U are kinematic and potential energies respectively, τ_i is an external torque such as an actuator torque, and q_i is a set of independent coordinates.

71

$$K = \frac{1}{2} M_d (r_{cd}{}^2 \dot{\theta}_3{}^2 + \dot{r}_{cd}{}^2) + \frac{1}{2} I_3 \dot{\theta}_3{}^2 \tag{66}$$

$$U = M_d g r_{cd} s_3 \tag{67}$$

$$L = K - U = \frac{1}{2} M_d (r_{cd}{}^2 \dot{\theta}_3^2 + \dot{r}_{cd}{}^2) + \frac{1}{2} I_3 \dot{\theta}_3^2 - M_d g r_{cd} s_3 \tag{68}$$

Consider $q_1 = \theta_3$:

$$\frac{\partial L}{\partial \dot{\theta}_3} = I_3 \dot{\theta}_3 + M_d r_{cd}{}^2 \dot{\theta}_3 \tag{69}$$

$$\frac{d}{dt} \frac{\partial L}{\partial \dot{\theta}_3} = I_3 \ddot{\theta}_3 + M_d r_{cd}^2 \ddot{\theta}_3 + 2 M_d r_{cd} \dot{r}_{cd} \dot{\theta}_3 \tag{70}$$

$$\frac{\partial L}{\partial \theta_3} = -M_d g r_{cd} c_3 \tag{71}$$

Consider $q_2 = r_{cd}$:

$$\frac{\partial L}{\partial \dot{r}_{cd}} = M_d \dot{r}_{cd} \tag{72}$$

$$\frac{d}{dt} \frac{\partial L}{\partial \dot{r}_{cd}} = M_d \ddot{r}_{cd} \tag{73}$$

$$\frac{\partial L}{\partial r_{cd}} = M_d \dot{\theta}_3^2 r_{cd} - M_d g s_3 \tag{74}$$

Where $I_3 = I_{zz3}$ [12, 17, 38] and I_{zz3} is the dipper inertia about z_3 axis.

From equations 66:

$$I_{zz3} \ddot{\theta}_3 + M_d r_{cd}^2 \ddot{\theta}_3 + 2 M_d r_{cd} \dot{r}_{cd} \dot{\theta}_3 + M_d g r_{cd} c_3 = \tau_3 \tag{75}$$

$$M_d \ddot{r}_{cd} - M_d \dot{\theta}_3^2 r_{cd} + M_d g s_3 = F_4 - F_{Hx} \tag{76}$$

Where: $\dot{r}_{cd} = \dot{d}_4$ and $\ddot{r}_{cd} = \ddot{d}_4$.

$$I_{zz3}\ddot{\theta}_3 + M_d r_{cd}^2 \ddot{\theta}_3 + 2M_d r_{cd}\dot{d}_4\dot{\theta}_3 + M_d g r_{cd}\theta_3 = \tau_3 \tag{77}$$

$$M_d\ddot{d}_4 - M_d\dot{\theta}_3^2 r_{cd} + M_d g s_3 = F_4 - F_{Hx} \tag{78}$$

By considering friction, I can summarize the dynamic equation for the simplified model of the cable shovel as:

$$\begin{aligned}
&\begin{bmatrix} I_{zz3}+M_d r_{cd}^2 & 0 \\ 0 & M_d \end{bmatrix}\begin{bmatrix} \ddot{\theta}_3 \\ \ddot{d}_4 \end{bmatrix} + \begin{bmatrix} 0 & 2M_d r_{cd}\dot{\theta}_3 \\ -M_d r_{cd}\dot{\theta}_3 & 0 \end{bmatrix}\begin{bmatrix} \dot{\theta}_3 \\ \dot{d}_4 \end{bmatrix} + \begin{bmatrix} f_{v3} & 0 \\ 0 & f_{v4} \end{bmatrix}\begin{bmatrix} \dot{\theta}_3 \\ \dot{d}_4 \end{bmatrix} + \begin{bmatrix} f_{c3} & 0 \\ 0 & f_{c4} \end{bmatrix}\mathrm{sgn}\begin{bmatrix} \dot{\theta}_3 \\ \dot{d}_4 \end{bmatrix} \\
&+ \begin{bmatrix} M_d g r_{cd}c_3 \\ M_d g s_3 \end{bmatrix} = \begin{bmatrix} \tau_3 \\ F_4 - F_{Hx} \end{bmatrix}
\end{aligned} \tag{79}$$

By considering equations (51), (53), and (55), equation (80) is expressed as:

$$\begin{aligned}
&\begin{bmatrix} I_{zz3}+M_d r_{cd}^2 & 0 \\ 0 & M_d \end{bmatrix}\begin{bmatrix} \ddot{\theta}_3 \\ \ddot{d}_4 \end{bmatrix} + \begin{bmatrix} 0 & 2M_d r_{cd}\dot{\theta}_3 \\ -M_d r_{cd}\dot{\theta}_3 & 0 \end{bmatrix}\begin{bmatrix} \dot{\theta}_3 \\ \dot{d}_4 \end{bmatrix} + \begin{bmatrix} f_{v3} & 0 \\ 0 & f_{v4} \end{bmatrix}\begin{bmatrix} \dot{\theta}_3 \\ \dot{d}_4 \end{bmatrix} + \begin{bmatrix} f_{c3} & 0 \\ 0 & f_{c4} \end{bmatrix}\mathrm{sgn}\begin{bmatrix} \dot{\theta}_3 \\ \dot{d}_4 \end{bmatrix} \\
&+ \begin{bmatrix} M_d g r_{cd}c_3 \\ M_d g s_3 \end{bmatrix} = \begin{bmatrix} K_H i_{HA}d_4 Sin\alpha_3 \\ K_C i_{CA} - K_H i_{HA}Cos\alpha_3 \end{bmatrix}
\end{aligned} \tag{80}$$

When the dipper has a payload, I assume the load center of gravity to be equal to d_4 and ignore the inertia of the payload in comparison to I_{zz3}, and thus I can write:

$$\begin{aligned}
&\begin{bmatrix} I_{zz3}+M_d r_{cd}^2+m_{Load}d_4^2 & 0 \\ 0 & M_d+m_{Load} \end{bmatrix}\begin{bmatrix} \ddot{\theta}_3 \\ \ddot{d}_4 \end{bmatrix} + \begin{bmatrix} 0 & 2(M_d r_{cd}+m_{Load}d_4)\dot{\theta}_3 \\ -(M_d r_{cd}+m_{Load}d_4)\dot{\theta}_3 & 0 \end{bmatrix}\begin{bmatrix} \dot{\theta}_3 \\ \dot{d}_4 \end{bmatrix} \\
&+ \begin{bmatrix} f_{v3} & 0 \\ 0 & f_{v4} \end{bmatrix}\begin{bmatrix} \dot{\theta}_3 \\ \dot{d}_4 \end{bmatrix} + \begin{bmatrix} f_{c3} & 0 \\ 0 & f_{c4} \end{bmatrix}\mathrm{sgn}\begin{bmatrix} \dot{\theta}_3 \\ \dot{d}_4 \end{bmatrix} + \begin{bmatrix} (M_d r_{cd}+m_{Load}d_4)g c_3 \\ (M_d+m_{Load})g s_3 \end{bmatrix} = \begin{bmatrix} K_H i_{HA}d_4 Sin\alpha_3 \\ K_C i_{CA} - K_H i_{HA}Cos\alpha_3 \end{bmatrix}
\end{aligned} \tag{81}$$

5.4 Cable Shovel Parameter Identification Using Load Information and Least-Squares Estimation Technique

Our first objective is to identify a number of cable shovel parameters. This can be effectively achieved by applying the least-squares estimation(LSE) technique using the

data I gathered from two cases: when the dipper is empty and when the dipper carries a known load.

The main criteria to be able to employ LSE is to use a model which is linear with respect to a suitably chosen set of parameters. This approach has been employed in the robotics field for dynamic identification of various manipulator structures [44, 45, 47, 50]. The following vector equation is used to identify the manipulator parameters:

$$\tau = W(q, \dot{q}, \ddot{q})\psi \tag{82}$$

Where ψ is a set of suitably defined cable shovel dynamic parameters, τ is the joint torque vector, and $W(q, \dot{q}, \ddot{q})$ is a matrix of nonlinear functions of joint displacements, velocities and accelerations. Our procedure for identifying the cable shovel parameters used in this thesis is as follows:

- Note that one of the major differences of our thesis in comparison to other work reported in the literature [39-46, 90] is that I am not able to directly sense the torques and forces applied at the joints. Therefore, I need to identify both the cable shovel parameters and the joint motor coefficients. To do this I use a known payload. I discuss the details of the novel approach later in this section.
- I minimize the parameters to be identified. I require identifying fewer parameters by considering only the dipper handle movement as a prominent two degrees of freedom.
- I use the cable shovel logged data for different trajectories and different payload discussed in section 4.8. I selected these trajectories based on several factors such as a study of earlier literature in similar area of research, our identification results taken from a virtual model of the cable shovel built in MATLAB environment, and last but not least the trajectories of the cable shovel during its normal operations.
- I identified the cable shovel parameters by using least square technique.

By taking into account that $r_{cd} = d_4 - L_{COGO}$, $r_{cd}^2 = d_4^2 + L_{COG\_Offser}^2 - 2d_4 L_{COG\_Offset}$, $\dot{r}_{cd} = \dot{d}_4$ and $\ddot{r}_{cd} = \ddot{d}_4$ equation 82 can be written as:

$$K_H i_{HA} d_4 Sin\alpha_3 - I_{zz3} \ddot{\theta}_3 - M_d d_4^2 \ddot{\theta}_3 - M_d L_{COGO}^2 \ddot{\theta}_3 + 2M_d d_4 L_{COGO} \ddot{\theta}_3$$

$$-m_{Load} d_4^2 \ddot{\theta}_3 - 2M_d \dot{d}_4 \dot{\theta}_3 d_4 + 2M_d \dot{d}_4 \dot{\theta}_3 L_{COGO} - 2m_{Load} d_4 \dot{d}_4 \dot{\theta}_3 \tag{83}$$

$$-f_{v3} \dot{\theta}_3 - f_{c3} \, \text{sgn}(\dot{\theta}_3) - M_d g c_3 d_4 + M_d g c_3 L_{COGO} - m_{Load} d_4 g c_3 = 0$$

$$K_C i_{CA} - K_H i_{HA} Cos\alpha_3 - M_d \ddot{d}_4 - m_{Load} \ddot{d}_4 + M_d d_4 \dot{\theta}_3^2 - M_d L_{COGO} \dot{\theta}_3^2 + m_{Load} d_4 \dot{\theta}_3^2$$

$$-f_{v4} \dot{d}_4 - f_{c4} \, \text{sgn}(\dot{d}_4) - M_d g s_3 - m_{load} g s_3 = 0 \tag{84}$$

Equation (84) and (85) can be written in the following form:

$$K_H i_{HA} d_4 Sin\alpha_3 - (I_{zz3} + M_d L_{COGO}^2) \ddot{\theta}_3 - M_d (2 \dot{d}_4 \dot{\theta}_3 d_4 + g c_3 d_4 + d_4^2 \ddot{\theta}_3)$$

$$+M_d L_{COGO} (g c_3 + 2 \dot{d}_4 \dot{\theta}_3 + 2 d_4 \ddot{\theta}_3) - f_{v3} \dot{\theta}_3 - f_{c3} \, \text{sgn}(\dot{\theta}_3) \tag{85}$$

$$=m_{Load} (d_4 g c_3 + d_4^2 \ddot{\theta}_3 + 2 d_4 \dot{d}_4 \dot{\theta}_3)$$

$$K_C i_{CA} - K_H i_{HA} Cos\alpha_3 + M_d (-g s_3 - \ddot{d}_4 + d_4 \dot{\theta}_3^2) - M_d L_{COGO} \dot{\theta}_3^2 +$$

$$-f_{v4} \dot{d}_4 - f_{c4} \, \text{sgn}(\dot{d}_4) = m_{load} (g s_3 + \ddot{d}_4 - d_4 \dot{\theta}_3^2) \tag{86}$$

Equations (86) and (87) can be rewritten as:

$$\Upsilon(q, \dot{q}, \ddot{q}, m_{load}) = \Lambda(q, \dot{q}, \ddot{q}, i_{HA}, i_{CA}) \Phi \tag{87}$$

where:

$$\Upsilon = \begin{bmatrix} m_{Load} (d_4 g c_3 + d_4^2 \ddot{\theta}_3 + 2 d_4 \dot{d}_4 \dot{\theta}_3) \\ m_{Load} (g s_3 + \ddot{d}_4 - \dot{\theta}_3^2 d_4) \end{bmatrix}$$

$$\Lambda = \begin{bmatrix} -(2 \dot{d}_4 \dot{\theta}_3 d_4 + g c_3 d_4 + d_4^2 \ddot{\theta}_3) & -(g c_3 + 2 \dot{d}_4 \dot{\theta}_3 + 2 d_4 \ddot{\theta}_3) & i_{HA} d_4 Sin\alpha_3 & 0 & -\ddot{\theta}_3 & -\dot{\theta}_3 & -\text{sgn}(\dot{\theta}_3) & 0 & 0 \\ (-g s_3 - \ddot{d}_4 + d_4 \dot{\theta}_3^2) & -\dot{\theta}_3^2 & -i_{HA} Cos\alpha_3 & i_{CA} & 0 & 0 & 0 & -\dot{d}_4 & -\text{sgn}(\dot{d}_4) \end{bmatrix}$$

$$\Phi = \begin{bmatrix} M_d \\ M_d L_{COGO} \\ K_H \\ K_C \\ (I_{zz3} + M_d L_{COGO}^2) \\ f_{v3} \\ f_{c3} \\ f_{v4} \\ f_{c4} \end{bmatrix}$$

$$\tag{88}$$

Where Φ is the vector of the cable shovel dynamic parameter plus K_H, and K_C. Φ can be estimated by least square technique [42, 44, 47] as:

$$\Phi = inv(\Lambda^{'}\Lambda)\Lambda^{'}\Upsilon \qquad (89)$$

In order to estimate Φ, I carried out the following steps:

1. I moved the dipper through a number of different trajectories while carrying no load and I ensured that the cable shovel did not swing. I logged two hoist motor armature currents, i_{HA_1} & i_{HA_2}, plus one crowd motor armature current, i_{CA}, as well as the dipper handle angle, θ_3, and the crowd extension d_4 at a 30Hz sample rate .

2. I next created a vector Υ_{NL} and a matrix Λ_{NL}, where NL stands for "No Load" for n set of data logged in step 1. Υ is be a $2n\ x1$ vector and Λ is a $2n\ x9$ matrix.

3. I repeated step 1 and step 2 while the dipper carried a known load and obtained and Υ_{WL} vector and Λ_{WL} matrix, where WL stands for "With Known Load". In order to measure the actual load, the shovel operator dropped the load into a truck and the truck was then weighed using a drive-over scale. The net load in the dipper was 8420 Kg in this experiment.

4. Next, I combined the Υ_{NL} and Υ_{WL} vectors and Λ_{NL} and Λ_{WL} matrices.

5. Then I estimated Φ vector which contains the cable shovel dynamic parameters and coefficients, K_H, and K_C from equation (97) by LSE technique:

$$\begin{bmatrix} \Upsilon_{NL} \\ \Upsilon_{WL} \end{bmatrix} = \begin{bmatrix} \Lambda_{NL} \\ \Lambda_{WL} \end{bmatrix} \Phi \qquad (90)$$

Figure 44 represents the diagram of our cable shovel parameter identification method. In equation (91), Υ_{NL} and Λ_{NL} contains the cable shovel internal parameters. Υ_{WL} and Λ_{WL} also contains the external forces in equation (91). An added advantage of this approach is that I estimated the friction coefficients in the presence of the known payload. These experiments are indeed free-space motion of the arm and any contact with the mine surface during data logging was avoided.
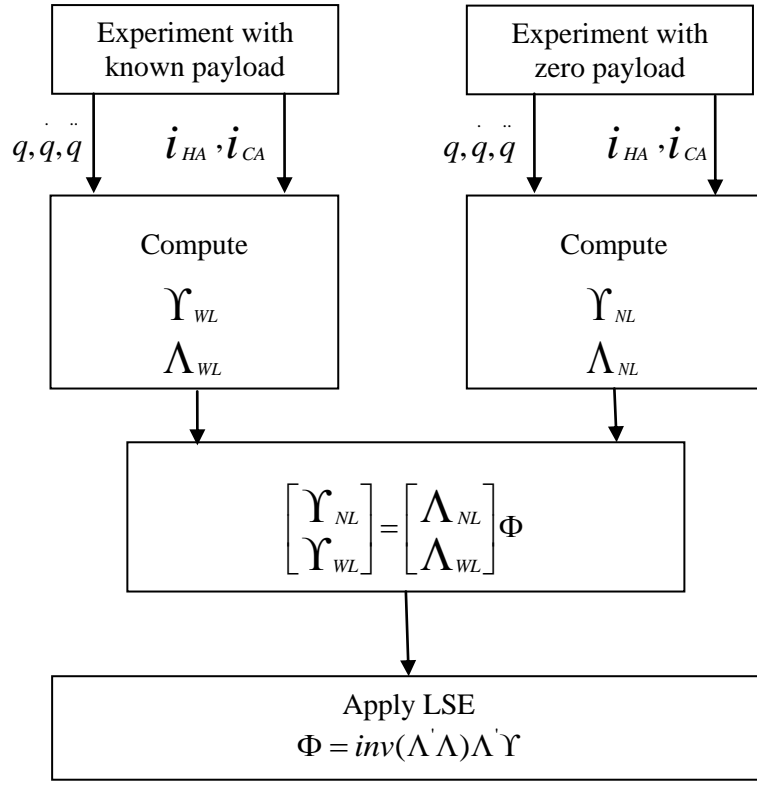
Figure 44: Identification of cable shovel parameters using LSE

5.5 Estimation of Gravitational Parameters

When the cable shovel dipper is stationary, the hoist and the crowd actuators must collectively balance the dipper and the dipper handle gravitational forces plus the payload. Thus, in the static condition, equation (88) can be expressed as:

$$
\begin{bmatrix} m_{Load}d_4 g c_3 \\ m_{Load} g s_3 \end{bmatrix} = \begin{bmatrix} -g c_3 d_4 & -g c_3 & i_{HA} d_4 Sin\alpha_3 & 0 \\ -g s_3 & 0 & -i_{HA} Cos\alpha_3 & i_{CA} \end{bmatrix} \begin{bmatrix} M_d \\ M_d L_{COGO} \\ K_H \\ K_C \end{bmatrix} \tag{91}
$$

Or:

$$
\Upsilon(q,m_{load}) = \Lambda(q,i_{HA},i_{CA})\Phi_S \tag{92}
$$

Equation (93) is linear in Φ_S which include the gravitational parameters M_d and $M_d L_{COGO}$ as well as the coefficients K_H and K_C. In order to estimate the cable shovel

77

gravitational parameters I carried out the five steps explained in section 5.4 and Figure 44 of this thesis in different static poses. The known load was again 8420Kg in our experiment.

In this work, I focused on the specific period of time when the cable shovel joint variables, the motor armature currents, and the motor field currents *all* remained nearly constant. After reviewing the data logged from different trajectories in the field trials at Sarcheshmeh Copper mine, I selected those data which met the above definition of a 'static' posture or geometry. Moreover, I averaged the values for the duration that the cable shovel remained motionless. I selected 50 different static postures positions of the dipper with different values for $i_{HA_1} \& i_{HA_2}$, i_{CA}, θ_3 , and d_4. The dipper was empty in all selected poses. Then, I created Υ_{NL} vector and Λ_{NL} matrix for that set of fifty logged data.

In the next stage, I chose a different set of fifty static positions when the dipper carried the known load. Then I created Υ_{WL} vector and Λ_{WL} matrices by using $i_{HA_1} \& i_{HA_2}$, i_{CA}, θ_3 , and d_4. All of these data were derived from those 50 static postures with a known load. Subsequently I combined Υ_{WL} vector and Λ_{WL} matrix with the Υ_{NL} and Λ_{NL} , and formed equation (91). In the next step I estimated the Φ_S vector from equation (90) employing LSE. Table 5 shows the cable shovel parameters I identified:

Table 5: Cable shovel parameters identified from different static positions

$M_d\,(Kg)$	$L_{COGO}\,(m)$	$K_H\,(N\,/\,A)$	$K_C\,(N\,/\,A)$
56960	3.27	1715	4418

5.6   Estimation of Dynamic Parameters and Friction Coefficients

As I discussed earlier in section 2.3 of this thesis, dynamic equations of the cable shovel motion can be expressed as:

$$D(q)\ddot{q} + C(q,\dot{q})\dot{q} + f_V \dot{q} + f_C \, \text{sgn}(\dot{q}) + G(q) = \tau \qquad (93)$$

I could identify $D(q)$, $C(q,\dot{q})$, $G(q)$ and the friction coefficients by using logged data from those trajectories where the joint velocities and accelerations of the cable shovel are not zero. However, as I discussed in section 5.5, I can only identify $G(q)$ in a static condition. At this stage, I am able to identify the full dynamic parameters of the cable shovel saddle block revolt joint and the crowd prismatic joint including gravitational parameters. Throughout our parameter identification procedure I examined a majority of trajectories and cycles in our data. I did not use two set of the logged data of the field trials in our cable shovel parameter identification. First, during the time that the hoist motor field current is reduced to 30A as represented in Figure 31. At this time, K_H would have a different value in comparison with the time that the hoist motor field current is 70 Amps. This situation usually occurs when the cable shovel lower is lowering the empty dipper. A second component, the data recorded during the digging cycle, is not used for parameter identification because the external forces applied to the dipper during the digging cycle are not measurable.

As I explained in section 5.6 I moved the dipper through a number of different trajectories while carrying no load in the bucket and logged i_{HA_1} & i_{HA_2}, i_{CA}, θ_3 , and d_4 at a 30 Hz sampling rate. Subsequently I created Υ_{NL} vector and Λ_{NL} for the set of 9000 data points which I logged for five minutes.

In the next phase, I loaded the dipper and again moved the dipper through a range of different trajectories and logged data at the same sampling rate. Following this I arranged for the shovel operator to dump the load into a truck. Using a truck scale, located within the mine, I measured the load in the truck bed with a high accuracy of 0.03%. The value we measured here is used as reference weight in this thesis. I carried out our experiment in Sarchechmeh copper mine located in Kerman, Iran. The cable shovel model was PH2100XP with the dipper capacity of 35,000 Kg. I moved the dipper handle horizontally to its maximum and minimum limits and vertically to its maximum and

minimum limits with the known load while logging data at the same time. I also moved the dipper through a range of normal operations that included a cabin swing. I discussed in considerable depth those trajectories and related scenarios in section 4.8 of this thesis. I also repeated the aforementioned experiments for several cycles with a known payload.

The main factor that limited our testing was cost: each hour of the normal shovel operation is worth more than US$100,000. Our experiments interrupted the normal operation of the shovel for approximately eight hour. A second limitation in our experiment was the maximum load that I could measure was 10 tonnes. Other factors that limited the maximum load in our study were the maximum capacity of the weigh scale at the mine and the relatively limited capacity and mass of the dump truck. I performed our cable shovel experiments on the empty dipper and full dipper over a course of four days.

After experimenting with the known load and logging the data, I computed Υ_{WL} vector and Λ_{WL} matrix; then combined them with the Υ_{NL} and Λ_{NL}, and formed equation (91). Similar to our experiment with an empty dipper, I used the 9000 set of data to compute Υ_{WL} vector and Λ_{WL} matrix. In the next step I estimated the Φ vector from equation (90) employing LSE. Table 6 represents the whole set of the cable shovel parameters that I identified from the logged data.

Table 6: Cable shovel parameters identified from dynamic experiments

$M_d\,(Kg)$	$L_{COGO}\,(m)$	$K_H\,(N/A)$	$K_C\,(N/A)$	$I_{zz3}(kgm^2)$	$f_{v3}(\frac{Nms}{rad})$	$f_{c3}(Nm)$	$f_{v4}(\frac{Ns}{m})$	$f_{c4}(N)$
54300	2.82	1940	3950	287900	3800	340	1473	480

Experimental results reveal that the cable shovel hoist and crowd friction coefficients change with the payload of the dipper [39]. Because the dipper has two different payload values, 0Kg and 8420Kg, in our experimental parameter identification approach, the estimated friction represented in table 8 are the best fit in the least square sense.

5.7　Dynamic Payload Monitoring

Payload estimation is a practical way to validate the accuracy of the parameters that I

identified [42, 90]. Further, an accurate payload estimate would enhance the efficiency of the mine, as I discussed in first chapter. I can express equation (94) as follow:

$$\Lambda(q,\dot{q},\ddot{q},i_{HA},i_{CA}) = \psi m_{load} \tag{94}$$

Where:

$$\psi = \frac{(d_4 g c_3 + d_4^2 \ddot{\theta}_3 + 2 d_4 \dot{d}_4 \dot{\theta}_3)}{\Phi} \tag{95}$$

Then I estimate m_{load} by least square technique as follow:

$$m_{load} = inv(\psi'\psi)\psi'\Lambda \tag{96}$$

To investigate the accuracy and repeatability of the parameters Φ that I identified in the first day of the field trial, I estimated the payload inside the dipper by using the identified parameters and the data that I logged in the second, third and fourth day of the field trial.

Figure 45 represented the estimated payload when the shovel operator lifts the dipper. The estimated average payload in this test is 8310 kg, which is approximately 1.3% less than actual payload of 8420 kg. I used Recursive Least Squares Estimation (RLSE) technique to estimate the payload while the dipper moves [42, 44, 47]. Figure 46 shows the related variables for the saddle block revolute joint and Figure 47 represents the related variables for the crowd prismatic joint. Together these were used to estimate the payload represented in Figure 45.

Based on different experiments I discovered that the best trajectory for the estimation of the payload is during the shovel swing regime. Figure 48 represents the estimated payload during the cable shovel swing. I estimated the average payload in this trajectory to be 8340 kg. However, throughout the shovel swing regime, I found that the current of the hoist and crowd motors, the angle of the dipper handle and the length of crowd all displayed little variation. Table 7 represents the estimated loads for different payloads and trajectories.

Figure 49 represents the dynamic payload estimated during lifting the dipper with 0Kg payload along with the cable shovel joint variables. The average estimated payload in the mentioned trajectory is 175 kg. Figure 50 represents the dynamic payload estimated during lifting the dipper when the dipper is full along with the cable shovel

joint variables. The average estimated payload in the mentioned trajectory is 35700 kg.

Table 7:   Payload estimation results

Trajectory	Payload(kg)	Estimated payload(kg)	Standard deviation
Shown in Figure 45	8420	8340	579
Shown in Figure 48	8420	8402	104
Shown in Figure 49	0	176	757
Shown in Figure 50	Full dipper	35700	1425
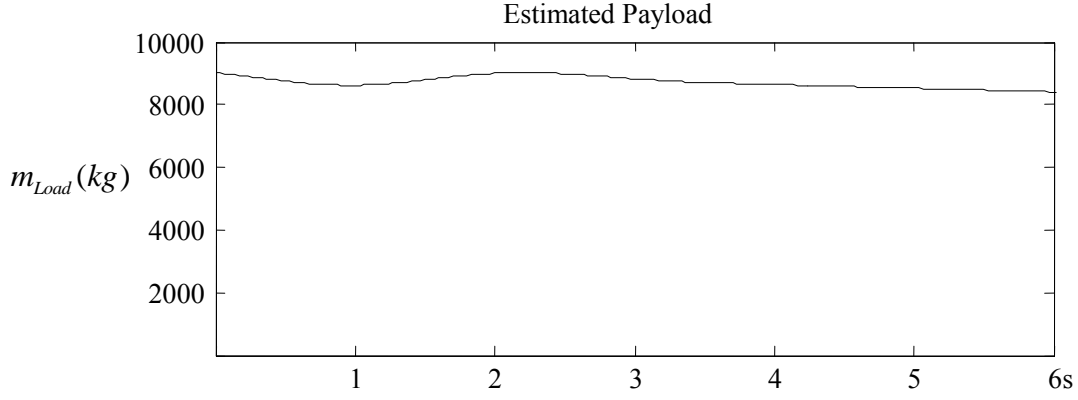
Estimated Payload

Figure 45: Dynamic estimated payload, dipper loaded with 8420 kg payload
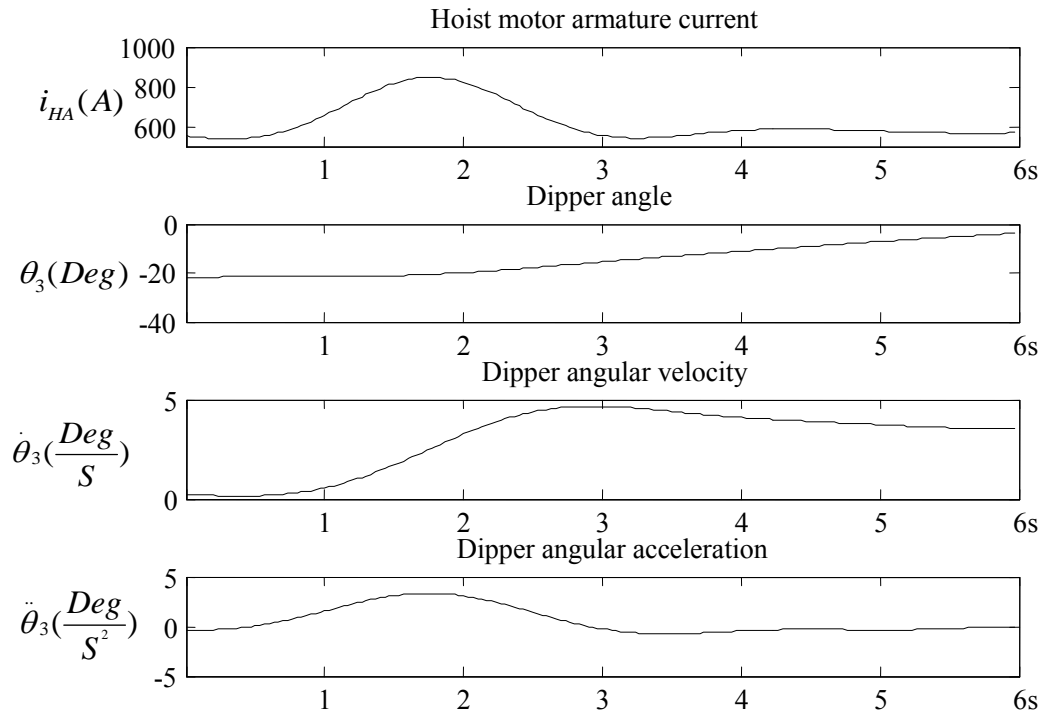
Figure 46: Saddle block revolute joint variables used to estimate payload shown in Figure 45
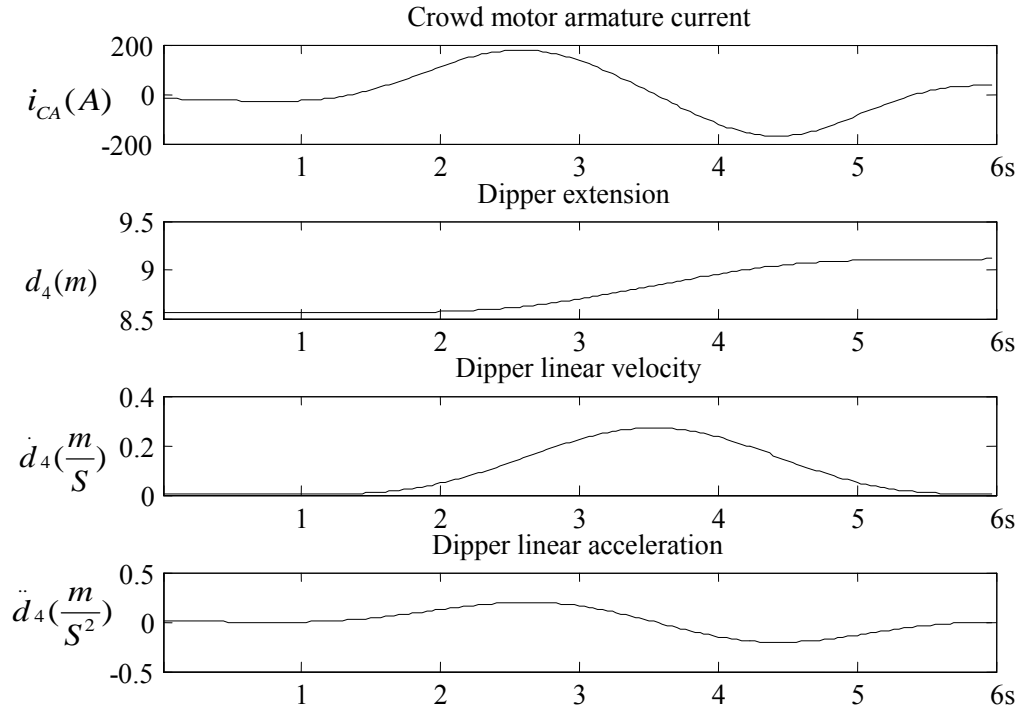
Figure 47: Crowd prismatic joint variables used to estimate payload shown in Figure 45
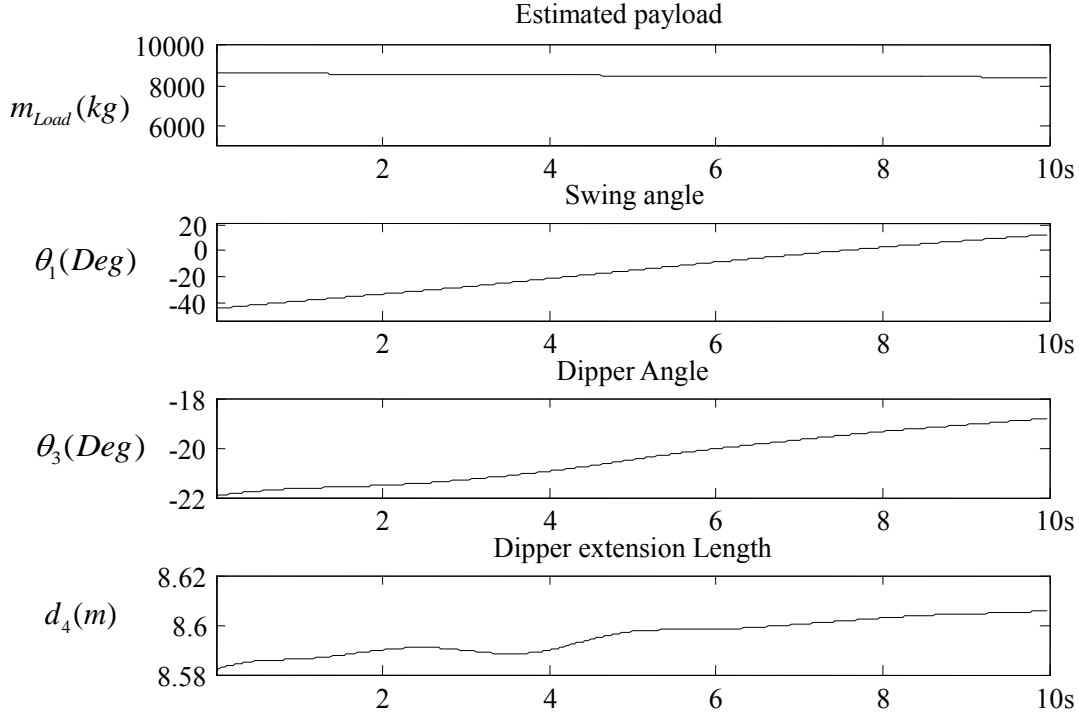
Figure 48: Estimated payload and joint variables during cable-shovel swing cycle, dipper loaded with 8420 kg payload
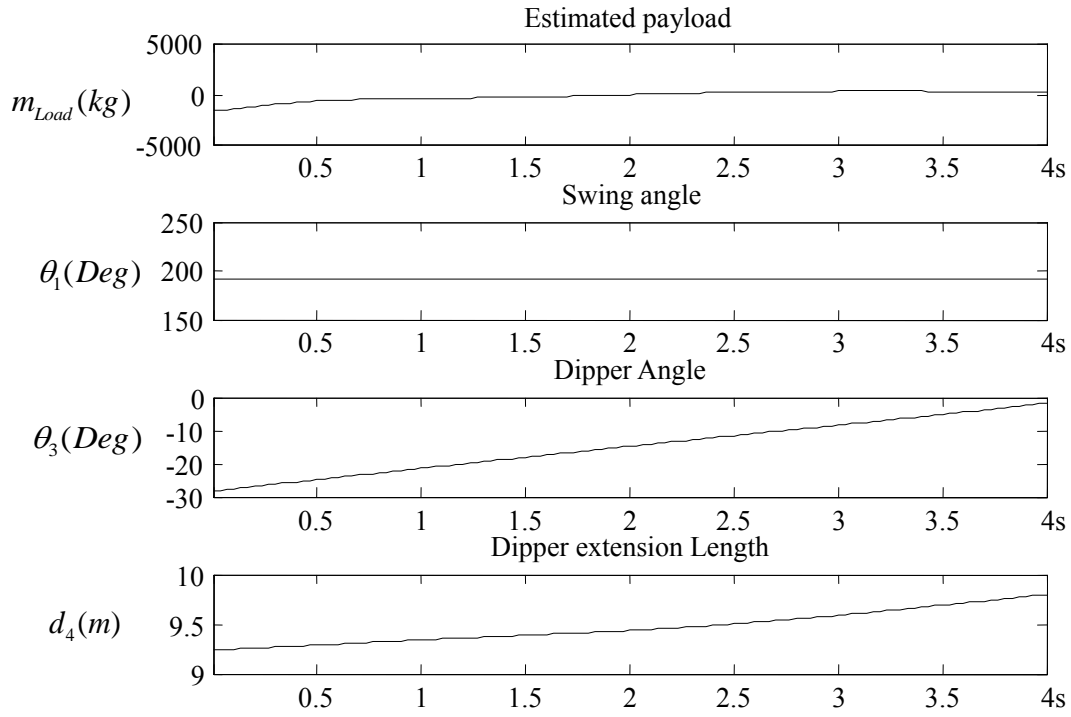
Figure 49: Estimated payload and joint variables, with empty dipper
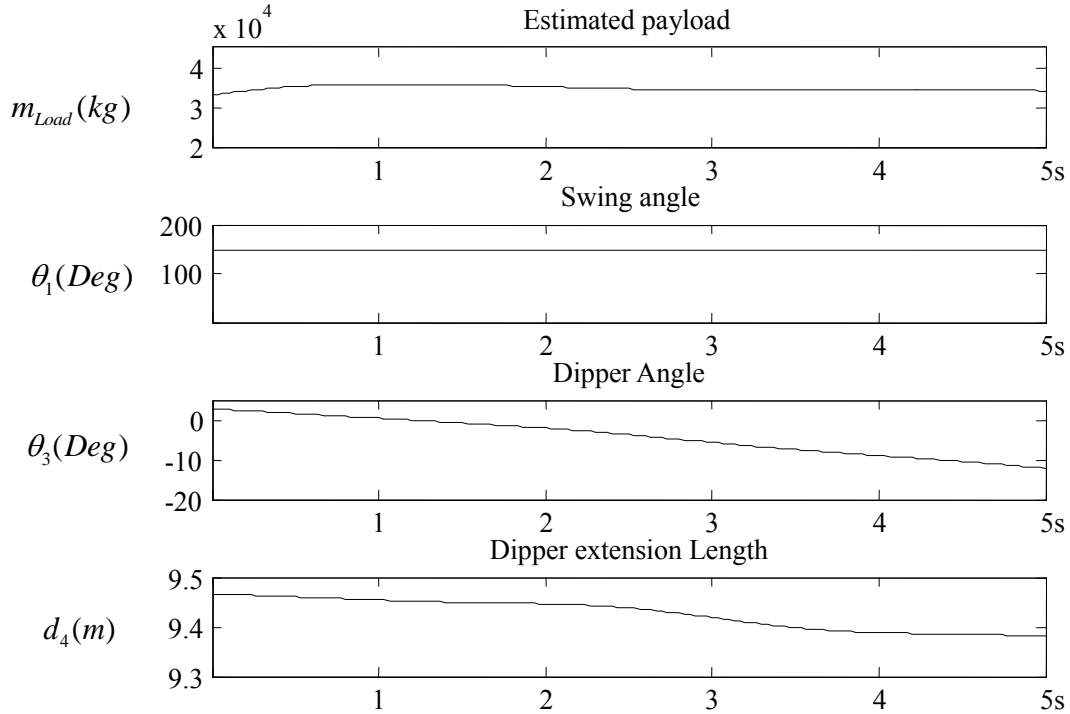
Figure 50: Estimated payload and joint variables cycle, dipper with an almost full dipper

5.8   Potential Effect of Sensor Inaccuracy on Payload Estimation

Errors in measurement of the joint variables and the various motor current measurements affect the overall accuracy of the payload estimation, shown in Table 8, below.   I estimated the payload by using the cable shovel parameters represented in Table 6. However, the impacts of these errors vary.   For example, our results demonstrate that just a two-percent error in the measurement of the hoist motor current generates a 190 kg error in payload weight, yet a 2% error in the dipper handle angle causes a 52 kg error; and finally a 2% error in the crowd length measurement produces a 100 kg error in the payload estimation.

Table 8:   Potential effect of sensor inaccuracy on payload estimation

Source of inaccuracy	Dipper load(kg)	Estimated load for Figure 46 trajectory (kg)	Error (kg)
Original measurement	8420	8312	-108
2% error in hoist armature current	8420	8510	90
2% error in crowd armature current	8420	8311	-109
2% error in θ_3 measurement	8420	8260	-160
2% error in d_4 measurement	8420	8218	-202

5.9   Discussions on Practical Results

Accuracy and repeatability of estimated payload in different trajectories and different days verify the following observations:

- The arm geometry sensor apparatus explained in chapter 3 is capable of

measuring the cable shovel joint variables despite shock and vibration, excessive magnetic field generated by the cable shovel thyristor rectifiers, and the presence of metal object around the cable shovel.

- I estimated the cable shovel joint velocity and acceleration values by numerically differentiations the position signals measured by the arm geometry sensor apparatus. This confirms that the response time of the novel AGS sensor apparatus is suitable to study the dynamics of the cable shovel.

- The simplified model explained in section 5.3 is a reliable and useful model. I was able to estimate the payload inside the dipper by using this simplified model with a good accuracy of 2%.

- The payload estimation results confirm that the cable shovel gravitational and dynamic parameters, K_C and K_H identified by using a known payload in this thesis are valid.

- The developed payload monitoring technique can be utilized in real-word mining application. We do not interrupt the shovel normal operation in order to estimate the payload and only estimate the payload when the shovel operator lifts the dipper or throughout the cable shovel swing regime. A computer program will record the amount of the load dumped inside the truck and report it to the shovel operator. Assuming the operator fills the truck in four cycles, operate would know the amount of the total load inside the truck before dumping the last scoop and can avoid of the truck overloading or underloading.

The factors contributes to payload estimation error are:

- The center of gravity of the payload and the dipper are not identical. We assumed these two are identical in section 5.3 in order to simplify the cable shovel model.

- The relationship between the hoist motor armature currents and the force exerted to the dipper by the hoist rope is not linear. In the simplified model, I assumed it is linear. In chapter 2, I discussed the detail model of the cable shovel.

- Friction coefficients are not constant and vary by the payload and possibly the cable shovel arm geometry. I assumed the friction coefficients are constant to simplify the cable shovel model.

- I ignored the hoist rope mass in the simplified model. I can calculate the hoist rope mass in any dipper position by knowing the weight per unit.

- I do not take into account the hoist rope and boom suspension cable spring effects in our payload monitoring method.

6   CONCLUSIONS AND FUTURE WORK

6.1   Contribution of Thesis

The major contributions of this thesis are summarized in the following:

1- I developed a comprehensive dynamic model of the cable shovel that accurately simulates various factors including DC motors, inertia, Coriolis, centripetal, gravity and cable spring effects. The effect of variation in the dipper handle length caused by its rotation, the effect of the point sheave and hoist cable torques on the torque of the boom, the suspension cable spring effect, and the hoist cable spring effect were also mathematically modeled. Furthermore, the relationship between the current driving a P&H type cable shovel motor and the torque applied to its joints, the shovel parameters, and the load carried by the dipper were established.

2- I devised a novel approach that enables non-contact sensing of all three active joint variables of a cable shovel in one location. I designed a prototype sensor apparatus that measures the dipper handle angle, the swing angle, and the dipper handle extension. I integrated an advanced 3D orientation sensor and a laser sensor inside the environmental enclosure of the shock mounted arm geometry sensor apparatus (AGS). I evaluated the effect of temperature, sunlight, vibration, the dipper handle speed,   magnets   or   magnetic   materials,   and   transient accelerations on the sensor apparatus performance. I successfully installed the AGS apparatus on the saddle block of a P&H2100 cable shovel and verified the apparatus is suitable for use in a mining applications.

3- I equipped the cable shovel employed for my study with numerous sensors. Subsequently I derived data from all possible cable shovel trajectories at a sampling rate of 30 Hz. All of the devices used in the preparation of this thesis were non-contact sensors including Hall effect current sensors, laser sensor, and 3DoF orientation tracker; therefore, no retrofitting or mechanical modification to the cable-shovel was required. I measured the following variables during the field test: swing motor armature and field currents, hoist motor armature and field currents, crowd motor armature and field currents, the cab swing angle, the

passive boom joint angle, the saddle block joint angle, the crowd joint displacement, and the cab roll and pitch angles.

4- I developed an efficient technique in order to identify the cable shovel parameters, including K_C (the coefficient related to the crowd motor torque coefficient and its gear ratio), and K_H (the coefficient related to the hoist motor torque coefficient its gear ratio, and the hoist drum radius). I have assumed, in our approach in this thesis that all cable shovel parameters, including the motor torque coefficients, were unknown. I gathered experimental data as the dipper moved through various trajectories both with zero and with a known non-zero payload. I later employed the Least Squares Estimation (LSE) in our approach to experimentally identify various parameters.

5- By gathering data when the dipper was in numerous different (although static) positions, I was able to identify the gravitational parameters, K_H, and K_C as they relate to the PH2100XP model cable shovel.

6- I identified and validated the symmetric joint-space inertia matrix $D(q)$, the Coriolis and centripetal effects $C(q, \dot{q})$, viscous friction coefficients f_V, Coulomb friction coefficients f_C, the gravity loading $G(q)$, K_H and K_C of the saddle block revolt joint and the crowd prismatic joint of PH2100XP cable shovel.

7- I developed an efficient technique for the real time estimation of the payload inside the dipper. I discovered that the payload could be estimated at any moment or in any position of the cable shovel movement simply by using the parameters I had identified. My experiments showed the best trajectories for estimating a payload were when the shovel swung or the hoist motor lifted the dipper in free space. The payload was estimated with better than 2% accuracy in this thesis. I employed a roadside truck scale to evaluate the accuracy of the dynamic payload monitoring system that I developed. Finally, the main objective of our thesis has been successfully achieved: the dynamic payload monitoring of the cable shovel.

8- I investigated the relationship between the sensor errors and the estimated payload error. I showed in this thesis that the inaccuracy in the hoist armature current

measurement could significantly increase the estimated payload error.

6.2   Suggestions for Future Work

The results of our research can be extended to the intelligent shovel excavation (ISE) technology, the study of material diggability in surface mining, the monitoring of contact forces during excavation, and the enhanced safety and productivity during mine haul (dump) truck loading. Future work might include but not be limited to the following:

1- Cable shovel energy efficiency can be increased by finding more suitable trajectories for the cable shovel operation. Our simplified dynamic model of the cable shovel can be used for energy calculation.

2- The cable shovel cutting force and the stress placed on the dipper and hoist rope during the digging cycle can be estimated. The unpredictable physical and mechanical properties of rocks being excavated during the digging cycle obviously have a severe impact on the hoist rope and the dipper teeth life span. During the digging cycle, the shovel operator could avoid exerting excessive forces on these components by monitoring the forces applied to the hoist rope and the dipper in real time.

3- Because the payload inside the dipper has a direct impact on the hoist cable tension, a hoist cable tension meter might be installed for high precision payload estimation.

4- A study might be undertaken of a predictive system that will forecast the imminent position of the dipper.   This device would help to avoid an unintended collision with other objects in the vicinity of the shovel. A three-dimensional laser scanner, or radar sensors, or GPS could provide the location of a dump truck with respect to the cable shovel dipper. An intelligent system onboard the cable shovel can predict an imminent collision and provide an alarm to warn the shovel operator or even engage the motor breaks to prevent a disaster.

5- The parameter coefficients for the swing-revolute joint and swing-motor torque might be better identified. K_H can be estimated more accurately for the instant when the hoist-motor field current is decreased. As represented in Figure 31, I observed that the hoist field current is significantly reduced when the shovel

operator lowers the dipper.

6- Similar approach can be used to identify the Bucyrus shovel or dragline parameters.

To summarize, in this thesis for the very first time I devised an integrated sensor for non-contact absolute sensing of the cable shovel joint variables. Later, I simplified the dynamic equations by accounting for only the two prominent degrees of freedom which correspond to the crowd angle and crowd extension. Next, I defined a suitable set of apace parameters (including inertia, friction, and DC motor specific parameters) that linearized our simplified model and enabled us to directly apply LSE for full experimental calibration of our model. Finally, I experimentally verified our model by showing precise dynamic payload estimation.

BIBLIOGRAPHY

[1] T. Joseph and G. Hansen, "Oil sands reaction to cable shovel motion," CIM Bulletin, pp. 62-64, 2002.

[2] R. Hardy, "Selection criteria for loading and hauling equipment–open pit mining applications," Curtin University of Technology, Sydney, PhD Thesis, 2007.

[3] P. R. Mcaree and D. H. Wauge, "Payload Estimation System and Method, " US Patent: 20090187527, 2009.

[4] D. Wauge, "Payload Estimation for Electric Mining Shovels," PhD Thesis, Mechanical Engineering, the University of Queensland, Australia, 2008.

[5] J. J. Slob, P.R. McAree, M. Steinbuch, and P.M. Siegrist, "Payload Estimation for Electric Mining Shovels using a Load Sensing Pin," Traineeship report, Eindhoven University of Technology, 2007.

[6] P&H mining equipment, "P&H electrical& operating manual," 1997.

[7] G. Mirzaeva, R. Betz and T. Summers, "Performance evaluation of DC motors for electric rope shovels based on air gap flux measurement," in Power Engineering Conference, 2009. AUPEC 2009. Australasian Universities, 2009, pp. 1-6.

[8] J. Rodríguez, L. Morán, J. Pontt, J. Espinoza, R. Díaz and E. Silva, "Operating experience of shovel drives for mining applications," Industry Applications, IEEE Transactions on, vol. 40, pp. 664-671, 2004.

[9] G. M. Brown, B. Elbacher and W. Koellner, "Increased productivity with AC drives for mining excavators and haul trucks," in Industry Applications Conference, 2000. Conference Record of the 2000 IEEE, 2002, pp. P28-P37.

[10] D. Wallis, R. Jefferey, P. Siegrist and P. McAree, "Control systems modelling of a 2100BLE electric mining shovel," in 2006 Australian Mining Technology Conference:'Value through Cost Control', 2010, pp. 105-118.

[11] S. Frimpong and Y. Hu, "Intelligent cable shovel excavation modeling and simulation," International Journal of Geomechanics, vol. 8, pp. 2-10, 2010.

[12] K. Awuah-Offei, S. Frimpong and H. Askari-Nasab, "Formation excavation resistance modelling for shovel dippers," International Journal of Mining and Mineral Engineering, vol. 1, pp. 127-146, 2009.

[13] S. Frimpong, Y. Li and K. Awuah-Offei, "Cable shovel health and longevity and operator efficiency in oil sands excavation," International Journal of Mining and Mineral Engineering, vol. 1, pp. 47-61, 2008.

[14] K. Awuah-Offei and S. Frimpong, "Cable shovel digging optimization for energy efficiency," Mechanism and Machine Theory, vol. 42, pp. 995-1006, 2007.

[15] K. Awuah-Offei and S. Frimpong, "Numerical simulation of cable shovel resistive forces in oil sands excavation," International Journal of Mining, Reclamation and Environment, vol. 20, pp. 223-238, 2006.

[16] S. Frimpong, Z. Chang and V. Kecojevic, "KANEXP03 cable shovel dynamics and PID control scheme for efficient surface mining excavation," Transactions Society for Mining Metallurgy and Exploration Incorporated, vol. 318, pp. 41, 2006.

[17] S. Frimpong, Y. Hu and K. Awuah-Offei, "Mechanics of cable shovel-formation interactions in surface mining excavations," J. Terramech., vol. 42, pp. 15-33, 2005.

[18] K. Awuah-Offei and S. Frimpong, "Geometric simulation of material weight resistance in cable shovel loading," in Modelling and Simulation: Fifteenth IASTED International Conference Proceedings, 2004 .

[19] S. Frimpong and Y. Hu, "Parametric simulation of shovel-oil sands interactions during excavation," International Journal of Mining, Reclamation and Environment, vol. 18, pp. 205-219, 2004.

[20] A. H. Kashani, W. S. Owen, N. Himmelman, P. D. Lawrence and R. A. Hall, "Laser Scanner-based End-effector Tracking and Joint Variable Extraction for Heavy Machinery," The International Journal of Robotics Research, vol. 29, pp. 1338, 2010.

[21] N. Himmelman, J. Borthwick, A. Kashani, L. Lin, A. Poon, R. Hall, P. Lawrence, S. Salcudean and W. Owen, "Rope shovel collision avoidance system," in Proceedings of Applications of Computers and Operations Research in the Mineral Industry (APCOM) Conference, 2009.

[22] A. Kashani, W. Owen, P. Lawrence and R. Hall, "Real-time robot joint variable extraction from a laser scanner," in 2007 IEEE International Conference on Automation and Logistics, 2007, pp. 2994-2999.

[23] N. P. Himmelman, "Dynamics modelling of an electric rope shovel for collision avoidance," M.A.Sc. Thesis, ECE, UBC, Vancouver, Canada, 2011.

[24] L. H. Lin, "Enhanced stereo vision SLAM for outdoor heavy machine rotation sensing," M.A.Sc. Thesis, ECE, UBC, Vancouver, Canada, 2010.

[25] L. H. Lin, P. Lawrence and R. Hall, "Stereo vision based swing angle sensor for mining rope shovel," in Intelligent Robots and Systems (IROS), 2010 IEEE/RSJ International Conference on, 2010, pp. 1714-1721.

[26] R. McAREE, "Collision Avoidance for Electric Mining Shovels,", US patent: US 2010/0036645 A1, Publication date: 02/11/2010.

[27] P. R. McAREE, A. W. Reid, K. J. Austin and P. M. Siegrist, "A Method for Postion-Calibration of a Digging Assembly for Electric Mining Shovels," US 2011/0029279 A1, 2011.

[28] A. Hall and P. R. McAree, "Robust bucket position tracking for a large hydraulic excavator," Mechanism and Machine Theory, vol. 40, pp. 1-16, 2005.

[29] S. Frimpong and N. Demirel, "Case Study: Planar Kinematics of Dragline for Efficient Machine Control," J. Aerospace Eng., vol. 22, pp. 112, 2009.

[30] S. Frimpong, Y. Li and N. Aouad, "Intelligent Machine Monitoring and Sensing for Safe Surface Mining Operations," Appropriate Technologies for Environmental Protection in the Developing World, pp. 217-227, 2009.

[31] Y. Li and S. Frimpong, "Hybrid virtual prototype for analyzing cable shovel component stress," The International Journal of Advanced Manufacturing Technology, vol. 37, pp. 423-430, 2008.

[32] K. Awuah-Offei, S. Frimpong and H. Askari-Nasab, "Dynamic simulation of cable shovel specific energy in oil sands excavation," Computer Applications in the Minerals Industry (CAMI 2005), Banff, Alberta, Canada, 2005.

[33] S. Frimpong and K. Awuah-Offei, "Efficient cable shovel excavation in surface mines," in International Conference on Energy, Environment, and Disasters, Charlotte, NC, 2005 .

[34] S. Patnayak and D. Tannant, "Performance monitoring of electric cable shovels," International Journal of Mining, Reclamation and Environment, vol. 19, pp. 276-294, 2005.

[35] M. Dunbabin and P. Corke, "Autonomous excavation using a rope shovel," in Field and Service Robotics, pp. 555-566.

[36] J. Roberts, G. Winstanley and P. Corke, "Three-dimensional imaging for a very large excavator," The International Journal of Robotics Research, vol. 22, pp. 467, 2003.

[37] Hendricks C., Daneshmend L., Wu S. and Scoble M., "Design of a simulator for proclivity analysis of electric mining shovels," in Mine Design for 21st Century, 1993.

[38] Daneshmend L., Hendricks C., Wu S. and Scoble M., "Design of a mining shovel simulator," in Innovative Mine Design for the 21st Century, 1993.

[39] K. J. Austin and P. R. McAree, "Transmission friction in an electric mining shovel," Journal of Field Robotics, vol. 24, pp. 863-875, 2007.

[40] G. Liu, K. Iagnemma, S. Dubowsky and G. Morel, "A base force/torque sensor approach to robot manipulator inertial parameter estimation," in IEEE International Conference on Robotics and Automation, 1998, pp. 3316-3321.

[41] C. H. An, C. G. Atkeson and J. M. Hollerbach, "Estimation of inertial parameters of rigid body links of manipulators," in Decision and Control, 1985 24th IEEE Conference on, 1985, .

[42] S. Tafazoli, P. Lawrence and S. Salcudean, "Identification of inertial and friction parameters for excavator arms," IEEE Trans. Rob. Autom., vol. 15, pp. 966-971, 1999.

[43] B. Bona and A. Curatella, "Identification of industrial robot parameters for advanced model-based controllers design," in Robotics and Automation, 2005. ICRA 2005. Proceedings of the 2005 IEEE International Conference on, 2005, pp. 1681-1686.

[44] J. Swevers, W. Verdonck and J. De Schutter, "Dynamic model identification for industrial robots," IEEE Control Syst. Mag., vol. 27, pp. 58-71, 2007.

[45] W. Khalil, E. Dombre and M. Nagurka, "Modeling, identification and control of robots," Appl. Mech. Rev., vol. 56, pp. B37, 2003.

[46] M. Khoshzaban, F. Sassani and P. Lawrence, "Dynamic calibration of hydraulic mobile manipulators," in Proceedings of the 1st World Automation Congress, pp. 255–262, 1994.

[47] J. Swevers, W. Verdonck, and B. Naumerand, "An experimental robot load identification method for industrial application," The International Journal of Robotics Research, vol. 21 no. 8 701-712 ,2002.

[48] J. J. Craig, Introduction to Robotics: Mechanics and Control. Prentice Hall, 2004.

[49] M. W. Spong, S. Hutchinson and M. Vidyasagar, Robot Modeling and Control. Wiley New Jersey, 2006.

[50] L. Sciavicco and B. Siciliano, Modelling and Control of Robot Manipulators. Springer Verlag, 2000.

[51] J. De Meester, R. Reekmans, A. Vandenput, R. Belmans and W. Geysen, "Microcomputer-controlled torque calculator in DC drives," IEEE Trans. Ind. Appl., vol. 25, pp. 113-118, 1989.

[52] A. Habbadi and F. Carrillo, "A new identification approach for closed loop dc electrical drive using prior knowledge," in 2004 IEEE International Symposium on Industrial Electronics, 2004.

[53] A. Haghighat Kashani, " 3D imaging for outdoor workspace monitoring, "PhD Thesis, ECE, UBC, Vancouver, Canada, 2011.

[54] S. Tafazoli, A.M. Ahani, and A. R. Rasuli, "Method and Apparatus for Determining A Spatial Positioning of Loading Equipment," US Patent application 13154230, Canada patent application 84122-8, June 6, 2011.

[55] F. Ghassemi, "An indirect method for non-contact sensing of robot joint angles using accelerometers with automatic in-situ calibration," M.A.Sc. Thesis, ECE, UBC, Vancouver, Canada, 2001.

[56] F. Ghassemi, S. Tafazoli, P. Lawrence and K. Hashtrudi-Zaad, "An accelerometer-based joint angle sensor for heavy-duty manipulators," in IEEE International Conference on Robotics and Automation, 2002. Proceedings. ICRA'02, 2002 .

[57] F. Ghassemi, S. Tafazoli, P. Lawrence and K. Hashtrudi-Zaad, "Design and Calibration of an Integration-Free Accelerometer-Based Joint-Angle Sensor," IEEE Transactions on Instrumentation and Measurement, vol. 57, pp. 150-159, 2008.

[58] J. Shigley and L. Mitchell, "Mechanical engineering design." McGraw-Hill Book Co., 1983, pp. 869, 1983.

[59] C. W. de Silva, Mechatronics: An Integrated Approach. CRC, 2005.

[60] P. C. Krause, O. Wasynczuk and S. D. Sudhoff, Analysis of Electric Machinery and Drive Systems. IEEE press, 2002.

[61] P. C. Sen, Principles of Electric Machines and Power Electronics. Wiley-India, 2007.

[62] Rasuli A., "Utilization of 16-bit Microcontrollers and Light-Triggered Thyristor in HVDC Systems," M.A.Sc. Thesis, K.N.T. University of Technology Tehran, Iran, 1995.

[63] E. Foxlin, "Pedestrian tracking with shoe-mounted inertial sensors," IEEE Comput. Graphics Appl., vol. 25, pp. 38-46, 2005.

[64] H. Ren and P. Kazanzides, "Investigation of attitude tracking using an integrated inertial and magnetic navigation system for hand-held surgical instruments," Mechatronics, IEEE/ASME Transactions on, pp. 1-8, 2010.

[65] R. Zhu and Z. Zhou, "A real-time articulated human motion tracking using tri-axis inertial/magnetic sensors package," Neural Systems and Rehabilitation Engineering, IEEE Transactions on, vol. 12, pp. 295-302, 2004.

[66] J. Favre, R. Aissaoui, B. Jolles, O. Siegrist, J. de Guise and K. Aminian, "3d joint rotation measurement using mems inertial sensors: Application to the knee joint," ISB-3D: 3-D Analysis of Human Movement, 28-30 June 2006, Valenciennes, France, vol. 18, 2006.

[67] A. Jiménez, F. Seco, C. Prieto and J. Guevara, "A comparison of pedestrian dead-reckoning algorithms using a low-cost MEMS IMU," in 6th IEEE International

Symposium on Intelligent Signal Processing, 26-28 August, Budapest, Hungary, 2009, pp. 37-42.

[68] H. Bullinger, J. Ziegler, C. Stephanidis, M. Smith, G. Salvendy, D. Harris, R. Koubeck, D. Meister, T. Enderwick and K. Stanney, Handbook of Virtual Environments: Design, Implementation, and Applications. 2002.

[69] F. H. Raab, E. B. Blood, T. O. Steiner and H. R. Jones, "Magnetic position and orientation tracking system," Aerospace and Electronic Systems, IEEE Transactions on, pp. 709-718, 1979.

[70] XSENS Motion Technologies, Ed., MTi and MTx User Manual and Technical Documentation. 2008.

[71] M. A. Nixon, B. C. McCallum, W. R. Fright and N. B. Price, "The effects of metals and interfering fields on electromagnetic trackers," Presence, vol. 7, pp. 204-218, 1998.

[72] G. Fu, P. Corradi, A. Menciassi and P. Dario, "An Integrated Triangulation Laser Scanner for Obstacle Detection of Miniature Mobile Robots in Indoor Environment," Mechatronics, IEEE/ASME Transactions on, pp. 1-6, 2011.

[73] J. Ryde and N. Hillier, "Performance of laser and radar ranging devices in adverse environmental conditions," Journal of Field Robotics, vol. 26, pp. 712-727, 2009.

[74] J. Pascoal, L. Marques and A. T. de Almeida, "Assessment of laser range finders in risky environments," in IEEE/RSJ International Conference on Intelligent Robots and Systems, 2008. IROS 2008, 2008, pp. 3533-3538.

[75] C. Ye, "Mixed pixels removal of a laser rangefinder for mobile robot 3-D terrain mapping," in Information and Automation, 2008. ICIA 2008. International Conference on, 2008, pp. 1153-1158.

[76] X. Luo and H. Zhang, "Characterization of acuity laser range finder," in Control, Automation, Robotics and Vision Conference, 2004. ICARCV 2004 8th, 2004, .

[77] M. C. Amann, T. Bosch, M. Lescure, R. Myllylä and M. Rioux, "Laser ranging: a critical review of usual techniques for distance measurement," Optical Engineering, vol. 40, pp. 10, 2001.

[78] M. Gavish and K. T. Chen, "System and method for laser range finder," 2001.

[79] W. Okkerse, S. Ottengraf and B. Osinga-Kuipers, "Biofilm thickness variability investigated with a laser triangulation sensor," Biotechnol. Bioeng., vol. 70, pp. 619-629, 2000.

[80] A. Reina and J. Gonzales, "Characterization of a radial laser scanner for mobile robotnavigation," in Intelligent Robots and Systems, 1997. IROS'97., Proceedings of the 1997 IEEE/RSJ International Conference on, 1997, .

[81] R. G. Dorsch, G. Häusler and J. M. Herrmann, "Laser triangulation: fundamental uncertainty in distance measurement," Appl. Opt., vol. 33, pp. 1306-1314, 1994.

[82] G. Beheim and K. Fritsch, "Range finding using frequency-modulated laser diode," Appl. Opt., vol. 25, pp. 1439-1442, 1986.

[83] N. Hillier, J. Ryde and E. Widzyk-Capehart, "Comparison of Scanning Laser Range-finders and Millimetre-wave Radar for Creating a Digital Terrain Map," .

[84] G. Brooker, R. Hennessey, C. Lobsey, M. Bishop and E. Widzyk-Capehart, "Seeing through dust and water vapor: Millimeter wave radar sensors for mining applications," Journal of Field Robotics, vol. 24, pp. 527-557, 2007.

[85] A. Rockseisen, "Method for the Contact-Free Measurement of the Distance of an Object According to the Principle of Laser Triangulation," US Patent 6088106, 2000.

[86] P&H MinePro Services, "Peak performance: Excavator section," 2003.

[87] E. Ramsden, Hall-Effect Sensors: Theory and Applications. Newnes, 2006.

[88] R. S. Popovic, "Hall-effect devices," Sensors and Actuators, vol. 17, pp. 39-53, 1989.

[89] C. Chien and C. Westgate, The Hall Effect and its Application. Plenum, New York, 1980.

[90] S. Tafazoli, "Identification of frictional effects and structural dynamics for improved control of hydraulic manipulators," PhD Thesis, ECE, UBC, Vancouver, Canada, 1997.

Appendix

Dynamic Analysis of the Cable Shovel

An effective dynamic model of a manipulator will create a relationship between the actuator torques and the joint variables (i.e., joint angles and displacements). A dynamic model can be useful:

- for simulating motion of a manipulator,
- for analyzing the cable shovel structure,
- for implementing payload and cutting force monitoring algorithms, and
- for designing advanced closed-loop control algorithms.

Several approaches have been proposed in the literature to model the dynamics of robots; two of the most well-known methods are: the Euler-Lagrange method and the Newton-Euler method. The Euler-Lagrange formulation is energy based and conceptually simple and systematic to derive. Newton-Euler formulation is based on a recursive algorithm to derive the model and is computationally more efficient since it exploits the typically open structure of the manipulator kinematic chain [48-50].

The Recursive Newton-Euler approach (RNE) is performed by first stepping forward through the chain of links to compute the kinematic parameters of the links (i.e. velocity, angular velocity, acceleration & angular acceleration) and then stepping backwards through the links and using Newton's Second Law $F = \dfrac{dP}{dt} = ma$, and Eulers equations $\tau = \dfrac{dH}{dt} = \dfrac{d}{dt}(I\omega)$, to compute the joint torques, where m is the mass, a is the acceleration, I is the moment of inertia, and ω is the angular velocity. The resulting dynamic equations for our 4DOF manipulator is given by [50]:

Forward chain for 1 to 4:

$$\omega_i^i = \begin{cases} R_i^{i-1T}\,\omega_{i-1}^{i-1} & \text{For a prismatic joint} \\[2mm] R_i^{i-1T}(\omega_{i-1}^{i-1} + \dot{q}_i\,z_0) & \text{For a revolute joint} \end{cases} \tag{97}$$

$$
\dot{\omega}_i^i = \begin{cases} R_i^{i-1T}\,\dot{\omega}_{i-1}^{i-1} & \text{For a prismatic joint} \\[2em] R_i^{i-1T}\,(\dot{\omega}_{i-1}^{i-1} + \ddot{q}_i\,z_0 + \dot{q}\,\omega_{i-1}^{i-1} \times z_0) & \text{For a revolute joint} \end{cases}
\tag{98}
$$

$$
\ddot{q}_i^i = \begin{cases} R_i^{i-1T}(\ddot{q}_{i-1}^{i-1} + \ddot{d}_i\,z_0) + 2\dot{d}_i\,\omega_i^i \times R_i^{i-1T}z_0 & \text{For a prismatic joint} \\ \quad + \dot{\omega}_i^i \times r_{i-1,i}^i + \omega_i^i \times (\omega_i^i \times r_{i-1,i}^i) \\[1em] R_i^{i-1T}\,\ddot{q}_{i-1}^{i-1} + \dot{\omega}_i^i \times r_{i-1,i}^i + \omega_i^i \times (\omega_i^i \times r_{i-1,i}^i) & \text{For a revolute joint} \end{cases}
\tag{99}
$$

$$
\ddot{q}_{C_i}^i = \ddot{q}_i^i + \dot{\omega}_i^i \times r_{i,C_i}^i + \omega_i^i \times (\omega_i^i \times r_{i,C_i}^i)
\tag{100}
$$

Where:

R_i^{i-1T} is the rotation matrix from frame i into $i-1$ frame

ω_i^i is the angular velocity of link i in frame i

$\dot{\omega}_i^i$ is the angular acceleration of link i in frame i

$\ddot{q}_{C_i}^i$ is the linear acceleration of the center of mass of link C_i in frame i

$\ddot{q}_i^i$ is the linear acceleration of the origin of frame i in frame i

$r_{i-1,i}^i$ is the vector from origin of frame $i-1$ to origin of frame i

r_{i,C_i}^i is the vector from the origin of frame i to the center of mass C_i

Forward chain for 1 to 4:

The base frame is fixed, therefore:

$$\omega_0^0 = \begin{bmatrix} 0 & 0 & 0 \end{bmatrix} \tag{101}$$

$$\dot{\omega}_0^0 = \begin{bmatrix} 0 & 0 & 0 \end{bmatrix} \tag{102}$$

$$\ddot{q}_0^0 = \begin{bmatrix} 0 & 0 & g \end{bmatrix} \tag{103}$$

These vectors are the initial conditions for the velocities and acceleration, and g is the gravitational constant.

$$\omega_1^1 = \begin{bmatrix} 0 & \dot{\theta}_1 & 0 \end{bmatrix} \tag{104}$$

$$\dot{\omega}_1^1 = \begin{bmatrix} 0 & \ddot{\theta}_1 & 0 \end{bmatrix} \tag{105}$$

$$\ddot{q}_1^1 = \begin{bmatrix} -\dot{\theta}_1^2 a_1 & g & -\ddot{\theta}_1 a_1 \end{bmatrix} \tag{106}$$

$$\ddot{q}_{c1}^1 = \begin{bmatrix} (-\dot{\theta}_1^2 a_1 - \dot{\theta}_1^2 a_1 r_{c1}) & g & (-\ddot{\theta}_1 a_1 - \ddot{\theta}_1 a_1 r_{c1}) \end{bmatrix} \tag{107}$$

$$\omega_2^2 = \begin{bmatrix} \dot{\theta}_1 s_2 & \dot{\theta}_1 c_2 & \dot{\theta}_2 \end{bmatrix} \tag{108}$$

$$\dot{\omega}_2^2 = \begin{bmatrix} (\ddot{\theta}_1 s_2 + c_2 \dot{\theta}_2 \dot{\theta}_1) & (\ddot{\theta}_1 c_2 - s_2 \dot{\theta}_2 \dot{\theta}_1) & \ddot{\theta}_2 \end{bmatrix} \tag{109}$$

$$\ddot{q}_2^2 = \begin{bmatrix} s_2 g - c_2 \dot{\theta}_1^2 a_1 - \dot{\theta}_1^2 c_2^2 a_2 - \dot{\theta}_2^2 a_2 \\ c_2 g + s_2 \dot{\theta}_1^2 a_1 + s_2 \dot{\theta}_1^2 c_2 a_2 + \ddot{\theta}_2 a_2 \\ a_2(\ddot{\theta}_1 c_2 - 2 s_2 \dot{\theta}_2 \dot{\theta}_1) - \ddot{\theta}_1 a_1 \end{bmatrix}^T \tag{110}$$

106

$$\ddot{q}_{c2}^{2} = \begin{bmatrix} s_2 g - c_2 \dot{\theta}_1^{2} a_1 - \dot{\theta}_1^{2} c_2^{2} a_2 - \dot{\theta}_2^{2} a_2 - r_{c2}(\dot{\theta}_1^{2} c_2^{2} + \dot{\theta}_2^{2}) \\ c_2 g + s_2 \dot{\theta}_1^{2} a_1 + s_2 \dot{\theta}_1^{2} c_2 a_2 + \ddot{\theta}_2 a_2 + r_{c2}(s_2 \dot{\theta}_1^{2} c_2 a_2 + \ddot{\theta}_2) \\ a_2(\ddot{\theta}_1 c_2 - 2s_2 \dot{\theta}_2 \dot{\theta}_1) - \ddot{\theta}_1 a_1 - r_{c2}(\ddot{\theta}_1 c_2 - 2s_2 \dot{\theta}_2 \dot{\theta}_1) \end{bmatrix}^{T} \tag{111}$$

$$\omega_3^{3} = \begin{bmatrix} \dot{\theta}_1 s_{23} & \dot{\theta}_{23} & -c_{23} \dot{\theta}_1 \end{bmatrix} \tag{112}$$

$$\dot{\omega}_3^{3} = \begin{bmatrix} (\ddot{\theta}_1 s_{23} + \dot{\theta}_1 s_{23}) & \ddot{\theta}_{23} & (\ddot{\theta}_1 s_{23} - \ddot{\theta}_1 c_{23}) \end{bmatrix} \tag{113}$$

$$\ddot{q}_3^{3} = \begin{bmatrix} \alpha_1 & \beta_1 & \delta_1 \end{bmatrix} \tag{114}$$

Where:

$$\alpha_1 = c_3(s_2 g - c_2 \dot{\theta}_1^{2} a_1 - \dot{\theta}_1^{2} c_2^{2} a_2 - \dot{\theta}_2^{2} a_2) + s_3(c_2 g + s_2 \dot{\theta}_1^{2} a_1 + s_2 \dot{\theta}_1^{2} c_2 a_2 + \ddot{\theta}_2 a_2)$$
$$- a_3 \dot{\theta}_{23}^{2} + (c_{23} \dot{\theta}_1)^{2} a_3$$

$$\beta_1 = a_2(-\ddot{\theta}_1 c_2 + s_2 \dot{\theta}_2 \dot{\theta}_1) - \ddot{\theta}_1 a_1 + a_2 s_2 \dot{\theta}_2 \dot{\theta}_1 + a_3[s_3(c_2 \dot{\theta}_2 \dot{\theta}_1 + s_2 \dot{\theta}_1^{2} + c_2 \dot{\theta}_3 \dot{\theta}_1)$$
$$- c_3(c_2 \dot{\theta}_1^{2} - s_2 \dot{\theta}_3 \dot{\theta}_1 - s_2 \dot{\theta}_2 \dot{\theta}_1)] + a_3 \ddot{\theta}_{23} + s_{23} \dot{\theta}_1$$

$$\delta_1 = s_3(s_2 g - c_2 \dot{\theta}_1^{2} a_1 - \dot{\theta}_1^{2} c_2^{2} a_2 - a_2 \dot{\theta}_2^{2}) - c_3(c_2 g + s_2 \dot{\theta}_1^{2} a_1 + s_2 \dot{\theta}_1^{2} c_2 a_2 + \ddot{\theta}_2 a_2)$$
$$- a_3 \ddot{\theta}_{23} - a_3 s_{23} \dot{\theta}_1^{2} c_{23}$$

$$\ddot{q}_{c3}^{3} = \begin{bmatrix} \alpha_2 & \beta_2 & \delta_2 \end{bmatrix} \tag{115}$$

Where:

$$\alpha_2 = c_3(s_2 g - c_2 \dot{\theta}_1^2 a_1 - \dot{\theta}_1^2 c_2{}^2 a_2 - \dot{\theta}_2^2 a_2) + s_3(c_2 g + s_2 \dot{\theta}_1^2 a_1 + s_2 \dot{\theta}_1^2 c_2 a_2 + \ddot{\theta}_2 a_2)$$
$$- a_3 \dot{\theta}_{23}^2 + (c_{23} \dot{\theta}_1)^2 a_3 - r_{c3}[\dot{\theta}_{23}^2 + (c_{23} \dot{\theta}_1)^2]$$

$$\beta_2 = a_2(-\ddot{\theta}_1 c_2 + s_2 \dot{\theta}_2 \dot{\theta}_1) - \ddot{\theta}_1 a_1 + a_2 s_2 \dot{\theta}_2 \dot{\theta}_1 + a_3[s_3(c_2 \dot{\theta}_2 \dot{\theta}_1 + s_2 \dot{\theta}_1^2 + c_2 \dot{\theta}_3 \dot{\theta}_1)$$
$$- c_3(c_2 \dot{\theta}_1 - s_2 \dot{\theta}_3 \dot{\theta}_1 - s_2 \dot{\theta}_2 \dot{\theta}_1)] + a_3 \dot{\theta}_{23} s_{23} \dot{\theta}_1 + r_{c3}[s_3(c_2 \dot{\theta}_2 \dot{\theta}_1 + s_2 \dot{\theta}_1^2 + c_2 \dot{\theta}_3 \dot{\theta}_1)$$
$$- c_3(c_2 \dot{\theta}_1 - s_2 \dot{\theta}_3 \dot{\theta}_1 - s_2 \dot{\theta}_2 \dot{\theta}_1] + r_{c3} \dot{\theta}_{23} s_{23} \dot{\theta}_1$$

$$\delta_2 = s_3(s_2 g - c_2 \dot{\theta}_1^2 a_1 - \dot{\theta}_1^2 c_2{}^2 a_2 - a_2 \dot{\theta}_2^2) - c_3(c_2 g + s_2 \dot{\theta}_1^2 a_1 + s_2 \dot{\theta}_1^2 c_2 a_2 + \ddot{\theta}_2 a_2)$$
$$- a_3 \ddot{\theta}_{23} - a_3 s_{23} \dot{\theta}_1^2 c_{23} - r_{c3} \ddot{\theta}_{23} - r_{c3} s_{23} \dot{\theta}_1^2 c_{23}$$

$$\omega_4^4 = \begin{bmatrix} \dot{\theta}_1 s_{23} & \dot{\theta}_{23} & -c_{23} \dot{\theta}_1 \end{bmatrix} \tag{116}$$

$$\dot{\omega}_4^4 = \begin{bmatrix} (\ddot{\theta}_1 s_{23} + \dot{\theta}_1 c_{23}) & \ddot{\theta}_{23} & (\ddot{\theta}_1 s_{23} - \ddot{\theta}_1 c_{23}) \end{bmatrix} \tag{117}$$

$$\tag{118}$$

$$\ddot{q}_4^4 = \begin{bmatrix} \alpha_3 & \beta_3 & \delta_3 \end{bmatrix}$$

Where:

$$\alpha_3 = c_3(s_2 g - c_2 \dot{\theta}_1^2 a_1 - \dot{\theta}_1^2 c_2{}^2 a_2 - \dot{\theta}_2^2 a_2) + s_3(c_2 g + s_2 \dot{\theta}_1^2 a_1 + s_2 \dot{\theta}_1^2 c_2 a_2 + \ddot{\theta}_2 a_2)$$
$$- a_3 \dot{\theta}_{23}^2 + (c_{23} \dot{\theta}_1)^2 a_3 + 2 \dot{d}_4 \dot{\theta}_{23} + d_4 \ddot{\theta}_{23} - d_4 s_{23} \dot{\theta}_1^2 c_{23}$$

$$\beta_3 = a_2(-\ddot{\theta}_1 c_2 + s_2 \dot{\theta}_2 \dot{\theta}_1) - \ddot{\theta}_1 a_1 + a_2 s_2 \dot{\theta}_2 \dot{\theta}_1 + a_3[s_3(c_2 \dot{\theta}_2 \dot{\theta}_1 + s_2 \dot{\theta}_1^2 + c_2 \dot{\theta}_3 \dot{\theta}_1)$$
$$- c_3(c_2 \dot{\theta}_1^2 - s_2 \dot{\theta}_3 \dot{\theta}_1 - s_2 \dot{\theta}_2 \dot{\theta}_1)] + a_3 \dot{\theta}_{23} s_{23} \dot{\theta}_1 - 2 \dot{d}_4 s_{23} \dot{\theta}_1 - d_4 \dot{\theta}_{23} \dot{\theta}_1^2 c_{23}$$
$$- d_4[c_3(c_2 \dot{\theta}_2 \dot{\theta}_1 + s_2 \dot{\theta}_1^2 + c_2 \dot{\theta}_3 \dot{\theta}_1) + s_3(c_2 \dot{\theta}_1 - s_2 \dot{\theta}_3 \dot{\theta}_1 - s_2 \dot{\theta}_2 \dot{\theta}_1)]$$

$$\delta_3 = s_3(s_2 g - c_2 \dot{\theta}_1^2 a_1 - \dot{\theta}_1^2 c_2{}^2 a_2 - a_2 \dot{\theta}_2^2) - c_3(c_2 g + s_2 \dot{\theta}_1^2 a_1 + s_2 \dot{\theta}_1^2 c_2 a_2 + \ddot{\theta}_2 a_2)$$
$$- a_3 \ddot{\theta}_{23} - a_3 s_{23} \dot{\theta}_1^2 c_{23} + \ddot{d}_4 - d_4(s_{23} \dot{\theta}_1)^2 - d_4 \dot{\theta}_{23}^2$$

$$\ddot{q}_{c4}^{\,4} = \begin{bmatrix} \alpha_4 & \beta_4 & \delta_4 \end{bmatrix} \qquad (119)$$

Where:

$$\alpha_4 = c_3(s_2 g - c_2\,\dot\theta_1^{\,2}\,a_1 - \dot\theta_1^{\,2} c_2^{\,2} a_2 - \dot\theta_2^{\,2} a_2) + s_3(c_2 g + s_2\,\dot\theta_1^{\,2}\,a_1 + s_2\,\dot\theta_1^{\,2} c_2 a_2 + \ddot\theta_2\,a_2)$$
$$- a_3\,\dot\theta_{23}^{\,2} + (c_{23}\,\dot\theta_1)^2 a_3 + 2\dot d\,\dot\theta_{23} + d_4\,\ddot\theta_{23}$$
$$- d_4 s_{23}\,\dot\theta_1^{\,2}\,c_{23} + r_{c4}\,\ddot\theta_{23} - r_{c4} s_{23}\,\dot\theta_1^{\,2}\,c_{23}$$

$$\beta_4 = a_2(-\ddot\theta_1 c_2 + s_2\,\dot\theta_2\,\dot\theta_1) - \dot\theta_1^{\,2}\,a_1 + a_2 s_2\,\dot\theta_2\,\dot\theta_1 + a_3[s_3(c_2\,\dot\theta_2\,\dot\theta_1 + s_2\,\dot\theta_1^{\,2} + c_2\,\dot\theta_3\,\dot\theta_1)$$
$$- c_3(c_2\,\dot\theta_1 - s_2\,\dot\theta_3\,\dot\theta_1 - s_2\,\dot\theta_2\,\dot\theta_1)] + a_3\,\ddot\theta_{23} s_{23}\,\dot\theta_1 - 2 d_4\,s_{23}\,\dot\theta_1$$
$$- d_4\,\ddot\theta_{23}\,\dot\theta_1^{\,2}\,c_{23} - d_4[c_3(c_2\,\dot\theta_2\,\dot\theta_1 + s_2\,\ddot\theta_1 + c_2\,\dot\theta_3\,\dot\theta_1) - r_{c4}\,\ddot\theta_{23}\,\dot\theta_1 c_{23}$$
$$+ s_3(c_2\,\ddot\theta_2 - s_2\,\dot\theta_3\,\dot\theta_1 - s_2\,\dot\theta_2\,\dot\theta_1)] - r_{c4}[c_3(c_2\,\dot\theta_2\,\dot\theta_1 + s_2\,\ddot\theta_1 + c_2\,\dot\theta_3\,\dot\theta_1)$$
$$+ s_3(c_2\,\ddot\theta_2 - s_2\,\dot\theta_3\,\dot\theta_1 - s_2\,\dot\theta_2\,\dot\theta_1)]$$

$$\delta_4 = s_3(s_2 g - c_2\,\dot\theta_1^{\,2}\,a_1 - \dot\theta_1^{\,2} c_2^{\,2} a_2 - a_2\,\dot\theta_2^{\,2}) - c_3(c_2 g + s_2\,\dot\theta_1^{\,2}\,a_1 + s_2\,\dot\theta_1^{\,2} c_2 a_2 + \ddot\theta_2\,a_2)$$
$$- a_3\,\ddot\theta_{23} - a_3 s_{23}\,\dot\theta_1^{\,2}\,c_{23} + \ddot d_4 - d_4(s_{23}\,\dot\theta_1)^2 - d_4\,\ddot\theta_{23} - c_{c4}(s_{23}\,\dot\theta_1)^2$$
$$- r_{c4}\,\dot\theta_{23}^{\,2}$$

Having computed the velocities and accelerations by forward recursion from the base link to the end effector, the forces and torques can be also calculated by a backward recursion [48, 50]:

The backward chain from 4 to 1 is as follows:

$$f_4 = M_4[s_3(s_2 g - c_2 \dot{\theta}_1^2 a_1 - \dot{\theta}_1^2 c_2^2 a_2 - a_2 \dot{\theta}_2^2) - c_3(c_2 g + s_2 \dot{\theta}_1^2 a_1 + s_2 \dot{\theta}_1^2 c_2 a_2 + \ddot{\theta}_2 a_2)$$
$$-a_3 \ddot{\theta}_{23} - a_3 s_{23} \dot{\theta}_1^2 c_{23} + \ddot{d} - d_4(s_{23}\dot{\theta}_1)^2 - d_4 \dot{\theta}_{23}^2 \tag{120}$$
$$-c_{c4}(s_{23}\dot{\theta}_1)^2 - r_{c4}\dot{\theta}_{23}^2] + f_{V4}\dot{d}_4 + f_{c4}\,\text{sgn}(\dot{d}_4)$$

$$\tau_3 = (-M_4[s_3(s_2 g - c_2 \dot{\theta}_1^2 a_1 - \dot{\theta}_1^2 c_2^2 a_2 - a_2 \dot{\theta}_2^2) - c_3(c_2 g + s_2 \dot{\theta}_1^2 a_1 + s_2 \dot{\theta}_1^2 c_2 a_2 + \ddot{\theta}_2 a_2)$$
$$-a_3 \ddot{\theta}_{23} - a_3 s_{23} \dot{\theta}_1^2 c_{23} + \ddot{d}_4 - d_4(s_{23}\dot{\theta}_1)^2 - d_4 \dot{\theta}_{23}^2 - c_{c4}(s_{23}\dot{\theta}_1)^2 - r_{c4}\dot{\theta}_{23}^2]$$
$$-M_3[s_3(s_2 g - c_2 \dot{\theta}_1^2 a_1 - \dot{\theta}_1^2 c_2^2 a_2 - a_2 \dot{\theta}_2^2) - c_3(c_2 g + s_2 \dot{\theta}_1^2 a_1 + s_2 \dot{\theta}_1^2 c_2 a_2 + \ddot{\theta}_2 a_2)$$
$$-a_3 \ddot{\theta}_{23} - a_3 s_{23} \dot{\theta}_1^2 c_{23} - r_{c3}\ddot{\theta}_{23} - r_{c3}s_{23}\dot{\theta}_1^2 c_{23}])(a_3 + r_{c3})$$
$$+M_4(c_3(s_2 g - c_2 \dot{\theta}_1^2 a_1 - \dot{\theta}_1^2 c_2^2 a_2 - a_2 \dot{\theta}_2^2) + s_3(c_2 g + s_2 \dot{\theta}_1^2 a_1 + s_2 \dot{\theta}_1^2 c_2 a_2 + \ddot{\theta}_2 a_2)$$
$$-a_3 \dot{\theta}_{23}^2 - (c_{23}\dot{\theta}_1)^2 a_3 + 2\dot{d}_4 \dot{\theta}_{23} + d_4 \ddot{\theta}_{23} - d_4 s_{23}\dot{\theta}_1^2 c_{23} + r_{c4}\ddot{\theta}_{23}$$
$$-r_{c4}s_{23}\dot{\theta}_1^2 c_{23})(d_4 + r_{c4}) + I_4(s_{23}\dot{\theta}_1^2 c_{23}) + M_4(s_3(s_2 g - \dot{\theta}_1^2 c_2^2 a_2 - a_2 \dot{\theta}_2^2)$$
$$-c_3(c_2 g + s_2 \dot{\theta}_1^2 a_1 + s_2 \dot{\theta}_1^2 c_2 a_2 + \ddot{\theta}_2 a_2) - a_3 \ddot{\theta}_{23} - a_3 s_{23}\dot{\theta}_1^2 c_{23} + \ddot{d}_4$$
$$-d_4(s_{23}\dot{\theta}_1)^2 - d_4 \dot{\theta}_{23}^2 - c_{c4}(s_{23}\dot{\theta}_1)^2 - r_{c4}\dot{\theta}_{23}^2)r_{c3} + I_3 s_{23}\dot{\theta}_1^2 c_{23} + f_{V3}\dot{\theta}_3 + f_{c3}\dot{\theta}_3$$
$$\tag{121}$$

$$\tau_2 = -\{-s_3[M_4(c_3(s_2g - c_2\dot\theta_1^2 a_1 - \dot\theta_1^2 c_2^2 a_2 - a_2\ddot\theta_2) + s_3(c_2g + s_2\dot\theta_1^2 a_1 + s_2\dot\theta_1^2 c_2 a_2 + \ddot\theta_2 a_2)$$

$$-a_3(\ddot\theta_2 + \ddot\theta_3)^2 - (c_{23}\dot\theta_1)^2 a_3 + 2\dot d(\ddot\theta_2 + \ddot\theta_3) + d_{PR}(\ddot\theta_2 + \ddot\theta_3) - d_{PR}s_{23}\dot\theta_1^2 c_{23} + r_{c4}(\ddot\theta_2 + \ddot\theta_3) - r_{c4}s_{23}\dot\theta_1^2 c_{23}]$$

$$+M_3[c_3(s_2g - c_2\dot\theta_1^2 a_1 - \dot\theta_1^2 c_2^2 a_2 - \ddot\theta_2^2 a_2) + S3(c_2g + s_2\dot\theta_1^2 a_1 + s_2\dot\theta_1^2 c_2 a_2 + \ddot\theta_2 a_2) - a_3(\ddot\theta_2 + \ddot\theta_3)^2$$

$$+(c_{23}\dot\theta_1)^2 a_3 - r_{c3}[(\ddot\theta_2 + \ddot\theta_3)^2 + (c_{23}\dot\theta_1)^2]] + c_3(M_4[s_3(s_2g - c_2\dot\theta_1^2 a_1 - \dot\theta_1^2 c_2^2 a_2 - a_2\ddot\theta_2)$$

$$-c_3(c_2g + s_2\dot\theta_1^2 a_1 + s_2\dot\theta_1^2 c_2 a_2 + \ddot\theta_2 a_2) - a_3(\ddot\theta_2 + \ddot\theta_3) - a_3s_{23}\dot\theta_1^2 c_{23} + \ddot d - d_{PR}(s_{23}\dot\theta_1)^2$$

$$-d_{PR}(\ddot\theta_2 + \ddot\theta_3)^2 - c_{c4}(s_{23}\dot\theta_1)^2 - r_{c4}(\ddot\theta_2 + \ddot\theta_3)^2] + M_3[s_3(s_2g - c_2\dot\theta_1^2 a_1 - \dot\theta_1^2 c_2^2 a_2 - a_2\ddot\theta_2)$$

$$-c_3(c_2g + s_2\dot\theta_1^2 a_1 + s_2\dot\theta_1^2 c_2 a_2 + \ddot\theta_2 a_2) - a_3(\ddot\theta_2 + \ddot\theta_3) - a_3s_{23}\dot\theta_1^2 c_{23} - r_{c3}(\ddot\theta_2 + \ddot\theta_3) - r_{c3}c_{23}\dot\theta_1^2 c_{23}]$$

$$-M_2(c_2g + s_2\dot\theta_1^2 a_1 + s_2\dot\theta_1^2 c_2 a_2 + \ddot\theta_2 a_2 + r_{c2}(s_2\dot\theta_1^2 c_2 a_2 + \ddot\theta_2))\}(a_2 + r_{c2})$$

$$-\{M_4[s_3(s_2g - c_2\dot\theta_1^2 a_1 - \dot\theta_1^2 c_2^2 a_2 - a_2\ddot\theta_2) - c_3(c_2g + s_2\dot\theta_1^2 a_1 + s_2\dot\theta_1^2 c_2 a_2 + \ddot\theta_2 a_2)$$

$$-a_3(\ddot\theta_2 + \ddot\theta_3) - a_3s_{23}\dot\theta_1^2 c_{23} + \ddot d - d_{PR}(s_{23}\dot\theta_1)^2 - d_{PR}(\ddot\theta_2 + \ddot\theta_3)^2 - c_{c4}(s_{23}\dot\theta_1)^2 - r_{c4}(\ddot\theta_2 + \ddot\theta_3)^2]$$

$$+M_3[s_3(s_2g - c_2\dot\theta_1^2 a_1 - \dot\theta_1^2 c_2^2 a_2 - a_2\ddot\theta_2) - c_3(c_2g + s_2\dot\theta_1^2 a_1 + s_2\dot\theta_1^2 c_2 a_2 + \ddot\theta_2 a_2)$$

$$-a_3(\ddot\theta_2 + \ddot\theta_3) - a_3s_{23}\dot\theta_1^2 c_{23} - r_{c3}(\ddot\theta_2 + \ddot\theta_3) - r_{c3}s_{23}\dot\theta_1^2 c_{23}]\}(a_3 + r_{c3}) + M_4(c_3(s_2g - c_2\dot\theta_1^2 a_1$$

$$-\dot\theta_1^2 c_2^2 a_2 - a_2\ddot\theta_2) + s_3(c_2g + s_2\dot\theta_1^2 a_1 + s_2\dot\theta_1^2 c_2 a_2 + \ddot\theta_2 a_2) - a_3(\ddot\theta_2 + \ddot\theta_3)^2 - (c_{23}\dot\theta_1)^2 a_3$$

$$+2\dot d(\ddot\theta_2 + \ddot\theta_3) + d_{PR}(\ddot\theta_2 + \ddot\theta_3) - d_{PR}s_{23}\dot\theta_1^2 c_{23} + r_{c4}(\ddot\theta_2 + \ddot\theta_3) - r_{c4}s_{23}\dot\theta_1^2 c_{23})(d + r_{c4}) - I_{4ZZ}(S_{23}\dot\theta_1^2 c_{23})$$

$$+M_4(s_3(s_2g - \dot\theta_1^2 c_2^2 a_2 - a_2\ddot\theta_2) - c_3(c_2g + s_2\dot\theta_1^2 a_1 + s_2\dot\theta_1^2 c_2 a_2 + \ddot\theta_2 a_2) - a_3(\ddot\theta_2 + \ddot\theta_3) - a_3s_{23}\dot\theta_1^2 c_{23}$$

$$+\ddot d - d_{PR}(s_{23}\dot\theta_1)^2 - d_{PR}(\ddot\theta_2 + \ddot\theta_3)^2 - c_{c4}(s_{23}\dot\theta_1)^2 - r_{c4}(\ddot\theta_2 + \ddot\theta_3)^2)r_{c3} + I_{3ZZ}s_{23}\dot\theta_1^2 c_{23}$$

$$-\{s_3(M_4[c_3(s_2g - c_2\dot\theta_1^2 a_1 - \dot\theta_1^2 c_2^2 a_2 - a_2\ddot\theta_2) + s_3(c_2g + s_2\dot\theta_1^2 a_1 + s_2\dot\theta_1^2 c_2 a_2 + \ddot\theta_2 a_2)$$

$$-a_3(\ddot\theta_2 + \ddot\theta_3)^2 - (c_{23}\dot\theta_1)^2 a_3 + 2\dot d(\ddot\theta_2 + \ddot\theta_3) + d_{PR}(\ddot\theta_2 + \ddot\theta_3) - d_{PR}s_{23}\dot\theta_1^2 c_{23} + r_{c4}(\ddot\theta_2 + \ddot\theta_3)$$

$$-r_{c4}s_{23}\dot\theta_1^2 c_{23}] + M_3[c_3(s_2g - c_2\dot\theta_1^2 a_1 - \dot\theta_1^2 c_2^2 a_2 - \ddot\theta_2^2 a_2) + s_3(c_2g + s_2\dot\theta_1^2 a_1$$

$$+s_2\dot\theta_1^2 c_2 a_2 + \ddot\theta_2 a_2) - a_3(\ddot\theta_2 + \ddot\theta_3)^2 + (c_{23}\dot\theta_1)^2 a_3 - r_{c3}[(\ddot\theta_2 + \ddot\theta_3)^2 + (c_{23}\dot\theta_1)^2])$$

$$-c_3(M_4[s_3(s_2g - c_2\dot\theta_1^2 a_1 - \dot\theta_1^2 c_2^2 a_2 - a_2\ddot\theta_2) - c_3(c_2g + s_2\dot\theta_1^2 a_1 + s_2\dot\theta_1^2 C_2 a_2 + \ddot\theta_2 a_2)$$

$$-a_3(\ddot\theta_2 + \ddot\theta_3) - a_3s_{23}\dot\theta_1^2 c_{23} + \ddot d - d_{PR}(s_{23}\dot\theta_1)^2 - d_{PR}(\ddot\theta_2 + \ddot\theta_3)^2 - c_{c4}(s_{23}\dot\theta_1)^2 - r_{c4}(\ddot\theta_2 + \ddot\theta_3)]$$

$$+M_3[s_3(s_2g - c_2\dot\theta_1^2 a_1 - \dot\theta_1^2 c_2^2 a_2 - a_2\ddot\theta_2) - c_3(c_2g + s_2\dot\theta_1^2 a_1 + s_2\dot\theta_1^2 c_2 a_2 + \ddot\theta_2 a_2)$$

$$-a_3(\ddot\theta_2 + \ddot\theta_3) - a_3s_{23}\dot\theta_1^2 c_{23} - r_{c3}(\ddot\theta_2 + \ddot\theta_3) - r_{c3}s_{23}\dot\theta_1^2 c_{23}])\}r_{c2} + I_{2zz}\ddot\theta_2 + f_{V2}\dot\theta_2$$